Published for SISSA by Springer

Received: *August 21, 2025*
Accepted: *September 15, 2025*
Published: *October 10, 2025*

Search for the production of a Higgs boson in association with a single top quark in pp collisions at $\sqrt{s} = 13$ TeV with the ATLAS detector

The ATLAS collaboration

E-mail: atlas.publications@cern.ch

Abstract: A search for the production of a Higgs boson in association with a single top quark, tH, is presented. The analysis uses proton-proton collision data corresponding to an integrated luminosity of 140 fb^{-1} at a centre-of-mass energy of 13 TeV, collected by the ATLAS detector at the LHC. The search targets Higgs-boson decays into $b\bar{b}$, WW^*, ZZ^*, and $\tau\tau$, accompanied by an isolated lepton (electron or muon) from the top-quark decay. Multivariate techniques are employed to enhance the separation between signal and background processes. The observed signal strength, μ_{tH}, defined as the ratio between the measured cross-section and the predicted Standard Model value, is $\mu_{tH} = 8.1 \pm 2.6\,(\text{stat.}) \pm 2.0\,(\text{syst.})$. The significance of the observed (expected) signal above the background-only expectation is 2.8 (0.4) standard deviations. The corresponding observed (expected) upper limit at the 95% confidence level on the tH cross-section is found to be 13.9 (6.1) times the value predicted by the Standard Model. An interpretation with an inverted sign of the top-quark Yukawa coupling is performed, and the signal strength and corresponding limit are reported.

Keywords: Hadron-Hadron Scattering

ArXiv ePrint: 2508.14695

https://doi.org/10.1007/JHEP10(2025)093

JHEP10(2025)093

Contents

1 Introduction

The discovery of a particle with properties consistent with the Higgs boson [1, 2] of the Standard Model (SM) in 2012 by the ATLAS and CMS experiments [3, 4] opened a new field of exploration in the realm of particle physics. Studying the Higgs-boson couplings is essential to test whether the observed particle corresponds to the Higgs boson predicted by the SM. In the SM, the strength of these interactions with other elementary particles is proportional to their masses (or masses squared).

Specifically, the Higgs boson interacts with fermions via Yukawa couplings [5]. Among these, the Yukawa coupling to the top quark, y_t, is of special interest as it is the largest with a value close to unity. Given its large value, y_t plays a crucial role in radiative corrections to the Higgs potential [6, 7], influencing the shape of the potential and, consequently, the stability of the electroweak (EW) vacuum [8]. In addition, it significantly affects the running of SM parameters, impacting the scale at which new physics might appear [7]. For all these reasons the Yukawa coupling of the Higgs boson to the top quark is considered a good probe for new physics. In particular, the study of its charge-conjugation and parity (CP) properties could provide insight into the observed baryon asymmetry of the universe [9–11].

The magnitude of y_t can be determined indirectly from Higgs-boson production via a top-quark loop or directly through cross-section measurements of top-quark pair production in association with a Higgs boson ($t\bar{t}H$). The $t\bar{t}H$ production process was observed [12, 13] in 2018. The production cross-section of the Higgs boson in association with a single top quark is sensitive to both the magnitude of y_t and its sign [14–18]. While the sign of y_t is not defined in an absolute sense, it is instead defined relative to the coupling strength of the W boson to the Higgs boson. In the following, this relative-sign convention is adopted throughout, and the sign of y_t is referred to accordingly, without explicitly restating its dependence on the W-boson coupling. Measurements of Higgs-boson processes conducted by the ATLAS and CMS Collaborations, such as the Higgs-boson decay into photon pairs ($H \to \gamma\gamma$) [19, 20], provide insight into the sign of the y_t coupling. Similar information comes from the combination of other Higgs-boson measurements. These include the simplified template cross-section (STXS) combination for gluon-gluon fusion (ggF), vector-boson fusion (VBF), and associated production with vector bosons (VH, where V refers to the W and Z bosons) or $t\bar{t}H$ in different decay channels [21, 22]. These measurements probe indirect effects in loop interactions and currently disfavour a negative value of the coupling [23], under the assumption that only SM particles contribute to the loops.

Higgs-boson production in association with a single top quark occurs via the EW interaction through three distinct production modes: t-channel (tHq), tWH and s-channel [24, 25]. The main production mode in proton-proton (pp) collisions at the Large Hadron Collider (LHC) [26] is the tHq process, followed by the associated tWH process and the s-channel. In this paper, the tHq and tWH processes are collectively referred to as tH production and are the ones used for the measurements presented, while s-channel production is neglected due to its extremely low production cross-section (3% of the total tH cross-section).

In the tHq process, an incoming light-flavour quark (i.e. up-type quark or down-type antiquark) from one of the colliding protons interacts with a b-quark by exchanging a space-like virtual W boson. The origin of the b-quark depends on the flavour scheme (FS) used in the calculation: in the five-flavour scheme (5FS), it is treated as a massless parton originating from the proton sea, while in the four-flavour scheme (4FS), where b-quarks are not included in the proton parton distribution functions (PDFs), it arises from gluon splitting into a $b\bar{b}$ pair [27–29]. In the tWH process, a gluon from one of the protons interacts with a b-quark from the other proton or from gluon splitting, via the exchange of a time-like virtual top

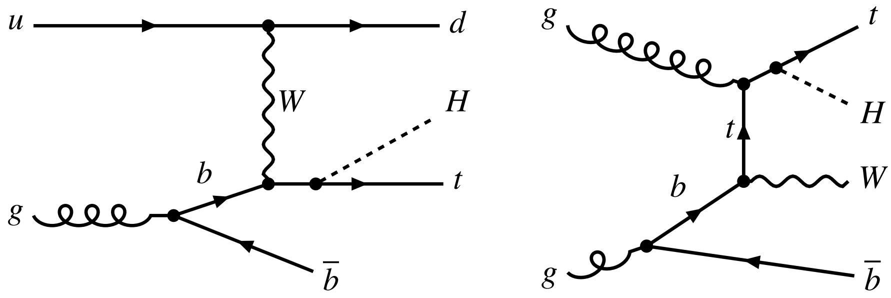

(a) (b)

Figure 1. Representative dominant Feynman diagrams for (a) tHq and (b) tWH production at LO, in the 4FS. The tHq event topology (a) is characterised by two heavy objects, the top quark and the Higgs boson plus an energetic light-flavour quark (dominantly a u-quark), referred to as the spectator quark, and an extra soft b-quark from gluon splitting. The tWH event topology (b) is characterised by three heavy objects, the top quark, the Higgs boson and a W boson and an extra soft b-quark from gluon splitting.

quark t. Two examples of dominant leading-order (LO) Feynman diagrams for the tHq and tWH processes, both in the 4FS, are shown in figure 1.

Under the SM hypothesis ($\kappa_t = y_t/y_t^{\mathrm{SM}} = +1$), the interference between diagrams in which the Higgs boson couples to the top quark and those where it couples to the W boson is destructive, leading to a strongly suppressed cross-section. In contrast, in scenarios beyond the SM, such as those involving CP-even and CP-odd admixtures in the top-quark Yukawa coupling structure, the relative sign between the Higgs-boson couplings to the top quark and the W boson can be altered, enhancing the tH cross-section up to an order of magnitude [24, 25]. The maximum enhancement occurs when $\kappa_t = -1$, corresponding to fully constructive interference between the contributing diagrams.

The tHq event topology is characterised by two heavy objects, a top quark and a Higgs boson, which is radiated from the latter, plus an energetic light-flavour quark (dominantly a u- or $\bar{d}$-quark), known as the spectator quark, and an extra soft b-quark from gluon splitting. The top-quark and Higgs-boson systems are produced in the central part of the detector recoiling against each other. The production of tWH is characterised by three heavy objects, the top quark, a W boson, a Higgs boson that is radiated from one of these two particles and an extra soft b-quark from gluon splitting. This event topology closely resembles $t\bar{t}H$ production and has an identical final state.

The CMS Collaboration searched for $tHq + tWH$ production in pp collisions at a centre-of-mass energy of $\sqrt{s} = 13\,\mathrm{TeV}$ with an integrated luminosity of $35.9\,\mathrm{fb}^{-1}$ [30]. The observed cross-section limits are 1.94 pb for the SM and 0.74 pb for the inverted top-quark Yukawa coupling (ITC) (i.e. $\mathrm{sign}(y_t) = \kappa_t = -1$) hypothesis. More recently, using the full Run-2 dataset, the CMS Collaboration reported updated $t\bar{t}H$ and $tHq + tWH$ results in the multi-lepton and $b\bar{b}$ final states in ref. [31] and ref. [32], respectively. In the multi-lepton final state, the measured signal strength is $\mu_{tHq+tWH} = 5.7 \pm 2.7\,(\mathrm{stat.}) \pm 3.0\,(\mathrm{syst.})$. In the $b\bar{b}$ final state, the observed upper limit relative to the SM prediction is 14.6 at 95% confidence level.

The analysis presented in this paper uses an integrated luminosity of 140 $\text{fb}^{-1}$of data collected with the ATLAS detector at $\sqrt{s} = 13$ TeV between 2015 and 2018 at the LHC. The search targets signatures that are primarily sensitive to $H \to b\bar{b}$, $H \to WW^*$, $H \to ZZ^*$ and $H \to \tau\tau$ decays. Backgrounds are estimated with a combination of simulation and data-driven techniques, and a global fit in all final states is used to extract the best estimate for the tH production rate under both the SM and ITC hypotheses.

2 Analysis strategy

The search described in this paper considers three mutually orthogonal final states, hereafter referred to as channels, distinguished by the number of light-flavour leptons (ℓ), i.e. electron (e) or muon (μ):

- one lepton ($H \to b\bar{b}$);
- two same-charge leptons (2ℓ SS);
- three leptons (3ℓ).

Events with τ-leptons decaying into an electron or a muon are part of selection, while events containing hadronically decaying τ-leptons (τ_{had}) are vetoed in all three channels.

Each channel targets different Higgs-boson decay modes. The $H \to b\bar{b}$ channel is most sensitive to the $H \to b\bar{b}$ decay, while the 2ℓ SS and 3ℓ channels mostly probe $H \to WW^*$. In the 2ℓ SS and 3ℓ channels, subleading contributions arise from $H \to \tau\tau$ and from $H \to ZZ^*$ decays.

These three channels are characterised by different background compositions, therefore they are analysed and fitted separately and combined afterwards.Each channel defines multiple analysis regions: signal regions (SRs), which are enriched in signal events, and control regions (CRs), which are designed to constrain the dominant background contributions. In the $H \to b\bar{b}$ channel, two regions are defined: one SR targeting the signal, and a CR dedicated to top-quark pair ($t\bar{t}$) production in association with b-jets, denoted CR($t\bar{t}+ \geq 1b$). In both the 2ℓ SS and 3ℓ channels, five regions are defined: one SR, three CRs to constrain backgrounds from non-prompt and fake leptons, and one CR targeting the associated production of a W boson with a top-quark pair ($t\bar{t}W$).

To enhance signal-to-background separation, all channels employ multivariate analysis techniques, specifically Boosted Decision Trees (BDTs). These methods are used both to discriminate signal from background and to separate different background components to better constrain them, as well as to define the analysis regions. Details are provided in section 6.

A profile likelihood fit, implemented using the TRExFitter framework [33], is used to simultaneously extract the signal strength, μ_{tH}, and the normalisations of the dominant backgrounds in each channel. The signal strength is first fitted separately in each channel, and then in a combined fit.

The manuscript is structured as follows: section 3 describes the ATLAS detector, while details of the data and MC simulated event samples used in the analysis are provided in

JHEP10(2025)093

section 4. Section 5 outlines the object definitions. The event selection, multivariate analysis techniques, and analysis region definitions for each channel are presented in section 6, while section 7 describes the background estimates and its results. All uncertainties considered in this measurement are discussed in section 8. The resulting constraints on the signal process in both the SM and ITC scenarios are shown in section 9, for each channel and their combination. Finally, the conclusions are presented in section 10.

3 ATLAS detector

The ATLAS detector [34] at the LHC covers nearly the entire solid angle around the collision point.[1] It consists of an inner tracking detector surrounded by a thin superconducting solenoid, electromagnetic and hadronic calorimeters, and a muon spectrometer incorporating three large superconducting air-core toroidal magnets.

The inner-detector system (ID) is immersed in a 2 T axial magnetic field and provides charged-particle tracking in the range of $|\eta| < 2.5$. The high-granularity silicon pixel detector covers the vertex region and typically provides four measurements per track, the first hit generally being in the insertable B-layer (IBL) installed before the LHC Run 2 [35, 36]. It is followed by the SemiConductor Tracker (SCT), which usually provides eight measurements per track. These silicon detectors are complemented by the Transition Radiation Tracker (TRT), which enables radially extended track reconstruction up to $|\eta| = 2.0$. The TRT also provides electron identification information based on the fraction of hits (typically 30 in total) above a higher energy-deposit threshold corresponding to transition radiation.

The calorimeter system covers the pseudorapidity range $|\eta| < 4.9$. Within the region $|\eta| < 3.2$, electromagnetic calorimetry is provided by barrel and endcap high-granularity lead/liquid-argon (LAr) calorimeters, with an additional thin LAr presampler covering $|\eta| < 1.8$ to correct for energy loss in material upstream of the calorimeters. Hadronic calorimetry is provided by the steel/scintillator-tile calorimeter, segmented into three barrel structures within $|\eta| < 1.7$, and two copper/LAr hadronic endcap calorimeters. The solid angle coverage is completed with forward copper/LAr and tungsten/LAr calorimeter modules optimised for electromagnetic and hadronic energy measurements, respectively.

The muon spectrometer (MS) comprises separate trigger and high-precision tracking chambers measuring the deflection of muons in a magnetic field generated by the superconducting air-core toroidal magnets. The field integral of the toroids ranges between 2.0 and 6.0 T m across most of the detector. Three layers of precision chambers, each consisting of layers of monitored drift tubes, cover the region $|\eta| < 2.7$, complemented by cathode-strip chambers in the forward region, where the background is highest. The muon trigger system covers the range $|\eta| < 2.4$ with resistive-plate chambers in the barrel, and thin-gap chambers in the endcap regions.

[1] ATLAS uses a right-handed coordinate system with its origin at the nominal interaction point (IP) in the centre of the detector and the z-axis along the beam pipe. The x-axis points from the IP to the centre of the LHC ring, and the y-axis points upwards. Cylindrical coordinates (r, ϕ) are used in the transverse plane, ϕ being the azimuthal angle around the z-axis. The pseudorapidity is defined in terms of the polar angle θ as $\eta = -\ln\tan(\theta/2)$. Angular distance is measured in units of $\Delta R \equiv \sqrt{(\Delta\eta)^2 + (\Delta\phi)^2}$.

The luminosity is measured mainly by the LUCID-2 [37] detector that records Cherenkov light produced in the quartz windows of photomultipliers located close to the beampipe.

Events were selected by the first-level trigger system implemented in custom hardware, followed by selections made by algorithms implemented in software in the high-level trigger [38]. The first-level trigger accepted events from the 40 MHz bunch crossings at a rate close to 100 kHz, which the high-level trigger further reduced in order to record complete events to disk at about 1.25 kHz.

A software suite [39] is used in data simulation, in the reconstruction and analysis of real and simulated data, in detector operations, and in the trigger and data acquisition systems of the experiment.

4 Data and simulated event samples

4.1 Data event samples

This analysis uses data from pp collisions at $\sqrt{s} = 13$ TeV collected with the ATLAS detector at the LHC during 2015–2018. Stringent detector and data-quality requirements were applied [40], resulting in a data sample corresponding to a total integrated luminosity of 140 fb^{-1}. The events were selected by single-lepton triggers with variable electron and muon transverse momentum (p_{T}) thresholds, and various identification and isolation criteria depending on the lepton flavour and the data-taking period [41, 42]. The lowest p_{T} threshold at trigger level used for electrons was 24 GeV (26 GeV), while for muons the threshold was 20 GeV (26 GeV) in 2015 (2016–2018).

4.2 Simulated event samples

Samples of simulated events were produced using different Monte Carlo (MC) event generators including parton shower (PS) and hadronisation models for both signal and background processes. The effect of multiple interactions in the same and neighbouring bunch crossings (pile-up) was modelled by overlaying the hard-scattering event with simulated minimum-bias events generated with Pythia 8.186 [43, 44] using the NNPDF2.3LO set of PDFs [45] and the A3 set of tuned parameters (A3 tune) [46]. Events were reweighted such that the distribution of the average number of interactions per bunch crossing matches that observed in data.

Table 1 presents a summary of all configurations used to generate events for signal (tHq and tWH) and background processes, for both nominal and alternative simulated samples. In all simulated signal and background samples, the top-quark mass was set to $m_{\mathrm{top}} = 172.5$ GeV and the Higgs-boson mass to $m_H = 125.0$ GeV. Moreover, the strong coupling constant was set to $\alpha_{\mathrm{s}} = 0.118$ [47] at the reference scale of the Z-boson mass. These values are also used in the computation of production cross-sections for processes involving these particles. The bottom and charm hadron decays were simulated with EvtGen [48] for all event samples, except those generated with Sherpa.

Systematic uncertainties from different modelling choices are evaluated by comparing alternative simulated samples to the nominal ones. These alternative samples are generated either through reweighting or with dedicated event generators. Each variation is applied

JHEP10(2025)093

Process	Generator	ME order	Parton shower	PDF set	Tune
tHq	MG5_aMC	NLO	Pythia 8	NNPDF3.0nlo	A14
	(MG5_aMC)	(NLO)	(Herwig 7)	(NNPDF3.0nlo)	(Herwig 7.1)
tWH	MG5_aMC	NLO	Pythia 8	NNPDF3.0nlo	A14
	(MG5_aMC)	(NLO)	(Herwig 7)	(NNPDF3.0nlo)	(Herwig 7.1)
$t\bar{t}$	Powheg Box	NLO	Pythia 8	NNPDF3.0nlo	A14
	(Powheg Box)	(NLO)	(Herwig 7)	(NNPDF3.0nlo)	(Herwig 7.1)
	(Powheg Box)	(NLO)	(Pythia 8)	(NNPDF3.0nlo)	(A14 $p_{\mathrm{T}}^{\mathrm{hard}}$)
	(MG5_aMC)	(NLO)	(Pythia 8)	(NNPDF3.0nlo)	(A14)
$t\bar{t}+b\bar{b}$	(Powheg Box Res)	(NLO)	(Pythia 8)	(NNPDF3.0nlo)	(A14)
$t\bar{t}H$	Powheg Box	NLO	Pythia 8	NNPDF3.0nlo	A14
	(Powheg Box)	(NLO)	(Herwig 7)	(NNPDF3.0nlo)	(Herwig 7.1)
	(MG5_aMC)	(NLO)	(Pythia 8)	(NNPDF3.0nlo)	(A14)
$t\bar{t}W$	Sherpa 2.2.10	NLO QCD+EW	Sherpa	NNPDF3.0nnlo	default
	(MG5_aMC)	(NLO QCD+EW)	(Pythia 8)	NNPDF3.0nnlo	(A14)
$t\bar{t}W$ (EW)	Sherpa 2.2.10	LO	Sherpa	NNPDF3.0nnlo	default
	(MG5_aMC)	(LO)	(Pythia 8)	(NNPDF3.0nlo)	(A14)
$t\bar{t}Z$	MG5_aMC	NLO	Pythia 8	NNPDF3.0nlo	A14
	(Sherpa 2.2.10)	(LO)	(Sherpa)	(NNPDF3.0nnlo)	(default)
	(MG5_aMC)	(NLO)	(Herwig 7)	(NNPDF3.0nlo)	(Herwig 7.1)
Single top quark (t-ch., tW, s-ch.)	Powheg Box	NLO	Pythia 8	NNPDF3.0nlo	A14
	(Powheg Box)	(NLO)	(Herwig 7)	(NNPDF3.0nlo)	(Herwig 7.1)
	(MG5_aMC)	(NLO)	(Herwig 7)	(NNPDF3.0nlo)	(Herwig 7.1)
$V+$jets	Sherpa 2.2.1	MEPS@NLO	Sherpa	NNPDF3.0nlo	default
VV, $qqVV$	Sherpa 2.2.2	MEPS@NLO	Sherpa	NNPDF3.0nnlo	default
	(Powheg Box)	(NLO)	(Pythia 8)	(NNPDF3.0nlo)	(A14)
VVV	Sherpa 2.2.2	MEPS@NLO	Sherpa	NNPDF3.0nnlo	default
tZ	MG5_aMC	NLO	Pythia 8	NNPDF3.1nlo	A14
tWZ	MG5_aMC	NLO DR1	Pythia 8	NNPDF2.3lo	A14
	(MG5_aMC)	(NLO DR2)	(Pythia 8)	NNPDF2.3lo	(A14)
$t\bar{t}t, t\bar{t}t\bar{t}$	MG5_aMC	QCD NLO	Pythia 8	NNPDF3.1nlo	A14
ggH, qqH	Powheg Box	QCD NLO	Pythia 8	CTEQ6L1	AZNLO
WH, ZH	Pythia 8	QCD NLO	Pythia 8	NNPDF2.3lo	A14

Table 1. The configurations used to generate events for signal (tHq and tWH) and background processes. The simulation samples used to estimate the systematic uncertainties are shown in parentheses and in grey.

independently, unless explicitly stated otherwise, to ensure a consistent evaluation of its individual impact on the analysis.

4.2.1 Simulated signal event samples

The production of a Higgs boson with a single top quark in the t-channel, tHq, was modelled using MadGraph5_aMC@NLO 2.6.2 [49] with matrix elements (MEs) at next-to-leading-order (NLO) accuracy in QCD in the 4FS using the NNPDF3.0nlo nf4 [50] PDF set. The renormalisation (μ_{r}) and factorisation (μ_{f}) scales were set to $0.5 \times \sum_i \sqrt{m_i^2 + p_{\mathrm{T},i}^2}$, summing over all ME-generated particles with mass m and transverse momentum p_{T}. Events were interfaced with Pythia 8.230 using the A14 set of tuned parameters (A14

JHEP10(2025)093

tune) [51] and the NNPDF2.3LO PDF set. The simulated tHq signal samples were normalised to the NLO QCD theory prediction without NLO EW corrections at $\sqrt{s} = 13$ TeV and in the 5FS of $74.3^{+6.5\%}_{-14.9\%}$ (QCD) $\pm$ 3.7% (PDF+α_s) fb [52, 53]. The PDF and α_s uncertainties are calculated using the PDF4LHC15_NLO_30_PDFAS PDF sets [54] and added in quadrature. The QCD uncertainty is computed from a combination of QCD scale variations and the difference of predictions in the 4FS and 5FS schemes, using the PDF4LHC15_NLO_NF4_100 PDF (central) set.

The associated production of a Higgs boson with a single top quark, tWH, was modelled using MadGraph5_aMC@NLO 2.8.1 with MEs at NLO accuracy in QCD in the 5FS using the NNPDF3.0NLO PDF set. The functional forms of the μ_r and μ_f scales were set the same as for the tHq simulation sample. The diagram-removal (DR) scheme (DR1) [55] was employed to remove the overlap between tWH and $t\bar{t}H$ simulation samples [56]. The events were interfaced with Pythia 8.245 using the A14 tune and the NNPDF2.3lo PDF set. The simulated tWH signal samples were normalised to the NLO QCD theory prediction in the 5FS [52, 53] and using the DR2 scheme [25] to handle the overlap between the tWH and $t\bar{t}H$ processes. At $\sqrt{s} = 13$ TeV the predicted cross-section is $\sigma(tWH)_{\text{NLO}} = 15.2^{+4.9\%}_{-6.7\%}$ (QCD scale) $\pm$ 6.3% (PDF+α_s) fb [52, 53].

To assess the modelling uncertainty due to the choice of the PS and hadronisation model, alternative event samples were produced for signal processes. Both tHq and tWH processes were produced using MadGraph5_aMC@NLO with the nominal set-up but interfaced with Herwig 7.1.6 [57, 58] using the MMHT2014nnlo [59] PDF set, with the Herwig 7.1 default set of tuned parameters (Herwig 7.1 tune) [58]. Moreover, simulated signal samples for both tHq and tWH with the ITC hypothesis were produced using similar set-ups as the ones used to produce SM simulated samples. In this case, the samples were normalised to the cross-section, for pp collisions at $\sqrt{s} = 13$ TeV, of $\sigma(tHq)^{\kappa_t=-1}_{\text{NLO}} = 873$ fb and $\sigma(tWH)^{\kappa_t=-1}_{\text{NLO}} = 114$ fb, respectively. For both nominal and ITC simulated signal samples, alternative variations of μ_r and μ_f scales and initial-/final-state radiation (ISR/FSR) were produced within the nominal set-up (i.e. MadGraph5_aMC@NLO +Pythia 8) as reweighted events.

4.2.2 Simulated background event samples

The production of $t\bar{t}$ events were modelled using Powheg Box v2 [60–63] at NLO QCD in 5FS with the NNPDF3.0NLO PDF set. In this case, the h_{damp} parameter[2] was set to $1.5 \times m_{\text{top}}$ [56]. Events were interfaced with Pythia 8.230 using the A14 tune and the NNPDF2.3LO PDF set. The simulated samples are normalised to the theory prediction at next-to-next-to-leading-order (NNLO) in QCD including the resummation of next-to-next-to-leading logarithmic (NNLL) soft-gluon terms calculated using Top++2.0 [64–70], equals to 834^{+29}_{-37} pb, where the uncertainty is the sum in quadrature of scale, PDF and α_s uncertainties.

A series of alternative $t\bar{t}$ simulated event samples were produced to evaluate the impact of modelling uncertainties. The effect of the choice of the PS and hadronisation model is quantified by comparing the nominal simulation with one produced using the same ME generator but interfaced with Herwig 7.1.6. To evaluate the impact of the choice of the NLO

[2]The h_{damp} parameter controls the p_T of the first additional emission beyond the LO Feynman diagram in the PS and therefore regulates the high-p_T emission against which the $t\bar{t}$ system recoils.

matching scheme two samples were produced: one where the parameter $p_{\mathrm{T}}^{\mathrm{hard}}$, which regulates the definition of the vetoed region of the PYTHIA 8 showering [71], was halved, and other event sample generated by MADGRAPH5_aMC@NLO and matched to HERWIG 7. Moreover, to assess the choice of the value of the h_{damp} parameter, alternative simulated samples generated using the nominal set-up but with $h_{\mathrm{damp}} = 3.0 \times m_{\mathrm{top}}$ were considered. A 4FS $t\bar{t} + b\bar{b}$ simulated sample was produced using POWHEG BOX RES with the OPENLOOPS [72–74] library and the NNPDF3.1NNLO nf4 PDF set, interfaced with PYTHIA 8.244. The simulation used a b-quark mass of 4.95 GeV and dynamic scales μ_{f} set to $0.5 \times \sum_{i=t,\bar{t},b,\bar{b},j} m_{\mathrm{T},i}$ and μ_{r} set to $0.5 \times \sqrt[4]{m_{\mathrm{T},t} \cdot m_{\mathrm{T},\bar{t}} \cdot m_{\mathrm{T},b} \cdot m_{\mathrm{T},\bar{b}}}$, where $m_{\mathrm{T},i} = \sqrt{m_i^2 + p_{\mathrm{T},i}^2}$ denotes the transverse mass of particle i. The h_{damp} parameter was defined as $0.5 \times \sum_{i=t,\bar{t},b,\bar{b}} m_{\mathrm{T},i}$, and the parameter h_{bzd} was set to 5. Here, h_{bzd} controls the suppression of the Born-zero configurations in POWHEG. This sample is considered to evaluate the impact of using the 4FS instead of the 5FS and also the effect of generating additional b-quarks explicitly at NLO in the ME in the 4FS, as opposed to their approximate treatment via the PS in the 5FS set-up.

The $t\bar{t}H$ events were simulated using POWHEG BOX v2 at NLO accuracy in QCD in 5FS with the NNPDF3.0NLO PDF set, and with μ_{r} and μ_{f} scales set to $\sqrt[3]{m_{\mathrm{T},t} \cdot m_{\mathrm{T},\bar{t}} \cdot m_{\mathrm{T},H}}$ [75]. Events were interfaced with PYTHIA 8.230 using the A14 tune and the NNPDF2.3LO PDF set. The NLO QCD+EW cross-section at $\sqrt{s} = 13$ TeV is 507^{+35}_{-50} fb [52], where the uncertainties were estimated from variations of α_{s} and the μ_{r} and μ_{f} scales. Additional variations use event weights for QCD scales and radiation, with an alternative PS simulated sample using HERWIG 7.04.

The $t\bar{t}W$ events were produced using SHERPA 2.2.10 [76] at NLO (LO) accuracy in QCD for up to one (two) additional partons. The NNPDF3.0NNLO PDF set was used along with the dedicated set of tuned PS parameters developed by the SHERPA authors. In addition, EW corrections were also produced with SHERPA 2.2.10 at LO accuracy for up to one additional parton. The $t\bar{t}W$ cross-section is calculated at NLO QCD with up to two additional partons using an improved MADGRAPH5_aMC@NLO FxFx merging procedure [77, 78] and combines it with leading $\mathcal{O}(\alpha^2\alpha_s^2)$ and subleading $\mathcal{O}(\alpha^3\alpha_s)$ NLO EW corrections. This calculation also includes on-shell LO decays of the $t\bar{t}W$ including the tree-level spin correlations within the narrow-width approximation. At $\sqrt{s} = 13$ TeV, this yields 722^{+70}_{-78} (scale)$^{+7}_{-7}$ (PDF) fb [78]. The choice of the NLO matching scheme was evaluated using an alternative simulated sample produced with MADGRAPH5_aMC@NLO 2.3.3 with the FxFx [77] merging scheme simulated samples including EW corrections.

The associated production of the Z boson with a top-quark pair ($t\bar{t}Z$) was simulated using MADGRAPH5_aMC@NLO 2.3.3 at NLO QCD with the NNPDF3.0NLO PDF set, interfaced with PYTHIA 8.210 using the A14 tune and the NNPDF2.3LO PDF set. The $t\bar{t}Z$ cross-section, including off-shell effects and Z/γ^* interference, was calculated at NLO QCD+EW as $0.88^{+0.09}_{-0.10}$ pb [52, 79], where the uncertainties were estimated from variations of α_{s} and the μ_{r} and μ_{f} scales. The choice of the NLO matching scheme was evaluated using an alternative simulated sample produced with SHERPA 2.2.0 at LO accuracy along with the NNPDF3.0NNLO PDF set, using the MEPS@LO prescription [80], with up to one additional parton for the $t\bar{t}Z(\to \ell\ell)$ sample and two additional partons for the $t\bar{t}Z(\to qq)$ and $t\bar{t}Z(\to \nu\nu)$ samples.

JHEP10(2025)093

All single top-quark events were generated with POWHEG BOX v2 at NLO in QCD with either the NNPDF3.0NLO nf4 or NNPDF3.0NLO PDF sets, with μ_f and μ_r scales set to $\sqrt{m_b^2 + p_{T,b}^2}$ [81, 82]. The t-channel was produced considering the 4FS, while the s-channel and associated tW processes used the 5FS. The latter process also employed the DR1 scheme to remove the overlap between tW and $t\bar{t}$ [56]. Events were interfaced with PYTHIA 8.230 using the A14 tune and the NNPDF2.3LO PDF set. Systematic variations include QCD μ_r and μ_f scales and radiation uncertainties, alternative PS using POWHEG BOX v2 with HERWIG 7.16, and matching scheme uncertainties using MADGRAPH5_aMC@NLO 2.6.2 with HERWIG 7.16 and the MMHT2014NNLO PDF set. For associated tW, an additional simulated sample using the diagram subtraction (DS) scheme was produced to evaluate the $t\bar{t}$ interference uncertainties.

The production of single-boson (V + jets), diboson (VV), and triboson (VVV) processes were simulated using either SHERPA 2.2.1 or SHERPA 2.2.2, with varying levels of QCD accuracy depending on the process. The NNPDF3.0NNLO PDF set was used along with a dedicated set of SHERPA-tuned PS parameters. For the V + jets processes, MEs were generated at NLO (LO) accuracy in QCD for up to two (four) partons, using the Comix library [83]. Simulated samples were normalised to NNLO predictions [84]. For the VV processes, MEs accounted for off-shell effects and included Higgs-boson contributions where relevant. Fully leptonic and semileptonic final states, where one boson decays leptonically and the other hadronically, were simulated at NLO (LO) accuracy in QCD for up to one (three) additional partons. Loop-induced processes $gg \to VV$ were generated at LO accuracy in QCD with up to one additional parton, for both fully leptonic and semileptonic final states. The EW production of a VV pair in association with two jets ($VVjj$) was simulated at LO accuracy in QCD. For the VVV processes, MEs were generated with factorised gauge-boson decays at NLO accuracy in QCD for the inclusive process and at LO accuracy in QCD for up to two additional parton emissions. In all cases, NLO MEs were matched to PS using a colour-exact variant of the MC@NLO algorithm [85]. Different jet multiplicities were merged via the CKKW matching procedure [86, 87], extended to NLO QCD accuracy through the MEPS@NLO [80] prescription, with a merging threshold set to 20 GeV. Leading-order MEs were merged using the MEPS@LO prescription. These calculations were performed in the G_μ scheme, which uses the Fermi constant as input, ensuring an optimal description of pure EW interactions at the EW scale.

To assess modelling uncertainties, scale uncertainties were evaluated using seven μ_r and μ_f variations (by factors of 0.5 and 2) as event weights. Furthermore, in the particular case of the VV processes, alternative event simulated samples were produced to evaluate the impact of different ME, PS, and hadronisation models by comparing the nominal diboson SHERPA event samples with POWHEG BOX v2 simulations of WW, WZ, and ZZ [88] processes at NLO accuracy in QCD. The effects of singly resonant amplitudes and interference due to Z/γ^* exchange, as well as same-flavour lepton combinations in the final state, were included where relevant. However, WW/ZZ interference in same-flavour lepton and neutrino final states was neglected. Events were interfaced with PYTHIA 8.186 using the AZNLO set of tuned parameters (AZNLO tune) [89]. The CT10 PDF set [90] was used for hard-scattering calculations, while the CTEQ6L1 [91] PDF set was applied for PS. The μ_f and μ_r scales were set to the boson-pair invariant mass, with a requirement of $m_{\ell\ell} > 4\,\text{GeV}$ at the ME level for same-flavour lepton pairs.

The tZq event sample was simulated using MadGraph5_aMC@NLO 2.3.3 at NLO accuracy in QCD in the 4FS with the NNPDF3.0nlo PDF set. The events were interfaced with Pythia 8.230 using the A14 tune and the NNPDF2.3lo PDF set. Off-resonance events away from the Z-mass peak were included. The functional form of the μ_r and μ_f scales was set to $4\sqrt{m_b^2 + p_{\text{T},b}^2}$, where the b-quark was the one produced by a gluon splitting in the event. The uncertainty due to initial-state radiation and to higher/lower parton radiation were estimated following exactly the same prescription as with the t-channel process.

The tWZ event production was modelled using MadGraph5_aMC@NLO 2.3.3 at NLO QCD with the NNPDF3.0nlo PDF set in the 5FS. Events were interfaced with Pythia 8.212, using the A14 tune and the NNPDF2.3lo PDF set. The DR1 scheme was used to remove the overlap between the tWZ and $t\bar{t}Z$ processes. Parton radiation uncertainties follow the same prescription as the t-channel process. An alternative DR scheme [25] was simulated to assess systematic uncertainty.

The production of three top-quark process ($t\bar{t}t$) events was modelled using MadGraph5_aMC@NLO 2.2.2 with NLO accuracy in QCD interfaced with Pythia 8.186, using the NNPDF2.3lo PDF set and the A14 tune. The production of four top-quark process ($t\bar{t}t\bar{t}$) events was modelled using MadGraph5_aMC@NLO 2.3.3 with NLO accuracy in QCD with the NNPDF3.1nlo PDF set. The events were interfaced with Pythia 8.230 for the PS and hadronisation, using the A14 tune and the NNPDF2.3lo PDF set.

Four SM Higgs-boson processes are considered as minor backgrounds: gluon-gluon fusion (ggH), VBF (qqH), and associated production with W and Z bosons (WH and ZH). The ggH and VBF events were modelled with either Powheg Box v2 or v1 (r2856) [92, 93], providing NLO accuracy in QCD with the CT10 PDF set. The μ_r and μ_f scales were set to $\sqrt{m_H^2 + p_{\text{T},H}^2}$. These generated events were interfaced with either Pythia 8.210 or 8.186 for PS and hadronisation, using the AZNLO tune and the CTEQ6L1 PDF set. The WH and ZH production was modelled with Pythia 8.186, using the A14 tune and the NNPDF2.3lo PDF set.

Most of the MC simulated samples used for the nominal estimates were processed through a simulation [94] of the ATLAS detector based on Geant4 [95], while those used for evaluating systematic uncertainties were processed with a fast simulation [94] that relies on a parameterisation of the calorimeter response [96]. Furthermore, fast-simulated event samples were used for certain nominal samples, particularly for the tHq and tWH signal processes and the $t\bar{t}t\bar{t}$ background process with no loss of accuracy.

5 Object definitions

Interaction vertices from the pp collisions are reconstructed from at least two tracks in the ID system with p_T larger than 500 MeV that are consistent with originating from the beam collision region in the x–y plane. If more than one primary vertex candidate is found in the event, the candidate for which the associated tracks form the largest sum of squared p_T is selected as the hard-scatter primary vertex [97].

JHEP10(2025)093

Electron candidates are reconstructed from energy clusters in the electromagnetic calorimeter matched to a track in the ID [98]. They are required to satisfy $p_{\mathrm{T}} > 10\,\mathrm{GeV}$ and $|\eta| < 2.47$, excluding the transition region between the endcap and barrel calorimeters ($1.37 < |\eta| < 1.52$). `Loose` and `Tight` electron identification working points are used, based on a likelihood discriminant employing calorimeter, tracking and combined variables that provide separation between electrons and jets.

Muon candidates are reconstructed from tracks measured in the ID matched to tracks measured in the MS [99, 100]. The resulting muon candidates are re-fitted using the complete track information from both detector systems. They are required to satisfy $p_{\mathrm{T}} > 10\,\mathrm{GeV}$ and $|\eta| < 2.5$. `Loose` and `Medium` muon identification working points are used.

Electron (muon) candidates are matched to the primary vertex by requiring that the significance of their transverse impact parameter, d_0,[3] satisfies $|d_0/\sigma(d_0)| < 5.0\,(3.0)$, where $\sigma(d_0)$ is the measured uncertainty in d_0, and by requiring that their longitudinal impact parameter, $z_0 \sin\theta$,[4] satisfies $|z_0 \sin\theta| < 0.5\,\mathrm{mm}$ [98, 99].

To further suppress leptons from heavy-flavour hadron decays, misidentified jets, or photon conversions (collectively referred to as "non-prompt leptons"), a BDT discriminant, referred to as the non-prompt-lepton BDT [101], based on isolation and lifetime information associated with a track jet that matches the selected electron or muon, is employed. The `Tight` working point based on the non-prompt-lepton BDT is used, which allows prompt muons (barrel/endcap electrons) to be selected with an efficiency that is about 60% (60%/70%) for $p_{\mathrm{T}} \sim 20\,\mathrm{GeV}$ and reaches a plateau of 95% (95%/90%) for $p_{\mathrm{T}} \sim 40$ (40/65)GeV, while the rejection factor against leptons from the decay of b-hadrons is about 20.

For the 2ℓSS channel, to further suppress electrons with incorrect charge assignment, a BDT discriminant based on calorimeter and tracking quantities [102] is used, reducing the signal by 1.9% and the total background by approximately 40%, both at preselection level (see section 6.2). The electron candidates are separated into three classes: "material conversion", "internal conversion", and "non-conversion" electron candidates. Most electrons originating from photon conversions, whether from material conversions in the detector or internal conversions, are rejected by the standard electron identification criteria. To further suppress remaining conversion electrons in the 2ℓSS and 3ℓ channels, additional vetoes are applied, except in control regions specifically targeting conversion electrons (e^*). Material conversion candidates have a reconstructed displaced vertex with radius $r > 20$ mm that includes the track associated with the electron.[5] The invariant mass of the associated track and the closest (in $\Delta\eta$) opposite-charge track reconstructed in the silicon detector, calculated at the conversion vertex, is required to be $< 100\,\mathrm{MeV}$. Internal conversion candidates must fail to satisfy the requirements for material conversions, and the di-track invariant mass, calculated here at the primary vertex, is required to be $< 100\,\mathrm{MeV}$.

The various lepton working points used are summarised in table 2. Lepton candidates are initially selected using relatively "*Loose*" criteria (labelled as L), and a subset may later

[3]The transverse impact parameter, d_0, is defined in the x–y plane as the distance of closest approach of the track to the beamline.

[4]The longitudinal impact parameter, z_0, is defined as the distance in z between the primary vertex and the point on the track used to evaluate d_0.

[5]The beampipe and IBL inner radii are 23.5 mm and 33 mm, respectively.

	Electron		Muon	
Lepton definition	L	T	L	T
Identification	`Loose`	`Tight`	`Loose`	`Medium`
Transverse impact parameter significance $\lvert d_0\rvert/\sigma_{d_0}$	< 5.0		< 3.0	
Longitudinal impact parameter z_0	$\lvert z_0 \sin\theta\rvert < 0.5$ mm			
Isolation (Non-prompt lepton BDT)	No	Yes	No	Yes
Electron charge-misassignment veto	No	Yes	–	
Electron conversion candidate veto	No	Yes (except e^*)	–	

Table 2. Description of the *Loose* (L) and *Tight* (T) lepton definitions. The electron e^* is required to fulfil, in addition to the corresponding lepton definition requirements, those corresponding to an internal or material conversion candidate.

be required to satisfy stricter "*Tight*" criteria (labelled as T) to further optimise the event selection. The choice of working point depends on the main background processes in each category. The specific selections adopted for the signal and control regions are described in section 6. The lepton working points used here (*Loose* and *Tight*) are not to be confused with the identification working points such as `Loose`, `Medium`, and `Tight`.

The constituents for jet reconstruction are identified by combining measurements from both the ID and the calorimeter using a particle flow (PFlow) algorithm [103]. Jet candidates are reconstructed from these PFlow objects using the anti-k_t algorithm [104, 105] with a radius parameter of $\Delta R = 0.4$. They are calibrated using simulation with corrections obtained by using in situ techniques in data [106]. Only jet candidates with $p_{\mathrm{T}} > 20$ GeV and within $|\eta| < 4.5$ are selected. To reduce the effect of pile-up, each jet with $p_{\mathrm{T}} < 60$ GeV and $|\eta| < 2.4$ must satisfy the `Tight` working point of the jet vertex tagger (JVT) [107] criteria used to identify jets that originate from the primary vertex. Moreover, jets within $2.5 < |\eta| < 4.5$ (hereafter called "forward jets") and $p_{\mathrm{T}} < 120$ GeV must satisfy the `Tight` working point of the forward jet vertex tagger (fJVT) [108] criteria. A set of quality criteria is also applied to reject events containing at least one jet arising from non-collision sources or detector noise [109].

Jets containing b-hadrons are identified (b-tagged) via the `DL1r` [110] algorithm that uses a deep feed-forward neural network based on the distinctive features of b-hadron decays, primarily the impact parameters of tracks and the displaced vertices reconstructed in the ID. Additional input to this network is provided by discriminating variables constructed by a recurrent neutral network (RNN) [111], which exploits the spatial and kinematic correlations between tracks originating from the same b-hadron. A multivariate b-tagging discriminant value is calculated for each jet. In this measurement, a jet is considered b-tagged if it passes the working point corresponding to 85%, 77%, 70%, or 60% average expected efficiency to tag a b-quark jet, with a light-jet[6] rejection factor of about 40 to 2500, and a charm-jet (c-jet) rejection factor of about 3 to 40, as determined for jets with $p_{\mathrm{T}} > 20$ GeV and

[6]'Light jet' or 'Light-flavour jet' refers to a jet originating from the hadronisation of a light-flavour quark (u, d, s) or a gluon.

JHEP10(2025)093

$|\eta| < 2.5$ in simulated $t\bar{t}$ events. This discrete version of the b-tagging discriminant, named pseudo-continuous b-tagging score (PCBT), is also exploited as jet variable.

The reconstruction of the τ_{had} is seeded by jets reconstructed via the anti-k_t algorithm, using calibrated energy clusters as inputs, with a distance parameter of $\Delta R = 0.4$ [112–115]. Jets seeding τ_{had} candidates are additionally required to have $p_{\text{T}} > 10\,\text{GeV}$ and $|\eta| < 2.5$. To separate the τ_{had} candidates initiated by hadronic τ-lepton decays from jets initiated by quarks or gluons, a RNN [114] identification method was trained on information from reconstructed charged-particle tracks and clusters of energy in the calorimeter associated with τ_{had} candidates as well as high-level discriminating variables. A separate multivariate discriminant based on a BDT [113, 115] is also used to reject backgrounds arising from electrons mimicking a τ_{had}. This discriminant (eBDT) is built using information from the calorimeter and the tracking detector. Transition radiation information from the TRT system plays a key role in the performance of this discriminant. Baseline τ_{had} are required to have one or three associated tracks, electric charge of ± 1, $p_{\text{T}} > 20\,\text{GeV}$ and $|\eta| < 2.5$, excluding the barrel-endcap transition region. Each τ_{had} must satisfy the `Medium` RNN identification selection requirement, with efficiencies of 75% for 1-prong and 60% for 3-prong taus, and the `Loose` eBDT requirement, with an efficiency of 95% [113, 115].

Ambiguities between independently reconstructed electrons, muons, jets and τ_{had} can arise. A sequential "overlap removal" procedure is performed to resolve these ambiguities and thus avoid double counting of candidates. This procedure is applied to electrons and muons satisfying the L criteria. If two electrons are separated by $\Delta R < 0.1$, only the one with the higher p_{T} is kept. If an electron and a muon overlap within $\Delta R < 0.1$, the muon is removed if it is reconstructed only from an ID track and calorimeter energy deposits consistent with a minimum-ionising particle (i.e. if it is "calorimeter-tagged"), otherwise the electron is removed. If an electron and a selected jet are found within $\Delta R < 0.2$, the jet is removed. Any electron later found within ΔR of 0.4 of a jet is removed. Muons associated with a jet must satisfy a jet-muon separation of $\Delta R < 0.4$. If the overlapping jet contains less than three tracks with $p_{\text{T}} > 500\,\text{MeV}$, the jet is removed, otherwise the muon is rejected. Any τ_{had} found within a ΔR of 0.2 of an electron is removed. Any τ_{had} found within a ΔR of 0.2 of any type of muon with p_{T} greater than 2 GeV is removed, although if the τ_{had} p_{T} is greater than 50 GeV, it will only be removed if it is found to overlap with a reconstructed muon. Finally, if a jet is found within a ΔR of 0.2 of a τ_{had}, the jet is removed.

The missing transverse momentum $\vec{p_{\text{T}}}^{\text{miss}}$ (with magnitude $E_{\text{T}}^{\text{miss}}$) is defined as the negative vector sum of the transverse momenta of all identified and calibrated objects and remaining unclustered energy, the latter of which is estimated from low-p_{T} tracks associated with the primary vertex but not assigned to any lepton or jet candidate [116]. The $E_{\text{T}}^{\text{miss}}$ is taken as a measurement of the undetectable particles, and is affected by energy losses due to detector inefficiencies and acceptance, and by energy resolution.

6 Event selection and classification

Events must satisfy the single-electron or single-muon trigger requirements described in section 4.1. Selected events are required to contain one lepton matched to the corresponding lepton reconstructed by the trigger within $\Delta R < 0.15$ and with $p_{\text{T}} > 27\,\text{GeV}$. These criteria ensure operation on the trigger efficiency plateau, thereby minimising the corrections needed in simulation to reproduce the per-lepton trigger efficiencies measured in data [41, 42].

Events selected by the trigger are required to have at least one primary vertex with at least two associated ID tracks with $p_{\mathrm{T}} > 0.5$ GeV. In each event, the primary vertex is defined as the reconstructed vertex having the highest scalar sum of squared p_{T} of associated tracks [97] among the vertices consistent with the average beam-spot position. These events are also required to contain either one lepton and at least three b-tagged jets (70% working point), two leptons with the same electric charge or three leptons, based on the *Loose* lepton definition introduced in section 5. Events containing τ_{had} leptons are explicitly vetoed in all three channels.

The sensitivity of the analysis relies on the discrimination provided by the multivariate response that combines different event-based variables. In each channel, BDTs with gradient boosting (BDTGs) are trained on simulated events in a preselection region using the `XGBoost` Python package [117]. The model performance is evaluated using the hold-out method, in which the considered data sample is randomly divided into an independent training-data sample and a test-data sample that is used as a proxy to evaluate the performance of the model on unseen data. In all channels, only the tHq process is considered as a signal in the BDTG training. This decision is driven by the similarities observed between the tWH and $t\bar{t}H$ topologies, so that including the tWH process in the training weakens the separation between tHq and $t\bar{t}H$ and other background processes. While the tWH sample is not part of the BDTG training, its contribution is fully accounted for in the signal yield and in the limit setting later on. A strong separation of the signal from the $t\bar{t}H$ process leads to a reduced interplay between $t\bar{t}H$ and the tH signal in the results.

Details on the definition of the preselection regions and the background composition are given in the following while the yields are reported in table 3.

6.1 $H \to b\bar{b}$ channel

The $H \to b\bar{b}$ preselection region is defined by requiring the presence of exactly one *Tight* lepton (electron or muon) with $p_{\mathrm{T}} > 27$ GeV. The 70% working point of the `DL1r` tagger is used to select at least three b-tagged jets. All events with at least five jets and at least four b-tagged jets are vetoed. This requirement has a negligible impact on the signal acceptance and will help any future combination with other $t\bar{t}H$ analyses. Given the presence of one neutrino coming from the W-boson decay, the event is expected to have a non-zero $E_{\mathrm{T}}^{\mathrm{miss}}$. For this reason an $E_{\mathrm{T}}^{\mathrm{miss}}$ >25 GeV requirement is applied.

As shown in Table 3, the main contribution to the background in the preselection region comes from $t\bar{t}$ + jets events, constituting 90% of the expected total yield. The $t\bar{t}$ + jets events are further classified depending on the flavour of the additional jets produced. Simulated events where at least one of the additional jets is matched to a b-hadron are classified as $t\bar{t}+ \geq 1b$ (30% of the expected $t\bar{t}$ + jets yield); if no matched b-jet is found but at least one jet is matched to a c-hadron the event is classified as $t\bar{t}+ \geq 1c$ (17% of the expected $t\bar{t}$ + jets yield) while all the other events are classified as $t\bar{t}+ \geq 0$ light (53% of the expected $t\bar{t}$ + jets yield). The latter contribution also includes $t\bar{t}$ events with no additional jets.

JHEP10(2025)093

Process	$H \to b\bar{b}$	2ℓ SS	3ℓ
tHq	91.1 ± 1.7	12.41 ± 0.17	3.15 ± 0.05
tWH	37.21 ± 0.26	3.97 ± 0.09	2.36 ± 0.07
$t\bar{t}$	–	1430 ± 14	324 ± 6
$t\bar{t}+\geq 1b$	60170 ± 90	–	–
$t\bar{t}+\geq 1c$	33585 ± 70	–	–
$t\bar{t}+\geq 0$ light	106290 ± 120	–	–
e/μ_{Fakes}	8028 ± 80	–	–
$t\bar{t}H$	1676.9 ± 1.5	126.6 ± 1.2	74.62 ± 0.25
$t\bar{t}W$	362.0 ± 1.6	798.0 ± 2.1	205.7 ± 1.1
$t\bar{t}Z$	891.0 ± 6	165.3 ± 1.0	567.8 ± 1.7
tZq	170.5 ± 1.3	88.9 ± 0.5	273 ± 0.9
tWZ	2.22 ± 0.22	18.73 ± 0.08	80.47 ± 0.16
Z/W+jets	4681 ± 34	518 ± 30	131 ± 25
VV, VVV	292 ± 6	298.6 ± 3.3	579 ± 4
Single-top	9331 ± 31	164 ± 4	20.1 ± 1.5
$t\bar{t}t$, $t\bar{t}t\bar{t}$	8.9 ± 0.1	4.81 ± 0.06	4.88 ± 0.06
VH, VBFH, ggH	25.0 ± 0.1	19 ± 4	7.4 ± 2.8
Total	225640 ± 190	3650 ± 33	2274 ± 26

Table 3. Preselection region yields as predicted by the MC simulation. The uncertainty is statistical only and the PDG rounding is applied. The $t\bar{t}$ background is split into $t\bar{t}+\geq 1b$, $t\bar{t}+\geq 1c$ and $t\bar{t}+\geq 0$ light categories for the $H \to b\bar{b}$ channel only; therefore the $t\bar{t}$ contribution for this channel is absent. Moreover, for the $H \to b\bar{b}$ channel only the data-driven estimate of the non-prompt and fake leptons background is given due to lack of a MC-based estimate.

In the $H \to b\bar{b}$ channel, the preselected events are used to train a five-dimensional BDTG including the categories tHq, $t\bar{t}+\geq 1b$, $t\bar{t}+\geq 1c$, $t\bar{t}+\geq 0$ light and others. The "others" category includes all the remaining backgrounds. A Deep Neural Network (DNN) is also tested to validate the results obtained with the BDTG. Since the BDTG shows slightly better performance, it is chosen for the final results.

In total, 25 variables were used in the training, such as the number of jets, the lepton charge and flavour information, invariant mass and angular separation of various reconstructed jets, the minimum χ^2 values from reconstructing the W-bosons and top-quark masses from their decay products under the $t\bar{t}+\geq 0$ light or $t\bar{t}+\geq 1b$ hypotheses, as well as the pseudo-continuous b-tagging discriminant of selected jets (see table 6). These variables are motivated by the expected kinematic properties of the signal. The tHq topology features a forward spectator jet from the scattered incoming light-flavour quark, a hadronically decaying top quark, and a different multiplicity of b-jets compared to the dominant $t\bar{t}$ background. The most important variables entering the BDTG reflect these features: the number of jets associated with the reconstructed hadronic top quark from different $t\bar{t}$ reconstruction techniques provides strong separation from the $t\bar{t}$ background; the lepton charge helps distinguish tHq events, as the incoming light-flavour quark is dominantly a u-quark from one of the colliding protons, leading mostly to positively charged top quarks (and hence positive leptons), from charge-

JHEP10(2025)093

Channel	Region	BDT score	Conversion cut	Jets	Leptons flavour (p_{T} ordered)	Other
$H \to b\bar{b}$	SR	—	—	$N^{70}_{\text{not-}b} < 2$ $N^{\text{jet}}_{\text{forward}} \geq 1$	—	—
	CR($t\bar{t}+ \geq 1b$)	—	—	$N^{70}_{\text{not-}b} \geq 2$ $N^{\text{jet}}_{\text{forward}} = 0$	—	
2ℓ SS	SR	BDT(tHq) > 0.65 BDT($t\bar{t}$) < 0.5 BDT($t\bar{t}W$) < 0.6 and BDT(VV) < 0.8	yes	—	—	—
	CR(μ_{HF})	BDT(tHq) < 0.65 BDT($t\bar{t}$) > 0.3 BDT($t\bar{t}W$) < 0.6 and BDT(VV) < 0.9	yes	—	$\mu\ \mu$	—
	CR(e_{HF})	BDT(tHq) < 0.65 BDT($t\bar{t}$) > 0.3 BDT($t\bar{t}W$) < 0.6 and BDT(VV) < 0.9	yes	—	$\mu\ e$, $e\ e$	$H_{\mathrm{T}}(\ell) < 225$ GeV
	CR(e_{conv})	BDT($t\bar{t}$) > 0.3	inverted	—	$\mu\ e$, $e\ e$	m($\ell\ell$) < 150 GeV
	CR($t\bar{t}W$)	BDT($t\bar{t}W$) > 0.6 BDT($t\bar{t}$) < 0.3	yes	—	—	—
3ℓ	SR	BDT(tHq) > 0.7 BDT($t\bar{t}$) < 0.9 BDT($t\bar{t}W$) < 0.8	yes	—	—	—
	CR(μ_{HF})	BDT(tHq) < 0.7 BDT($t\bar{t}$) > 0.5 BDT($t\bar{t}W$) < 0.8	yes	—	$\mu\ \mu\ \mu$, $e\ \mu\ \mu$, $\mu\ e\ \mu$, $e\ e\ \mu$	—
	CR(e_{HF})	BDT(tHq) < 0.7 $BDT(t\bar{t}) > 0.5$ $BDT(t\bar{t}W) < 0.8$	yes	—	$\mu\ \mu\ e$, $e\ \mu\ e$ $\mu\ e\ e$, $e\ e\ e$	—
	CR(e_{conv})	—	inverted	—	$\mu\ \mu\ e$, $e\ \mu\ e$, $\mu\ e\ e$, $e\ e\ e$	—
	CR($t\bar{t}W$)	BDT($t\bar{t}W$) > 0.8	yes	—	—	—

Table 4. Regions selection requirements for $H \to b\bar{b}$, 2ℓ SS and 3ℓ channels. The regions are defined using a mixture of requirements on the BDTGs outputs, the flavour of the leptons, the number of jets and b-tagged jets, the sum of the transverse momentum of the leptons H_{T} (ℓ), the leptons invariant masses ($m(\ell\ell)$) and the conversion criteria.

symmetric backgrounds such as $t\bar{t}$, $t\bar{t}W$, $t\bar{t}Z$ or $t\bar{t}H$; the p_{T} of the highest-p_{T} forward jet is characteristic of the spectator jet in tHq production; and the event sphericity encodes the more isotropic topology of $t\bar{t}$ events compared to the typically more forward-backward structure of tHq events [118]. The complete lists of input variables can be found in section A. Variable importance is evaluated using the "gain" metric provided by the `XGBoost` algorithm, which reflects the relative improvement in model accuracy due to each variable.

The preselection phase-space is then split into two regions, defined by rectangular requirements on the number of forward jets ($N^{\text{jet}}_{\text{forward}}$) and the number of central jets failing to meet the `DL1r` tagger 70% working-point requirement ($N^{70}_{\text{not-}b}$). In the $H \to b\bar{b}$ channel, a jet is classified as forward if its pseudorapodity is $2.5 < |\eta| < 4.5$ or if its pseudorapodity is $2 < |\eta| < 2.5$ and it fails to meet the 70% b-tagging requirement. The two regions are enhanced in the tH contribution and $t\bar{t}+ \geq 1b$ and they are referred to as SR and CR($t\bar{t}+ \geq 1b$), respectively. The SR selection requires at least one forward jet and at most one central jet failing to meet the 70% b-tagging requirement, while for CR($t\bar{t}+ \geq 1b$) no forward jet should be present and at least two central jets must fail to meet the 70% b-tagging requirement. table 4 summarises the selections applied to define the SR and CR.

JHEP10(2025)093

6.2 2ℓ SS channel

The 2ℓ SS preselection region is defined by requiring exactly two *Tight* light leptons (electrons or muons) with the same electric charge. For the selected events, the leading lepton must have $p_{\mathrm{T}} > 27\,\mathrm{GeV}$ and the sub-leading lepton must have $p_{\mathrm{T}} > 20\,\mathrm{GeV}$.

The number of jets with $|\eta| < 4.5$ is required to be between one and six. The 70% working point of the `DL1r` tagger is used to select b-jets. The number of b-jets is required to be between one and three.

As shown in Table 3, the dominant source of background in the preselection region stems from $t\bar{t}$ followed by $t\bar{t}W$ and $Z+$jets production. Both $t\bar{t}$ and $Z+$jets enter the preselection region if a non-prompt or fake lepton is in the event or if the charge of one of the electrons is wrongly measured. The rest of the background processes consists of $t\bar{t}W$, $t\bar{t}Z$ or diboson production.

Four binary-classifier BDTGs are trained in the 2ℓ SS channel, each targeting the tHq signal or one of the main background processes ($t\bar{t}$, $t\bar{t}W$, and diboson) against the sum of the remaining three classes. These classifiers are used to define mutually exclusive enriched regions. In total, 52 variables were used in the training: 28, 19, 29 and 27 for the four BDTGs, respectively. These variables include kinematic and topological quantities that characterise the signal and its main backgrounds. The most important variables include the charge of the two leptons, H_{T},[7] the number of b-tagged jets, the invariant masses and angular separations of pairs of reconstructed jets and leptons (see table 6). The charge of the two leptons is highly discriminating, since the tHq process favours positively charged top quarks as explained before, while dominant backgrounds such as $t\bar{t}$, $t\bar{t}H$, and diboson production are charge-symmetric. Invariant masses of leptons and jets also provide discriminating power, as the decay kinematics and spatial correlations in the tHq topology produce characteristic patterns between leptons from top-quark decays and the forward spectator jet or b-jet. In contrast, in backgrounds such as $t\bar{t}$, $t\bar{t}H$, and dibosons, these correlations are absent or substantially altered due to additional heavy resonances or differing event topologies. The other variables further exploit differences in global event activity, jet and b-jet multiplicities, and the more isotropic topology of $t\bar{t}$, $t\bar{t}W$ and $t\bar{t}Z$ compared to the forward — backward structure of tHq events. The complete lists of input variables can be found in section A.

Five regions are defined in the 2ℓ SS channel: the SR is designed to maximise the tHq contribution, while the CRs target the main background processes. The regions are defined using a mixture of requirements on the BDTGs outputs, selecting a given flavour for the two leptons in the final state or cutting on event kinematic variables such as H_{T} or leptons invariant masses. The material- or internal-conversion cuts defined in section 5 are applied to all the electrons in all regions, except for the conversion control region, $\mathrm{CR}(e_{\mathrm{conv}})$, where this requirement is inverted. The regions described here are orthogonal to one another. table 4 summarises the selections applied to define the SR and CRs. Three CRs are defined to derive mis-identified leptons background: $\mathrm{CR}(\mu_{\mathrm{HF}})$, $\mathrm{CR}(e_{\mathrm{HF}})$ and $\mathrm{CR}(e_{\mathrm{conv}})$. The $\mathrm{CR}(e_{\mathrm{conv}})$ is enriched in events with one electron stemming from γ-conversion (e_{conv}), while $\mathrm{CR}(\mu_{\mathrm{HF}})$

[7]The H_{T} variable is defined performing the scalar sum of the transverse momentum of all the reconstructed objects in the final state, in this case jets and leptons. The $H_{\mathrm{T}}(\ell)$ variable instead is computed including only leptons.

and CR(e_{HF}) are enriched in contributions from non-prompt electrons or muons stemming from heavy-flavoured (containing a b- or c-quark) hadron decay, e_{HF} and μ_{HF}, respectively. One CR is defined to target the irreducible $t\bar{t}W$ background.

6.3 3ℓ channel

The 3ℓ preselection region is defined by requiring the presence of exactly three *Tight* light leptons (electrons or muons). The sum of the leptons' charges is required to be ± 1. The light leptons are ordered based on their p_{T}, with the leading lepton having $p_{\mathrm{T}} > 27\,\mathrm{GeV}$, the sub-leading lepton required to have $p_{\mathrm{T}} > 20\,\mathrm{GeV}$ and the softest lepton to have $p_{\mathrm{T}} > 10\,\mathrm{GeV}$. The number of jets with $|\eta| < 4.5$ is required to be between one and six. The 70% working point of the `DL1r` tagger is used to select b-jets. The number of b-jets is required to be between one and three. As shown in Table 3, the dominant background contributions in the preselection region arise from diboson, $t\bar{t}Z$, and $t\bar{t}$ processes.

Three binary-classifier BDTGs are trained in the 3ℓ channel, each targeting the tHq signal or one of the main background processes ($t\bar{t}$ and $t\bar{t}W$) against the sum of the remaining two classes. These classifiers are used to define regions enriched in tHq and in each of the background processes included in the training. A total of 50 input variables are used in the training: 22, 19, and 30 for each of the three classifiers, respectively. These variables include kinematic and topological quantities that characterise the signal and its main backgrounds. The most important ones include the invariant masses of leptons, the p_{T} of leptons, the sum of leptons' charges, and the multiplicity of central and b-tagged jets. The dilepton invariant masses are powerful discriminants, since in backgrounds such as $t\bar{t}Z$ and diboson production leptons often originate from on-shell Z bosons, producing peaks around the Z-boson mass, while in tHq events they mainly arise from W-boson decays and do not show such resonant structures (see table 6). The sum of leptons' charges is also discriminant similarly to the other two channels. The lepton transverse momenta provide additional separation, as backgrounds with extra vector bosons typically yield harder leptons than those expected in tHq events. Finally, the number of b-tagged jets provides discrimination, as tHq process typically features fewer central and b-jets than backgrounds such as $t\bar{t}$, $t\bar{t}H$, $t\bar{t}W$, and $t\bar{t}Z$. The complete lists of input variables can be found in section A.

Five orthogonal regions are defined in the 3ℓ channel: one SR to maximise the tHq contribution, three CRs to estimate in data the mis-identified leptons background and one CR to estimate the $t\bar{t}W$ background. The regions are defined using a mixture of requirements on the BDTGs outputs, the number of jets and invariant masses. The material- and internal-conversion requirements defined in section 5 are applied to all the electrons in all regions, except for one region where this requirement is inverted to enhance the contribution of the process targeted by that region. Table 4 summarises the selection criteria applied to define the SR and CRs.

7 Background estimation

The background processes satisfying the SR and CR selections are categorised into irreducible and reducible backgrounds. Irreducible backgrounds arise from processes that have an identical number of prompt leptons from weak boson or leptonic τ-lepton decays, and a

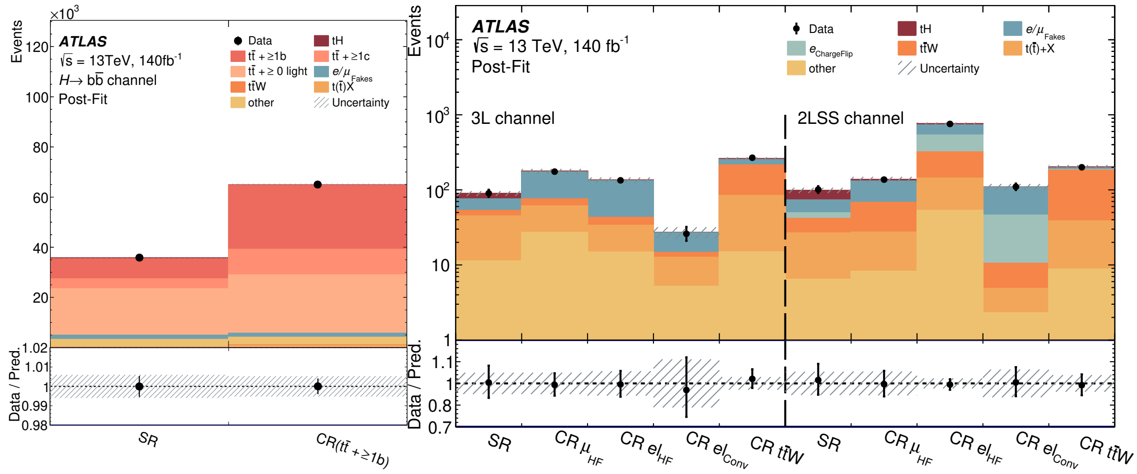

(a) (b)

Figure 2. The data and estimated signal-plus-background yields in the SR and CRs of the (a) $H \to b\bar{b}$ channel and (b) 3ℓ and 2ℓ SS channels. The term e/μ_{Fakes} refers to backgrounds from non-prompt or misidentified leptons, namely contributions from heavy-flavour decays and photon conversions. Both signal and background events are estimated with a likelihood fit to data ("Post-Fit"), as described in sections 7 and 9. The uncertainty band includes statistical and systematic contributions.

similar number of b-jets as the targeted signal. Reducible backgrounds arise instead from particle mis-identification in the detector, mis-assigning of the lepton charge or mis-tagging a charm or light-flavoured jet as a b-jet. Fake and non-prompt leptons can originate from different sources like decays of bottom or charm mesons, photon conversions or light jets creating accidentally a detector signature similar to a light lepton.

The contribution of irreducible backgrounds is generally derived through the respective simulated samples and constrained in CRs where needed. A data-driven estimate is provided for most of the reducible backgrounds and for background processes where the MC prediction is not in good agreement with the data. Figure 2 compares the total data yields in all SRs and CRs as defined in section 6 for the three analysis channels to the signal plus background predictions obtained by the likelihood fit to data described in section 7 and section 9.

7.1 Background estimation in the $H \to b\bar{b}$ channel

As already discussed in section 6.1, the main source of background in the $H \to b\bar{b}$ channel consists of $t\bar{t}$ +jets events. The production of the $t\bar{t}$ in association with heavy flavour jets is known to be not well modelled by the simulation. For this reason, simulated $t\bar{t}$ +jets events are split into $t\bar{t}+\geq 1b$, $t\bar{t}+\geq 1c$ and $t\bar{t}+\geq 0$ light categories and the CR($t\bar{t}+\geq 1b$) is included in the fit to constrain its contribution from data. The normalisation factor of the $t\bar{t}+\geq 1b$ background found in the combined fit to data is $k(t\bar{t}+\geq 1b) = 1.24^{+0.17}_{-0.15}$. The $t\bar{t}+\geq 1c$ predicted yield has no dedicated correction factor due to the difficulty in building a pure CR. Instead, an overall uncertainty on the $t\bar{t}+\geq 1c$ prediction is included in the fit as described in section 8.2. The remaining irreducible backgrounds are all estimated by using the MC predictions. The small contribution of reducible background from non-prompt and fake leptons is estimated using the matrix-method technique described in ref. [119].

7.2 Background estimation in the 2ℓ SS and 3ℓ channels

In the 2ℓ SS channel, the main irreducible backgrounds originate from $t\bar{t}W$ production, having final states and kinematic properties inherently similar to the tHq signal. Smaller contributions originate from the following rare processes: tZq, $t\bar{t}H$ and tWZ production. Backgrounds with prompt leptons are directly estimated from simulation using the samples described in section 4, except for $t\bar{t}W$, for which the normalisation is fitted. In the 3ℓ channel instead, the main irreducible backgrounds originate from diboson production, $t\bar{t}Z$ and tZq. Other minor irreducible backgrounds are triboson, other Higgs-boson production modes such as ggH, VBF (qqH) and VH, and $t\bar{t}t$ and $t\bar{t}t\bar{t}$. A CR dedicated to the $t\bar{t}W$ background, CR($t\bar{t}W$), is defined in both the 2ℓ and 3ℓ channel to better constrain its contribution from data. The normalisation factor associated with the $t\bar{t}W$ background as estimated from the combined fit is found to be $k(t\bar{t}W) = 1.09 \pm 0.11$.

The most important sources of reducible background in both the 2ℓ SS and 3ℓ channels are the $t\bar{t}$, W/Z+jets and single-top-quark processes. These processes can satisfy the preselection requirement due to the presence of a fake or non-prompt lepton in the final state. These backgrounds are estimated from simulation, with the normalisation determined by the likelihood fit through the use of the dedicated CRs introduced earlier. The non-prompt leptons in the simulated event samples are labelled according to whether they originate from heavy-flavour or light-flavour hadron decays, or from a material/internal conversion. The light-flavour category is negligible. In the 2ℓ SS channel, normalisation factors are extracted to be $k(e_{\mathrm{conv}})_{2\ell\,\mathrm{SS}} = 1.20\pm0.47$, $k(e_{\mathrm{HF}})_{2\ell\,\mathrm{SS}} = 0.55\pm0.65$ and $k(\mu_{\mathrm{HF}})_{2\ell\,\mathrm{SS}} = 0.80\pm0.32$. In the 3ℓ channel, the normalisation factors extracted are $k(e_{\mathrm{conv}})_{3\ell} = 0.82\pm0.59$, $k(e_{\mathrm{HF}})_{3\ell} = 1.47\pm0.42$ and $k(\mu_{\mathrm{HF}})_{3\ell} = 0.91 \pm 0.24$.

Electrons with mis-identified electric charge ("charge-flip"), with one electron either undergoing hard bremsstrahlung followed by an asymmetric conversion ($e^\pm \to e^\pm\gamma^* \to e^\pm e^+ e^-$) or having mismeasured track curvature, represent another source of reducible background. This contribution is negligible in the 3ℓ channel and sizeable in the 2ℓ SS channel. The muon charge misassignment rate is negligible in the p_{T} range relevant to this analysis. The electron charge misassignment rate is measured in data by using samples of $Z \to e^+e^-$ events reconstructed as either same-charge pairs or opposite-charge pairs, with the non-Z background subtracted via a sideband method utilising events outside the Z-boson mass window. The charge misassignment rate is extracted from the ratio of the numbers of same-charge and opposite-charge events close to the Z-boson mass through a likelihood approach taking into account the possibility that both electron charges are misassigned. The rates are parameterised as a function of electron p_{T} and $|\eta|$, and vary from about 10^{-5} for low-p_{T} electrons ($17 \leq p_{\mathrm{T}} \leq 50\,\mathrm{GeV}$) with $|\eta| \leq 1.37$, to about 4×10^{-3} for high-p_{T} electrons ($p_{\mathrm{T}} \geq 100\,\mathrm{GeV}$) with $2 \leq |\eta| \leq 2.47$. To estimate the charge-flip background in each 2ℓ SS region, the measured charge misassignment rate is applied to data events satisfying the requirements of the region, except that the two leptons must have opposite charges.

8 Sources of systematic uncertainty

Different sources of systematic uncertainty are considered for this measurement. They are grouped into three categories: instrumental uncertainties that affect physics object reconstruction; modelling uncertainties relevant for MC simulation-based estimations; and uncertainties affecting the estimate of fake and non-prompt lepton backgrounds. All uncertainties include both shape and normalisation effect, unless otherwise stated in their description.

The description of the sources of systematic uncertainties is organised as follows: first, those common to all three channels are presented, followed by sections addressing uncertainties specific to the $H \to b\bar{b}$ channel and the 2ℓSS and 3ℓ channels.

8.1 Common systematic uncertainties

Instrumental systematic uncertainties considered are related to: trigger efficiency; lepton reconstruction, identification and isolation efficiencies; lepton calibration; jet calibration; JVT and fJVT efficiencies; b-tagging efficiency; $E_{\mathrm{T}}^{\mathrm{miss}}$ calibration. The experimental systematic uncertainties are applied either as an event-reweighting correction factor or as a rescaling or smearing of the object energy and momentum for scale and resolution uncertainties.

Uncertainties associated with the lepton selection arise from the trigger, reconstruction, identification and isolation efficiencies, and the lepton momentum scale and resolution as described in refs. [98–100]. Uncertainties on the efficiency of the BDT designed to reject non-prompt leptons are estimated through a $Z \to \ell\ell$ tag-and-probe method and cover contributions related to the $Z(\to \ell\ell)$+jets MC modelling, the template cut/shape, the $m_{\ell\ell}$ window, the tag-and-probe lepton selections, the multijet background, the non-prompt lepton background, the luminosity, the cross-sections of the considered processes, and the limited number of events in simulation and data.

Uncertainties associated with jet reconstruction and calibration arise from the jet energy scale (JES), jet energy resolution (JER) and the JVT/fJVT requirements. The JES uncertainty accounts for contributions from composition of jet flavour, η-intercalibration, punch-through, single-particle response, calorimeter response and pile-up making up for a total of 31 independent variations [106]. The JER is measured separately for data and MC using an in-situ technique and the associated uncertainties are split into 13 components [106]. The JVT efficiency is measured in data and correction factors are applied to simulated events to correct the simulated performance. The uncertainty associated with the JVT performance is obtained by varying the correction factors [107].

The uncertainty in $E_{\mathrm{T}}^{\mathrm{miss}}$ results from the propagation of the uncertainties in the energy scales and resolutions of photons, leptons and jets, and from the modelling of its soft term [120].

The efficiency of the b-tagging algorithm is measured for each jet flavour using control samples in data and in simulation. From these measurements, correction factors are derived to correct the tagging rates in the simulation. For b-jets, the correction factors and their uncertainties are estimated from data using dileptonic $t\bar{t}$ events [110, 121]. For c-jets, they are derived from jets arising from W boson decays in $t\bar{t}$ events [122]. For light-flavour jets, the correction factors are derived from $Z+$jets events [123]. Uncertainties from sources affecting the b-tagging efficiencies of b-jets, c-jets and light-jets are evaluated as a function of jet p_{T}, including bin-to-bin correlations.

The uncertainty in the reweighting of the MC pile-up distribution to match the distribution in data is evaluated by varying the reweighting factors and has a very small impact on either the combined or individual results. The uncertainty in the combined 2015–2018 integrated luminosity is 0.83% [124], obtained using the LUCID-2 detector for the primary luminosity measurements, complemented by measurements using the inner detector and calorimeters.

Systematic uncertainties in the tHq and tWH MC predictions due to missing higher-order QCD corrections in the modelling are estimated by doubling and halving the μ_{r} and μ_{f} scales chosen for the nominal sample. A systematic uncertainty due to the choice of the PS model is estimated as the relative difference between the Powheg +Pythia 8 and Powheg +Herwig 7 predictions and applied to the nominal predictions. An uncertainty is considered on the cross-section summing in quadrature the contributions from QCD scale, flavour scheme, PDF and α_s from a NLO QCD prediction: the values obtained are equal to 15.4% and 9.2% for tHq and tWH, respectively [52, 53].

The uncertainty in the $t\bar{t}$ modelling due to the choice of the h_{damp} parameter, which controls the resummation of higher-order terms, is estimated by comparing the nominal prediction with a Powheg +Pythia 8 sample where the parameter is set to $3 \times m_{\mathrm{top}}$. Reweighted events are used to assess the impact of ISR simulation within the nominal Powheg +Pythia 8 simulation: μ_{f} and μ_{r} scales are varied by 0.5 (high radiation) or 2.0 (low radiation) together with the PS tune `Var3c` [51]. The μ_{r} and μ_{f} scales are varied in both the hard-scatter process and PS and they are modified independently. The hadronisation model uncertainty and other non-perturbative effects in the PS are evaluated by comparing the nominal sample with Powheg+Herwig 7.2.1. The PS scale uncertainty is evaluated using the `Var3c` eigentune variation of the A14 tune [125]. The impact of FSR is evaluated by varying the renormalisation scale for PS emissions by factors of 0.5 and 2.0, using reweighted events.

The uncertainty in $t\bar{t}H$ modelling due to the ISR is estimated by using weights in the ME calculation and the PS. The μ_{r} and μ_{f} scales are varied, and ISR α_{s} variations are evaluated similarly to the $t\bar{t}$ process. The impact of FSR is evaluated using PS weights that vary the renormalisation scale for QCD emission in the FSR by a factor of 0.5 and 2.0. Additionally, uncertainties in the ME (PS, hadronisation and underlying-event modelling) are estimated by comparing the nominal Powheg +Pythia 8 MC simulation with aMC@NLO +Pythia 8 (Powheg +Herwig 7). The predicted $t\bar{t}H$ cross-section uncertainty is $^{+5.8\%}_{-9.2\%}$(scale) + 3.6%(PDF+α_{s}) [52] and the two components are considered uncorrelated.

Systematic uncertainties in the $t\bar{t}W$ MC predictions due to missing higher-order QCD corrections in the modelling are considered. To estimate the uncertainty due to ambiguities in the ME and PS algorithm and parameter choices, the nominal Sherpa prediction is compared with the prediction of the MadGraph5_aMC@NLO +Pythia 8 FxFx sample described in section 4. In addition, a dedicated PS model uncertainty is estimated as the relative difference between the Powheg +Pythia 8 and Powheg +Herwig 7 predictions and applied to the nominal $t\bar{t}W$ prediction. Modelling uncertainties due to μ_{r} and μ_{f} scales [126], and the amounts of ISR/FSR are evaluated similarly to the $t\bar{t}$ and $t\bar{t}H$ processes. Uncertainties in the PDF modelling are included by varying the value of α_{s} and using different PDF sets.

The predicted $t\bar{t}W$ cross-section uncertainty is $^{+9.7\%}_{-10.8\%}$(scale) + 7.2%(PDF+α_s) [78] and the two components are considered uncorrelated. The uncertainty on the theoretical prediction of the $t\bar{t}W$ cross-section is dropped in the 3ℓ and 2ℓSS channels as the normalisation of this background is estimated from data.

Uncertainties due to missing higher orders in QCD are estimated for $t\bar{t}Z$ production by varying the nominal μ_r and μ_f scales are evaluated similarly to the $t\bar{t}$, $t\bar{t}H$ and $t\bar{t}W$ processes. Uncertainties in additional-jet modelling are estimated with ISR α_s variations taken from the A14 tune. To estimate the uncertainty due to ambiguities in the ME and PS algorithm and parameter choices, the nominal prediction is compared with Sherpa. PS, hadronisation and underlying-event modelling uncertainties are estimated by comparing the nominal aMC@NLO +Pythia 8 MC simulation with MadGraph5+Herwig 7. The predicted $t\bar{t}Z$ cross-section uncertainty is $^{+9.6\%}_{-11.3\%}$(scale) + 4%(PDF+α_s) [52].

Systematic uncertainties due to missing higher-order QCD corrections are also considered for the three single-top-quark processes: t-channel, tW and s-channel. The uncertainty due to the choice of the hadronisation model and the other non-perturbative aspects of the PS is evaluated comparing the nominal prediction with that provided by the Powheg+Herwig 7.1.6 simulation. An uncertainty is also attributed to the choice of the Powheg approach to perform the matching between the hard-scatter and the PS. This uncertainty is estimated comparing the nominal Powheg+Pythia 8 prediction with the aMC@NLO+Pythia 8 simulation for the tW process, and the Powheg+Herwig 7.1.6 with the aMC@NLO+Herwig 7.1.6 prediction for the t-channel and s-channel. An additional uncertainty is quoted for the tW process to estimate the difference between the DS and DR schemes. Finally, a conservative 5% uncertainty on the theoretical cross-section of single-top-quark processes (t-channel, tW and s-channel) is considered in the $H \to b\bar{b}$ channel. In the 3ℓ channel, a 5.4% uncertainty on the tW production cross-section [127] is considered. For the 2ℓSS channel, where single-top-quark contributions are negligible, no uncertainty from these processes is included.

Uncertainties in diboson modelling due to missing higher orders in QCD are estimated by varying the nominal μ_r and μ_f scales by factors of 0.5 and 2.0. In addition, a normalisation uncertainty of 24.5% is considered, as a result of adding in quadrature the theory uncertainty (5%) and 24% per additional jet, accordingly to the Berends-Giele scaling [128].

For minor backgrounds such as Z+jets, W+jets, tZq, tWZ, rare top-quark ($t\bar{t}t$ and $t\bar{t}t\bar{t}$) and other Higgs-boson production modes (ggH, VBF and VH) only the theoretical uncertainty on the predicted cross-section is considered. A normalisation uncertainty of 35% and 40% is considered for the Z+jets and W+jets processes in the $H \to b\bar{b}$ channel only. This is the result of adding in quadrature the theory uncertainty (4% for W+jets and 5% for Z+jets) and 24% per additional jet. In the 2ℓSS and 3ℓ channels, the normalisation of these processes is derived from data as part of the fake and non-prompt leptons estimate. The predicted tZq cross-section uncertainty is $^{+7.7\%}_{-7.9\%}$(scale) + 0.9%(PDF+α_s) [49] and the two components are considered uncorrelated. The contribution of the tWZ, rare top-quark and other Higgs-boson production processes is small in all the channels, for this reason a conservative 50% uncertainty on their cross-section is applied.

8.2 Channel-specific uncertainties: $H \to b\bar{b}$ channel

In the $H \to b\bar{b}$ channel, the effect of every modelling uncertainty associated to the $t\bar{t}$ simulation are considered independently for the three categories, $t\bar{t}+\geq 1b$, $t\bar{t}+\geq 1c$ and $t\bar{t}+\geq 0$ light. In the $t\bar{t}+\geq 1b$ case, since its yield is estimated from data, the normalisation of alternative samples is rescaled to match the nominal prediction in the preselection region. In addition to the $t\bar{t}$ modelling uncertainties common to all the channels, one from the NLO matching scheme in the $t\bar{t}$ simulated sample is also included comparing the nominal sample to the $p_{\mathrm{T}}^{\mathrm{hard}}$ varied one. A modelling uncertainty due to the differences between the nominal $t\bar{t}+\geq 1b$ simulation in the 5FS and an alternative $t\bar{t}+b\bar{b}$ simulation in the 4FS is considered [129]. The uncertainty is applied independently to three sub-components of the $t\bar{t}+\geq 1b$ background, defined according to the number of hadrons matched to the additional jet produced in association with the top-quark pair. The three sub-components are:

- $t\bar{t}$ $+1b$, if one additional jet in the event is matched to a single b-hadron,
- $t\bar{t}$ $+1B$, if one additional jet in the event is matched to a gluon splitting $g \to b\bar{b}$,
- $t\bar{t}$ $+2b$, if two additional jets in the event are matched to a single b-hadron each.

A 50% uncertainty on the normalisation of the $t\bar{t}+\geq 1c$ is also considered in the fit model [130]. Finally, a theoretical uncertainty of 6% is applied on the $t\bar{t}+\geq 0$ light normalisation as estimated in a dedicated validation region.

A systematic uncertainty is included to account for the difference between lepton fake rates originating from heavy-flavour decays versus those from misidentified jets. This uncertainty is evaluated separately for muons and electrons and its normalisation component contributes approximately 10% for muons and 30% for electrons.

8.3 Channel-specific uncertainties: 2ℓ SS and 3ℓ channels

For both the 2ℓ SS and 3ℓ channels, all the common $t\bar{t}$ modelling uncertainties are considered, as the $t\bar{t}$ simulation is used to estimate non-prompt lepton backgrounds originating from heavy-flavour decays and conversions. The modelling uncertainties associated to $t\bar{t}$ simulation are considered correlated among the various non-prompt leptons categories and between the 2ℓ SS and 3ℓ channels. Their effect is shape only as the normalisation of these backgrounds is estimated from data. In addition to the $t\bar{t}$ modelling uncertainties common to all the channels, one from the NLO matching scheme in the $t\bar{t}$ simulated sample is also included comparing predictions from Powheg+Herwig 7.1.3 and MadGraph5_aMC@NLO+Herwig 7.1.3 simulations. A conservative uncertainty of 50% is assigned to a small fraction of events, roughly 3% in the preselection region, where the origin of the non-prompt lepton could not be identified.

In the 2ℓ SS channel a systematic uncertainty of 10%–60% is assigned to the estimation of background from electrons with misidentified charge as described in section 7.2.

9 Results

A maximum-likelihood fit to all bins in the three SRs and the nine CRs (see table 4) is performed to simultaneously determine the background and the tH signal yields in the data.

The discriminant variable used in the SRs is defined as follows: for the $H \to b\bar{b}$ channel, it is the BDTG response for tHq signal-like events, $\mathrm{P}(tHq)$; for the 2ℓ SS and 3ℓ channels, it is given by the output of the BDTG trained to target tHq events, $\mathrm{BDT}(tHq)$. In the $\mathrm{CR}(t\bar{t}+\geq 1b)$, the discriminant is the BDTG response for $t\bar{t}+\geq 1b$-like events, $\mathrm{P}(t\bar{t}+\geq 1b)$. The H_{T} variable is used in all the CRs of the 2ℓ SS channel and in the 3ℓ channel control region targeting the $t\bar{t}W$ process. Finally, the $\Delta R(\ell_C, \ell_A + \ell_B)$ variable[8] is used in the $\mathrm{CR}(\mu_{\mathrm{HF}})$ and $\mathrm{CR}(e_{\mathrm{HF}})$ of the 3ℓ channel while the BDTG response of the binary classifier targetting $t\bar{t}$ is used in the $\mathrm{CR}(e_{\mathrm{conv}})$.

The likelihood function $\mathcal{L}(\mu, \vec{k}, \vec{\theta})$ is constructed as a product of Poisson probability terms over all bins considered in the measurement, and depends on the following: the signal-strength parameter, μ, defined as a multiplicative factor applied to the predicted yield for the tHq and tWH signal processes; $\vec{k}$, the normalisation factors for several backgrounds; and $\vec{\theta}$, a set of nuisance parameters (NPs) encoding systematic uncertainties in the signal and background expectations [131]. Systematic uncertainties can impact the estimated signal and background rates, the migration of events between categories, and the shape of the fitted distributions; they are summarised in section 8. Both μ and $\vec{k}$ are treated as free parameters in the likelihood fit. The NPs $\vec{\theta}$ allow variations of the expectations for signal and background according to the systematic uncertainties, subject to Gaussian constraints in the likelihood fit. Their fitted values represent the deviations from the nominal expectations that are needed to provide the best fit to the data. Statistical uncertainties in each bin due to the limited size of the simulated event samples are taken into account with dedicated parameters, using the Beeston-Barlow "lite" technique [132]. All systematic uncertainties are fully correlated across channels, except for those that are specific to a given channel.

The best-fit value of the tHq and tWH signal strength, μ_{tH}, is:

$$\mu_{tH} \;=\; 8.1 \;\pm\; 2.6 \;\;(\mathrm{stat.}) \;\pm\; 2.0 \;\;(\mathrm{syst.})\,.$$

This value corresponds to a measured value of the cross-section of $\sigma(tH) = 720 \pm 270\,\mathrm{fb}$. Figure 3(a) shows the signal strength measured in the different channels together with their combined value.

The compatibility of the signal strength evaluated from the different channels and the combined value is assessed by performing a likelihood ratio test and a p-value of 91% is obtained. The significance of the observed (expected) signal above the background-only expectation is 2.8 (0.4) standard deviations. The significance of the observed signal compared with the signal-plus-background hypothesis is instead 2.4. In the absence of a significant deviation from the background-only hypothesis, a 95% CL upper limit on the signal strength is set at 13.9 (6.1) times the observed (expected) SM prediction, as shown in figure 3(b). To quantify how well the fit model describes the data, a goodness-of-fit test is performed. The test consists of comparing the nominal model to a so-called saturated model [133], one constructed with enough degrees of freedom to describe the data perfectly. The probability obtained for the goodness-of-fit test is 98%, confirming excellent fit quality.

[8] Among the three leptons in the event in the 3ℓ channel, the lepton with the highest p_{T} is called ℓ_A, the one with the second highest p_{T} is called ℓ_B while the lepton with the softest p_{T} is called ℓ_C. The variable $\Delta R(\ell_C, \ell_A + \ell_B)$ is defined computing the ΔR value of the ℓ_C lepton with the system composed by summing the four vectors of leptons ℓ_A and ℓ_B.

JHEP10(2025)093

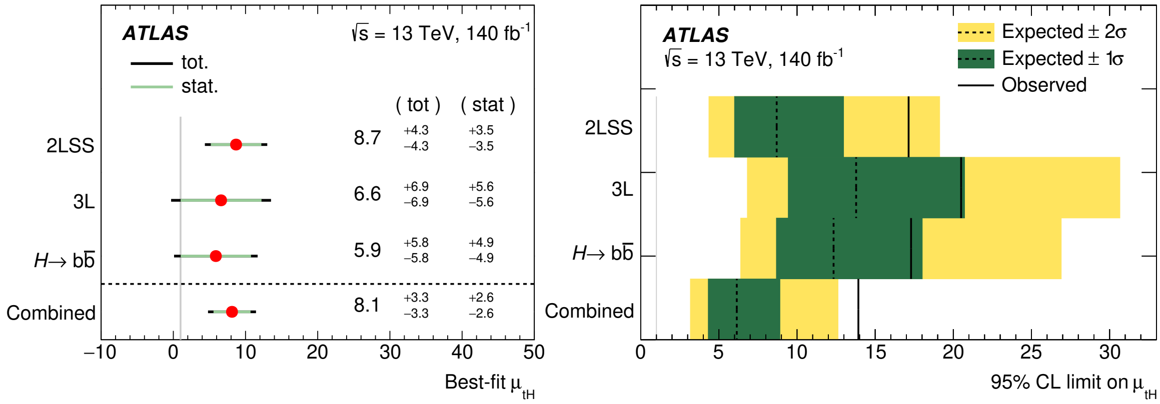

Figure 3. The (a) fitted values of the μ_{tH} and (b) 95% CL upper limits in the individual channels and in the combined measurement. The values reported for the individual channels are obtained by fitting μ_{tH} separately for each channel, whereas the combined measurement is derived by simultaneously fitting all channels together. The observed limits are shown (solid black lines), together with the expected limits under the SM hypothesis (dotted black lines). A grey line is added in correspondence of the μ_{tH} equal to one. In the case of the expected limits, the one- and two-standard-deviation uncertainty bands are also shown.

The contributions from the different sources of uncertainty affecting the measured μ_{tH} are evaluated using the covariance-matrix decomposition method [134] and are shown, grouped by category, in table 5. The leading source of uncertainty is the statistical uncertainty. The largest source of systematic uncertainty is the theoretical uncertainty with the biggest contribution coming from the uncertainty on the signal prediction and $t\bar{t}$. Among the experimental uncertainties, the leading contribution stems from the JES and JER.

The impact of the top 20 NPs in the fit on μ_{tH} is shown in figure 4 for the SM scenario and it is assessed as follows: if the uncertainty on the parameter is σ_k, the uncertainty on μ_{tH} is σ_μ, and the correlation between the parameter and μ_{tH} is $\rho_{k,\mu}$, the impact is computed as $\sigma_k \rho_{k,\mu} \sigma_\mu$. The plot shows the measured NPs and their agreement with the expected values. The most constrained NP corresponds to the PS uncertainty in the $t\bar{t}+\geq 0$ light category. All pulls are below one standard deviation with the strongest pull stemming from the PS uncertainty on the $t\bar{t}+\geq 1b$ category, suggesting a mild mis-modelling of this contribution in the $H \to b\bar{b}$ channel. Overall, the lack of significant pulls or constraints in the NPs indicates a good agreement between data and the fit model, supporting the robustness of the fit and the reliability of the extracted signal strength.

The observed and expected yields in the three SRs and the nine CRs after the combined likelihood fit under the signal-plus-background hypothesis are compared with data in figures 5 and 6. Detailed tables showing pre-fit and post-fit yields for all regions are reported in section B. A good agreement between data and prediction is found in all the regions.

Additional measurements are performed using the ITC hypothesis ($\kappa_t = -1$) as signal model. The best-fit value of the tH signal strength under the ITC hypothesis is:

$$\mu_{tH}(\kappa_t = -1) \;=\; 1.2 \;\pm\; 0.4 \;\;(\text{stat.}) \;\pm\; 0.5 \;\;(\text{syst.})\,.$$

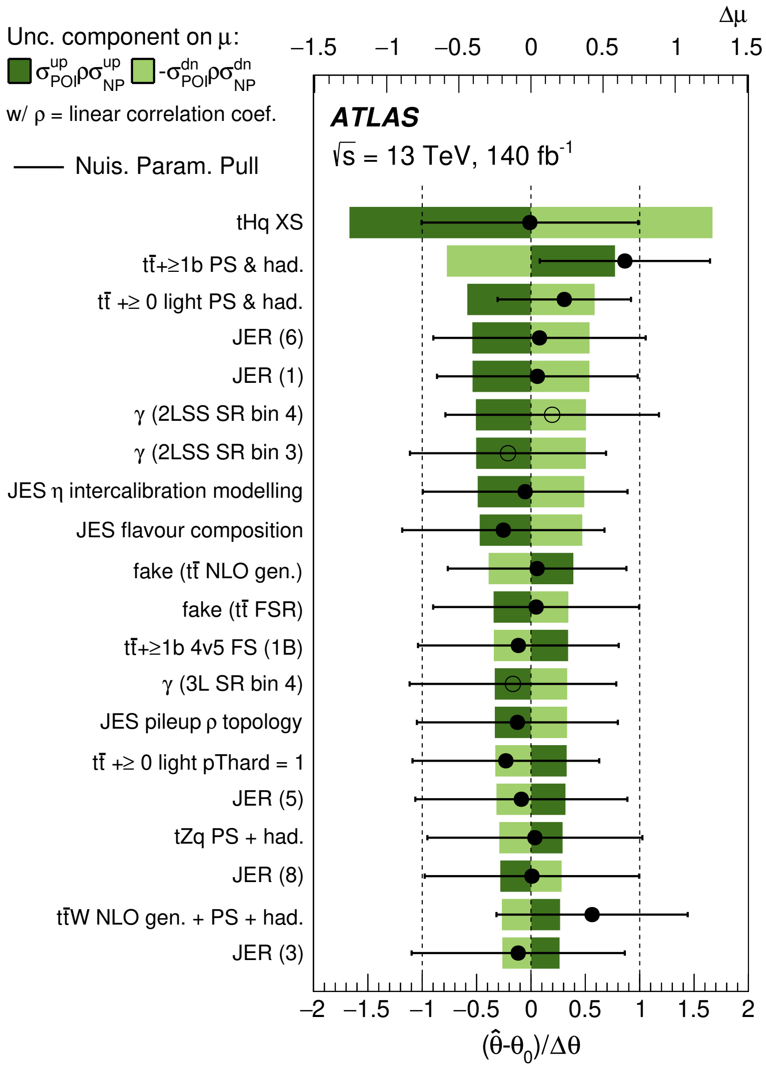

Figure 4. The impact of the top 20 most important systematic uncertainties on the fitted μ_{tH} in the SM scenario. The uncertainties are listed in decreasing order of their impact on μ_{tH}. The filled boxes show the relative impact on μ_{tH}, referring to the top x-axis. The points, referring to the bottom x-axis, show the deviations on the fitted NPs $\boldsymbol{\theta}_0$ from their nominal values, expressed in terms of standard deviations with respect to their nominal uncertainties. The associated black uncertainty bars show the fitted uncertainties of the NPs, relative to their nominal uncertainties. Filled markers refer to systematic uncertainties, while empty black markers refer to statistical uncertainties in the MC simulation in a given bin of an analysis region and they are labelled as γ. The results shown are extracted from the fit including all channels.

Source	Impact on μ_{tH}			
	Combination	$H \to b\bar{b}$	2ℓ SS	3ℓ
Theory uncertainties (modelling)	1.69	2.97	1.64	2.63
Signal	1.26	0.88	1.33	1.22
$t\bar{t}+\geq 1b$	0.70	2.57	—	—
$t\bar{t}+\geq 0$ light and $t\bar{t}+\geq 1c$	0.54	1.04	—	—
$t\bar{t}W$	0.23	<0.01	0.52	0.18
$t\bar{t}$	0.43	—	0.52	1.95
Rest of backgrounds	0.50	0.60	0.63	1.23
Experimental uncertainties	1.07	0.95	1.61	2.61
JES and JER	1.00	0.51	1.57	2.51
Non-prompt lepton bkg. modelling	0.25	0.59	0.22	0.07
Flavour tagging	0.17	0.52	0.13	0.17
Muons	0.12	< 0.01	0.12	0.40
$E_{\mathrm{T}}^{\mathrm{miss}}$	0.10	0.04	0.20	0.03
Pile-up	0.12	0.04	0.05	0.44
Electrons	0.10	0.07	0.11	0.32
Charge mis-identification	0.07	—	0.06	—
JVT and fJVT	0.04	0.10	0.11	0.06
Luminosity	0.09	0.09	0.10	0.14
Total systematic uncertainty	2.01	3.11	2.30	4.06
Statistical uncertainty	2.56	4.87	3.5	5.60
Normalisation factors	0.50	0.04	0.84	0.73
MC statistics	0.64	< 0.01	1.05	1.67
Total	3.3	5.8	4.3	6.9

Table 5. The absolute contribution of the main sources of uncertainty on the signal strength μ_{tH}. Some NPs with small impacts are grouped into categories, with the impact of the category being the quadrature sum of individual parameter impacts. Indentation is used to denote subcategories.

The observed and expected yields in the three SRs after the combined likelihood fit under the signal-plus-background hypothesis are compared with data in figure 7 for the ITC hypothesis.

The measured inverted-coupling signal strengths in the individual channels and the combined result are summarised in figure 8(a). The corresponding observed (expected) 95% CL exclusion limit is 2.4 (1.2), which is shown in figure 8(b) for both the individual channels and the combined measurement. The goodness-of-fit test probability for the $\kappa_t = -1$ scenario fit is 95%. In contrast to the SM case, under the ITC hypothesis the channel with the highest sensitivity is the $H \to b\bar{b}$ channel, overtaking the multi-lepton channels despite its modest signal-to-background ratio in the SM case (see section B). This inversion arises from the strong enhancement of the tHq cross-section together with the discriminating power of key variables in the $H \to b\bar{b}$ channel, such as the number of jets and number of jets associated with the reconstructed hadronic top quark from different $t\bar{t}$ reconstruction

JHEP10(2025)093

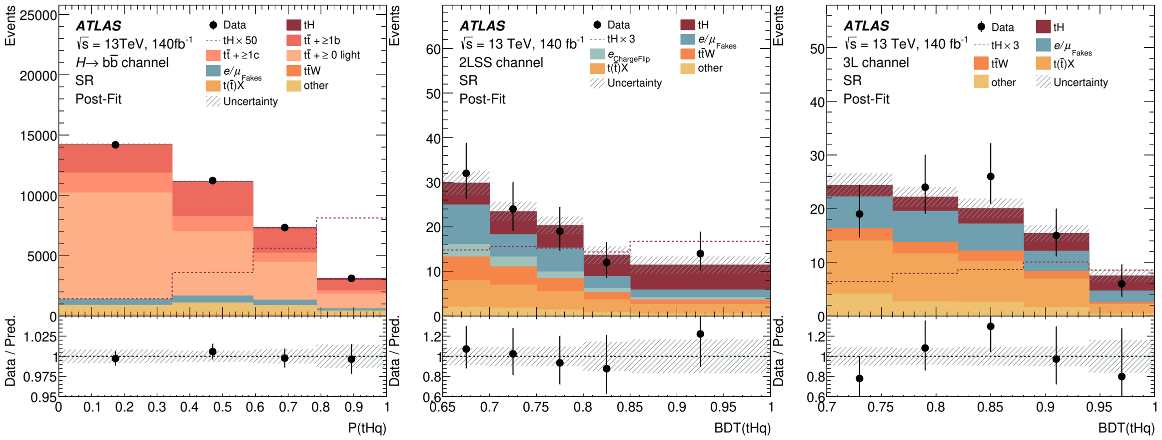

(a) (b) (c)

Figure 5. Comparison between data and the signal-plus-background prediction for the event yields in the (a) $H \to b\bar{b}$, (b) 2ℓ SS and (c) 3ℓ SRs. The term e/μ_{Fakes} refers to backgrounds from non-prompt or misidentified leptons, namely contributions from heavy-flavour decays and photon conversions. The SM signal and the background contributions after the likelihood fit to data ("Post-Fit") under the signal-plus-background hypothesis are shown as filled histograms. A dashed red line is added to the plot to show the signal contribution normalised to the measured value multiplied by 50 for the $H \to b\bar{b}$ channel and by 3 for the 2ℓ SS and 3ℓ channels. The ratio of the data to the total post-fit prediction ("Pred.") is shown in the lower panel. The combined statistical and systematic uncertainty in the prediction is indicated by the grey hatched band.

techniques. By contrast, variables used in training the BDT(tHq) classifiers in the 2ℓ SS and 3ℓ channels, such as invariant masses or angular distances of leptons, show a similar behaviour as the background under the $\kappa_t = -1$ hypothesis, leading to a loss of signal-to-background discrimination power. The uncertainty on the measured signal strength for the ITC hypothesis is dominated by systematic sources. In particular, the absolute uncertainty on $\mu_{tH}(\kappa_t = -1)$ from the theoretical uncertainty in the $t\bar{t}+ \geq 1b$ category is 0.25, the JES and JER together contribute 0.20, the uncertainty from the signal theoretical prediction is 0.18, and that from the modelling of $t\bar{t}$ in the 2ℓ SS and 3ℓ channels is 0.17.

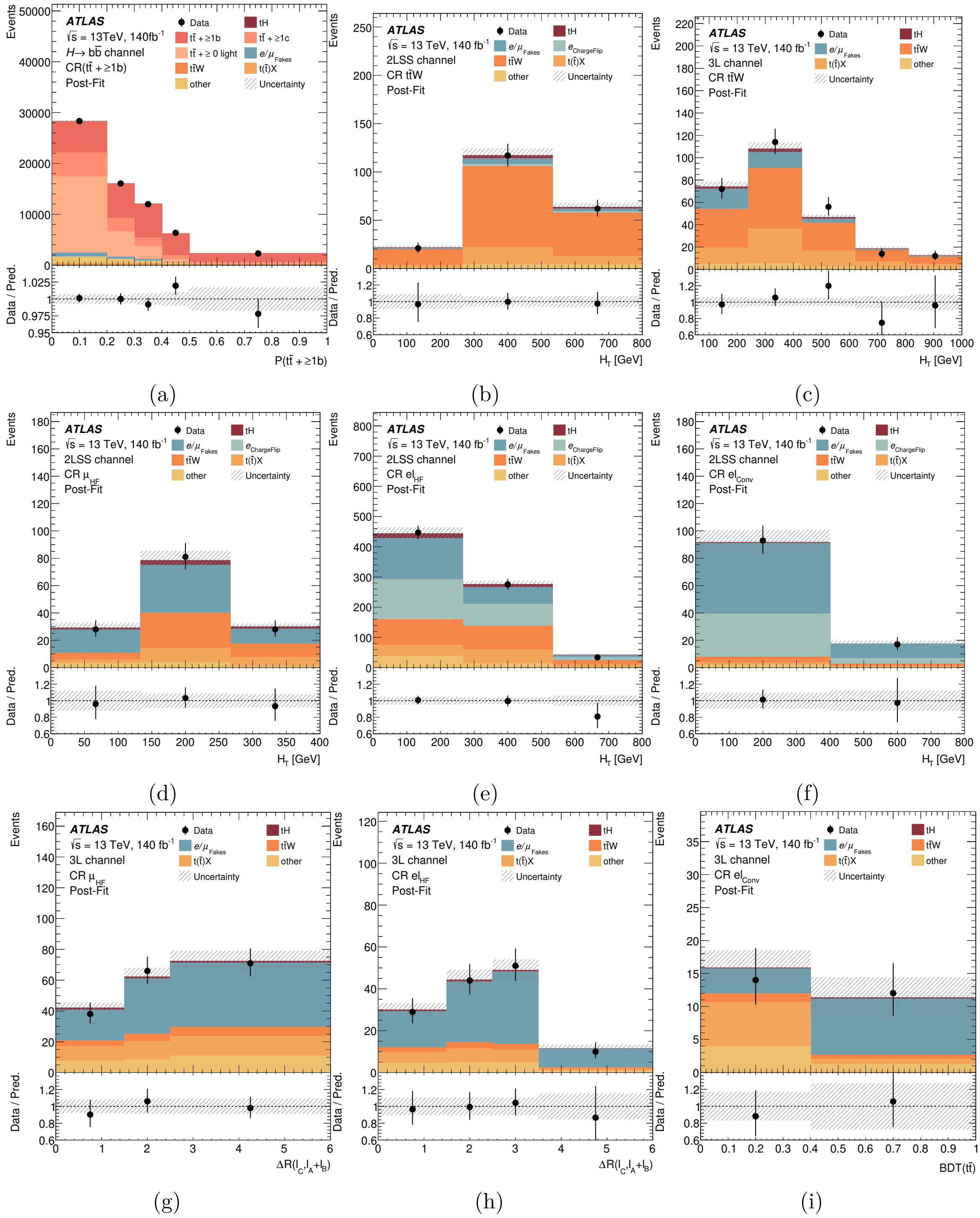

Figure 6. Comparison between data and the signal-plus-background prediction for the event yields in the nine CRs. The term e/μ_{Fakes} refers to backgrounds from non-prompt or misidentified leptons, namely contributions from heavy-flavour decays and photon conversions. The signal and background contributions after the likelihood fit to data ("Post-Fit") under the signal-plus-background hypothesis are shown as filled histograms. The ratio of the data to the total prediction ("Pred.") is shown in the lower panel. The combined statistical and systematic uncertainty in the prediction is indicated by the grey hatched band.

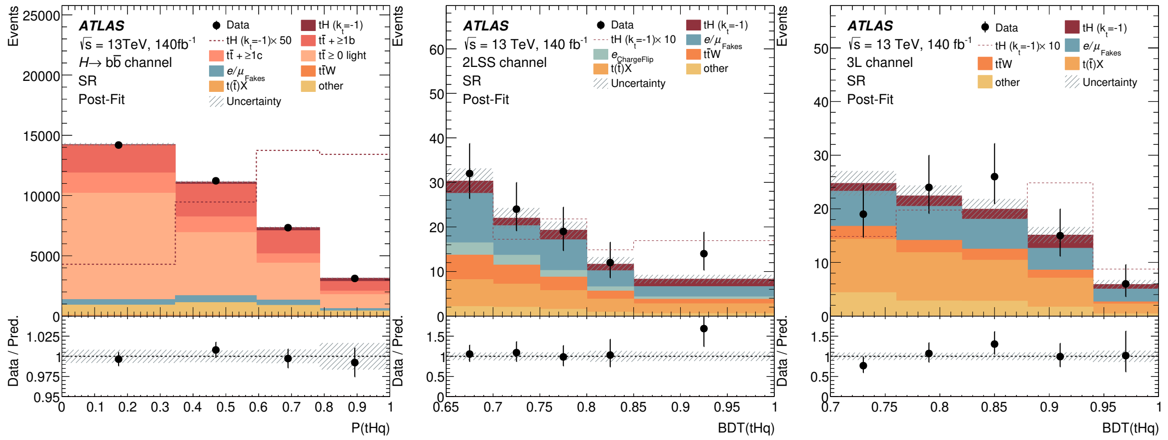

(a) (b) (c)

Figure 7. Comparison between data and the signal-plus-background prediction for the event yields in the (a) $H \to b\bar{b}$, (b) 2ℓ SS and (c) 3ℓ SRs in the ITC hypothesis. The term e/μ_{Fakes} refers to backgrounds from non-prompt or misidentified leptons, namely contributions from heavy-flavour decays and photon conversions. The ITC signal and the background contributions after the likelihood fit to data ("Post-Fit") under the signal-plus-background hypothesis are shown as filled histograms. A dashed red line is added to the plot to show the signal contribution normalised to the measured value multiplied by 50 for the $H \to b\bar{b}$ channel and by 10 for the 2ℓ SS and 3ℓ channels. The ratio of the data to the total post-fit prediction ("Pred.") is shown in the lower panel. The combined statistical and systematic uncertainty in the prediction is indicated by the grey hatched band.

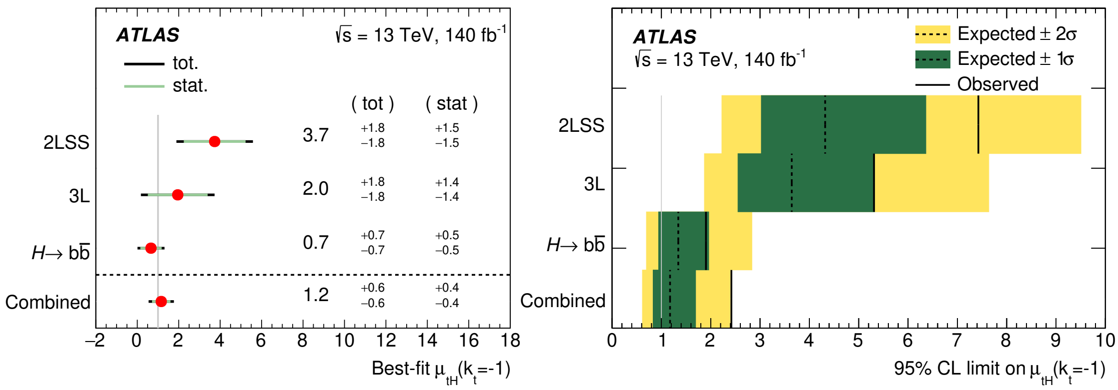

(a) (b)

Figure 8. Fitted values of (a) $\mu_{tH}(\kappa_t = -1)$ and (b) the 95% CL upper limits, shown for the individual channels and the combined measurement. The values reported for the individual channels are obtained by fitting $\mu_{tH}(\kappa_t = -1)$ separately for each channel, whereas the combined measurement is derived by simultaneously fitting all channels together. The observed limits are shown (solid black lines), together with the expected limits under the ITC hypothesis (dotted black lines). A grey line is added in correspondence of the $\mu_{tH}(\kappa_t = -1)$ equal to one. In the case of the expected limits, the one- and two-standard-deviation uncertainty bands are also shown.

10 Conclusion

The search for the production of a Higgs boson in association with a single top quark (tH) is presented. The analysis is based on pp collision data at 13 TeV with an integrated luminosity of 140 fb^{-1}, recorded from 2015 to 2018 with the ATLAS detector at the LHC. The signal regions are split into final states with one, two same-sign or three isolated leptons (electrons or muons) probing the $H \to b\bar{b}$, $H \to WW^*$, $H \to ZZ^*$ and $H \to \tau\tau$ decays of the Higgs boson. Additional background-enriched regions are used in the fit to improve the modelling of several leading backgrounds, such as $t\bar{t}+ \geq 1b$, $t\bar{t}W$ and three different categories of the fake and non-prompt leptons background. The tH signal strength is found to be $\mu_{tH} = 8.1 \pm 2.6$ (stat.) ± 2.0 (syst.) in the SM hypothesis. The measured value of the SM cross-section is $\sigma(tH) = 720 \pm 270$ fb. The main source of uncertainty for this measurement is the one associated with the available experimental data, therefore a better constraint can be obtained analysing a larger event sample. Despite the analysis being optimised to set the best tH limit under the SM hypothesis, it is possible to also test the ITC hypothesis. The signal strength value in this case is found to be $\mu_{tH}(\kappa_t = -1) = 1.2 \pm 0.4$ (stat.) ± 0.5 (syst.). The excess in data favours the ITC hypothesis, but both hypotheses are compatible with the data.

Acknowledgments

We thank CERN for the very successful operation of the LHC and its injectors, as well as the support staff at CERN and at our institutions worldwide without whom ATLAS could not be operated efficiently.

The crucial computing support from all WLCG partners is acknowledged gratefully, in particular from CERN, the ATLAS Tier-1 facilities at TRIUMF/SFU (Canada), NDGF (Denmark, Norway, Sweden), CC-IN2P3 (France), KIT/GridKA (Germany), INFN-CNAF (Italy), NL-T1 (Netherlands), PIC (Spain), RAL (U.K.) and BNL (U.S.A.), the Tier-2 facilities worldwide and large non-WLCG resource providers. Major contributors of computing resources are listed in ref. [135].

We gratefully acknowledge the support of ANPCyT, Argentina; YerPhI, Armenia; ARC, Australia; BMWFW and FWF, Austria; ANAS, Azerbaijan; CNPq and FAPESP, Brazil; NSERC, NRC and CFI, Canada; CERN; ANID, Chile; CAS, MOST and NSFC, China; Minciencias, Colombia; MEYS CR, Czech Republic; DNRF and DNSRC, Denmark; IN2P3-CNRS and CEA-DRF/IRFU, France; SRNSFG, Georgia; BMFTR, HGF and MPG, Germany; GSRI, Greece; RGC and Hong Kong SAR, China; ICHEP and Academy of Sciences and Humanities, Israel; INFN, Italy; MEXT and JSPS, Japan; CNRST, Morocco; NWO, Netherlands; RCN, Norway; MNiSW, Poland; FCT, Portugal; MNE/IFA, Romania; MSTDI, Serbia; MSSR, Slovakia; ARIS and MVZI, Slovenia; DSI/NRF, South Africa; MICIU/AEI, Spain; SRC and Wallenberg Foundation, Sweden; SERI, SNSF and Cantons of Bern and Geneva, Switzerland; NSTC, Taipei; TENMAK, Türkiye; STFC/UKRI, United Kingdom; DOE and NSF, United States of America.

Individual groups and members have received support from BCKDF, CANARIE, CRC and DRAC, Canada; CERN-CZ, FORTE and PRIMUS, Czech Republic; COST, ERC, ERDF, Horizon 2020, ICSC-NextGenerationEU and Marie Skłodowska-Curie Actions, European

Union; Investissements d'Avenir Labex, Investissements d'Avenir Idex and ANR, France; DFG and AvH Foundation, Germany; Herakleitos, Thales and Aristeia programmes co-financed by EU-ESF and the Greek NSRF, Greece; BSF-NSF and MINERVA, Israel; NCN and NAWA, Poland; La Caixa Banking Foundation, CERCA Programme Generalitat de Catalunya and PROMETEO and GenT Programmes Generalitat Valenciana, Spain; Göran Gustafssons Stiftelse, Sweden; The Royal Society and Leverhulme Trust, United Kingdom.

In addition, individual members wish to acknowledge support from CERN: European Organization for Nuclear Research (CERN DOCT); Chile: Agencia Nacional de Investigación y Desarrollo (FONDECYT 1230812, FONDECYT 1240864, Fondecyt 3240661); China: Chinese Ministry of Science and Technology (MOST-2023YFA1605700, MOST-2023YFA1609300), National Natural Science Foundation of China (NSFC — 12175119, NSFC 12275265); Czech Republic: Czech Science Foundation (GACR — 24-11373S), Ministry of Education Youth and Sports (ERC-CZ-LL2327, FORTE CZ.02.01.01/00/22_008/0004632), PRIMUS Research Programme (PRIMUS/21/SCI/017); EU: H2020 European Research Council (ERC — 101002463); European Union: European Research Council (BARD No. 101116429, ERC — 948254, ERC 101089007), European Regional Development Fund (SMASH COFUND 101081355, SLO ERDF), Horizon 2020 Framework Programme (MUCCA — CHIST-ERA-19-XAI-00), European Union, Future Artificial Intelligence Research (FAIR-NextGenerationEU PE00000013), Italian Center for High Performance Computing, Big Data and Quantum Computing (ICSC, NextGenerationEU); France: Agence Nationale de la Recherche (ANR-21-CE31-0022, ANR-22-EDIR-0002); Germany: Baden-Württemberg Stiftung (BW Stiftung-Postdoc Eliteprogramme), Deutsche Forschungsgemeinschaft (DFG — 469666862, DFG — CR 312/5-2); China: Research Grants Council (GRF); Italy: Istituto Nazionale di Fisica Nucleare (ICSC, NextGenerationEU), Ministero dell'Università e della Ricerca (NextGenEU 153D23001490006 M4C2.1.1, NextGenEU I53D23000820006 M4C2.1.1, NextGenEU I53D23001490006 M4C2.1.1, SOE2024_0000023); Japan: Japan Society for the Promotion of Science (JSPS KAKENHI JP22H01227, JSPS KAKENHI JP22H04944, JSPS KAKENHI JP22KK0227, JSPS KAKENHI JP24K23939, JSPS KAKENHI JP24KK0251, JSPS KAKENHI JP25H00650, JSPS KAKENHI JP25H01291, JSPS KAKENHI JP25K01023); Norway: Research Council of Norway (RCN-314472); Poland: Ministry of Science and Higher Education (IDUB AGH, POB8, D4 no 9722), Polish National Science Centre (NCN 2021/42/E/ST2/00350, NCN OPUS 2023/51/B/ST2/02507, NCN OPUS nr 2022/47/B/ST2/03059, NCN UMO-2019/34/E/ST2/00393, UMO-2022/47/O/ST2/00148, UMO-2023/49/B/ST2/04085, UMO-2023/51/B/ST2/00920, UMO-2024/53/N/ST2/00869); Portugal: Foundation for Science and Technology (FCT); Spain: Ministry of Science and Innovation (MCIN & NextGenEU PCI2022-135018-2, MICIN & FEDER PID2021-125273NB, RYC2019-028510-I, RYC2020-030254-I, RYC2021-031273-I, RYC2022-038164-I); Sweden: Carl Trygger Foundation (Carl Trygger Foundation CTS 22:2312), Swedish Research Council (Swedish Research Council 2023-04654, VR 2021-03651, VR 2022-03845, VR 2022-04683, VR 2023-03403, VR 2024-05451), Knut and Alice Wallenberg Foundation (KAW 2018.0458, KAW 2022.0358, KAW 2023.0366); Switzerland: Swiss National Science Foundation (SNSF — PCEFP2_194658); United Kingdom: Royal Society (NIF-R1-231091); United States of America: U.S. Department of Energy (ECA DE-AC02-76SF00515), Neubauer Family Foundation.

A List of input variables used to train the different BDTGs

For the 2ℓSS and 3ℓ channels, leptons are ordered in three different ways:

- *Transverse momentum* ordering: the lepton with the highest p_{T} is called ℓ_A, the one with the second highest p_{T} is called ℓ_B while the lepton with the softest p_{T} is called ℓ_C;
- *Charge and ΔR between leptons* ordering: the lepton with the charge opposite to the sum of the three lepton charges is called ℓ_0, the lepton with the smallest ΔR to ℓ_0 is called ℓ_1, the remaining lepton is called ℓ_2;
- *Charge and ΔR with leading b-jet* ordering: the lepton with the charge opposite to the sum of the three lepton charges is called $\hat{\ell}_0$, the lepton with the smallest ΔR with the leading b-jet is called $\hat{\ell}_1$ while the remaining lepton is called $\hat{\ell}_2$.

The jet satisfying the 70% b-tagging requirement and having the highest p_{T} is called leading b-jet. The jet that fails the b-tagging requirement and maximises the invariant mass with the leading b-jet is called spectator jet, j_{s}. Every jet having $|\eta| > 2.5$ is called forward jet, j_{f}. A forward jet is defined as leading if it has the highest p_{T} among all the forward jets. Every jet with $|\eta| < 2.5$ is called central jet. Using the aforementioned leptons and jet definitions, several variables are constructed.

Variable	$H \to b\bar{b}$	2ℓ SS BDT($t\bar{t}$)	2ℓ SS BDT(VV)	2ℓ SS BDT($t\bar{t}W$)	2ℓ SS BDT(tHq)	3ℓ BDT(tHq)	3ℓ BDT($t\bar{t}$)	3ℓ BDT($t\bar{t}W$)	Description
$p^*_{\ell_A}$(b-jet)	—	—	—	—	—	—	—	×	Momentum of lepton with respect to the leading b-jet rest frame.
$p^*_{\ell_B}$(b-jet)	—	—	—	—	—	×	—	—	
$p^*_{\ell_C}$(b-jet)	—	—	—	—	—	—	—	×	
$p_{\mathrm{T,min}}$	—	×	—	×	×	—	—	—	p_{T} of softest lepton.
$\Delta R(\ell_A, \ell_B + \ell_C)$	—	—	—	—	—	—	—	×	ΔR between lepton and the system of the other two leptons.
$\Delta R(\ell_B, \ell_A + \ell_C)$	—	—	—	—	—	—	—	×	
$\Delta R(\ell_A, b\text{-jet})$	—	—	—	—	—	×	—	×	ΔR between lepton and leading b-jet.
$\Delta R(\ell_B, b\text{-jet})$	—	—	—	—	—	—	—	×	
$\Delta R(\text{non-}b\text{-jet}, \ell_1)$	—	—	—	—	×	—	—	—	ΔR or $\Delta\eta$ between lepton and its closest b-jet or non-b-jet.
$\Delta R(\text{non-}b\text{-jet}, \ell_2)$	—	—	—	—	×	—	—	—	
$\Delta R(\ell_1, b\text{-jet})$	—	×	×	—	—	—	—	—	
$\Delta R(\ell_2, b\text{-jet})$	—	×	×	—	—	—	—	—	
$\Delta\eta(\ell_1, b\text{-jet})$	—	×	×	—	—	—	—	—	
$\Delta\eta(\ell_2, b\text{-jet})$	—	×	×	—	—	—	—	—	
$m(\ell,\ell)_{\mathrm{SS}}$	—	—	—	—	—	×	×	×	Invariant mass, ΔR, $\Delta\phi$ or $\Delta\eta$ of same-sign leptons.
$\Delta\eta(\ell,\ell)_{\mathrm{SS}}$	—	—	—	—	×	×	—	—	
$\Delta\phi(\ell,\ell)_{\mathrm{SS}}$	—	—	—	×	—	—	—	—	
$\Delta R(\ell,\ell)_{\mathrm{SS}}$	—	×	—	×	—	—	—	—	
$m(\ell_0, \ell_2)$	—	—	—	—	—	×	×	—	Invariant mass and ΔR of leptons, jets and/or leading b-jet. The lepton ordering is charge and ΔR based.
$m(\ell_0, \ell_1)$	—	—	—	—	—	×	×	×	
$m(\ell_1, b\text{-jet})$	—	—	—	—	—	×	—	×	
$m(\ell_2, b\text{-jet})$	—	—	—	—	—	×	×	—	
$\Delta R(\ell_0, \ell_1)$	—	—	—	—	—	—	—	×	
$m(\ell_2, \mathrm{j}_2)$	—	×	×	×	×	—	—	—	
$m(\ell_2, \mathrm{j}_1)$	—	×	×	—	×	—	—	—	
$m(\ell_1, \mathrm{j}_2)$	—	—	—	—	×	—	—	—	
$m(\ell_1 + \ell_2, \mathrm{j}_2)$	—	—	—	×	—	—	—	—	
$m(\ell_1 + \ell_2, \mathrm{j}_1 + \mathrm{j}_2)$	—	—	—	×	×	—	—	—	
$m(\ell_1 + \ell_2, \mathrm{j}_1)$	—	×	—	—	—	—	—	—	
$m(\mathrm{j}_1 + \mathrm{j}_2)$	—	—	×	×	×	—	—	—	
$m(\ell_1 + \ell_2)$	—	×	×	×	×	—	—	—	
$m_H(WW)$	—	×	—	×	×	—	—	—	Mass of a candidate Higgs Boson when decays into a pair of W bosons.
$m(\text{jet},\text{jet})_W$	—	—	×	×	×	—	—	—	Mass of the best two jet candidates for the W boson.
$m(\text{jet},\text{jet})_{\text{top}}$	—	×	×	×	×	—	—	—	Mass of the best top-quark candidate from jets.
$m(\hat{\ell}_0, \hat{\ell}_1)$	—	—	—	—	—	—	×	—	Invariant mass of $\hat{\ell}_0$ and $\hat{\ell}_1$.
$m(\hat{\ell}_0, \hat{\ell}_2)$	—	—	—	—	—	×	—	×	Invariant mass and ΔR of $\hat{\ell}_0$ and $\hat{\ell}_2$.
$\Delta R(\hat{\ell}_0, \hat{\ell}_2)$	—	—	—	—	—	—	—	×	
$m(\hat{\ell}_2, b\text{-jet})$	—	—	—	—	—	×	—	×	Invariant mass and ΔR of leading b-jet and $\hat{\ell}_1$ and $\hat{\ell}_2$.
$\Delta R(\hat{\ell}_2, b\text{-jet})$	—	—	—	—	—	—	×	—	
$m(\ell, b\text{-jet})_{\text{top}}$	—	—	—	—	—	—	×	×	Invariant mass of lepton and b-jet giving best top-quark visible mass.
$m(\ell,\ell)_{\text{top}}$	—	—	—	—	—	×	×	—	Invariant mass of two leptons giving best top-quark visible mass.
p_{FW1}	—	—	—	×	—	—	—	—	First Fox-Wolfram moment [136, 137].

Variable	$H \to b\bar{b}$	2ℓ SS BDT($t\bar{t}$)	2ℓ SS BDT(VV)	2ℓ SS BDT($t\bar{t}W$)	2ℓ SS BDT(tHq)	3ℓ BDT(tHq)	3ℓ BDT($t\bar{t}$)	3ℓ BDT($t\bar{t}W$)	Description
p_{FW4}	—	×	×	—	—	—	—	×	Fourth Fox-Wolfram moment.
$p_{\text{T,min}}$	—	—	—	—	—	×	×	×	p_{T} of the softest lepton.
$m(j_{\text{s}})$	—	—	—	—	×	—	—	—	Mass of the spectator jet.
$E(j_{\text{s}})$	—	—	—	—	×	—	—	—	Energy of the spectator jet.
$p_{\text{T}}(j_{\text{s}})$	—	—	—	—	×	—	—	—	p_{T} of the spectator jet.
$E_{\text{T}}^{\text{miss}}/H_{\text{T}}$	—	—	×	—	—	—	—	×	Ratio between $E_{\text{T}}^{\text{miss}}$ and H_{T}.
N(jet)	×	—	—	—	—	—	—	—	Number of non-b-tagged jets.
N(non-b-jet)	—	—	—	—	—	—	—	×	Number of non-b-tagged jets.
N(central-jet)	—	—	—	—	—	×	×	×	Number of central jets.
N(b-jet)	—	—	—	—	—	—	×	×	Number of b-tagged jets.
$\Delta m(Z, \ell\ell_{\text{SF}})_{\text{min}}$	—	×	×	×	—	—	×	×	Minimum difference between the reconstructed invariant mass of two leptons with the same flavour and Z-boson mass.
$\Delta m(Z, \ell\ell)_{\text{min}}$	—	—	—	—	—	×	×	×	Minimum difference between the reconstructed invariant mass of two leptons and Z-boson mass.
$E_{\text{T}}^{\text{miss}}$	—	×	×	×	×	×	×	×	$E_{\text{T}}^{\text{miss}}$.
$\Sigma_i \text{charge}(\ell_i)$	—	×	×	×	×	—	—	—	Sum of lepton charges.
$m(b\text{-jet}, j_{\text{s}})$	—	—	—	×	×	×	—	—	Invariant mass, $\Delta\phi$, $\Delta\eta$ and ΔR of leading b-jet and spectator jet.
$\Delta\phi(b\text{-jet}, j_{\text{s}})$	—	—	—	—	—	×	—	—	
$\Delta\eta(b\text{-jet}, j_{\text{s}})$	—	×	—	—	—	—	—	—	
$\Delta R(b\text{-jet}, j_{\text{s}})$	—	—	—	×	×	—	—	×	
$\Delta R(\ell, j_{\text{f}})$	—	×	—	—	—	—	—	—	ΔR and $\Delta\eta$ between the leading forward jet and its closest lepton.
$\Delta\eta(\ell, j_{\text{f}})$	—	—	—	—	×	—	—	—	
$\Sigma_i q(\ell_i)$	—	—	—	—	—	×	×	×	Sum of lepton charges.
Lepton flavours	—	×	—	—	—	—	—	—	Identification of the flavour of the leptons.
$id(\ell_0)$	×	—	—	—	—	—	—	—	identification number of the lepton combining charge and flavour information.
$e\mu$-events	—	×	×	—	—	—	—	—	Identification of the events $e\mu$.
ee-events	—	—	×	×	×	—	—	—	Identification of the events ee.
H_{T}	—	—	×	—	×	×	×	×	H_{T}.
$H_{\text{T}}(\ell)$	—	×	—	×	×	—	—	—	Sum of the transverse momentum of the leptons.
H_{T}(jets)	—	×	—	×	—	—	—	—	Sum of the transverse momentum of the jets.
$\tilde{m}_{lep}$	—	×	×	×	×	×	—	—	$\sqrt{\Sigma_i(E_{\ell_i}^2 + p_{T,\ell_i}^2)}$.
$\Delta R(\ell, \ell)_{\text{min}}$	—	—	—	—	—	—	—	×	Minimum ΔR between two leptons.
$\Delta\phi(\phi_T^{\text{miss}}, \ell_2)$	—	—	—	×	—	—	—	—	$\Delta\phi$ between ϕ_T^{miss} and ℓ_2.
"custom" χ^2	—	×	×	×	—	—	—	—	$\chi^2(m(\ell_i, \ell_j)_{\text{top}})_{\text{min}}$, minimum χ^2 value between the masses of top-quark candidates given by the combination of leptons.
$m(\ell, \ell)_{\text{top}}$	—	×	×	×	—	—	—	—	Invariant mass of two leptons giving best top-quark visible mass.
$\eta(\text{No-}b\text{-jet})_{\text{max}}$	—	—	—	×	—	—	—	—	Maximum η value among non-b-tagged jets.
$\Delta\eta(\ell_2, \text{non-}b\text{-jet})$	—	—	—	—	—	—	×	—	$\Delta\eta$ between ℓ_2 and closest non-b-tagged jets.
$\Delta\eta(\ell, j_{\text{f}})$	—	—	—	—	—	×	—	—	$\Delta\eta$ between leading forward jet and closest lepton.
N(non-b-jet)	—	—	×	—	×	—	—	—	Number of non b-tagged jets.
N(central-jet)	—	×	×	×	×	—	—	—	Number of central jets.
N(b-jet)	—	×	×	×	—	—	—	—	Number of b-tagged jets.
$b\text{-score}_1$	—	×	×	×	×	×	×	×	Binned DL1r score (calibrated) of leading b-jet.
$b\text{-score}_2$	—	×	×	×	—	—	—	×	Binned DL1r score (calibrated) of second b-jet.

Variable	$H \to b\bar{b}$	2ℓ SS BDT($t\bar{t}$)	BDT(VV)	BDT($t\bar{t}W$)	BDT(tHq)	3ℓ BDT(tHq)	BDT($t\bar{t}$)	BDT($t\bar{t}W$)	Description
b-score$_3$	—	×	×	×	—	—	—	×	Binned DL1r score (calibrated) of third b-jet.
"custom" n_j	×	—	—	—	—	—	—	—	$n_{j,t_{\text{had}}}(\chi^2_{\text{min, ttl}}$, PCBT-bin 4), number of jets that belong to the hadronic top-quark found from reconstructing $t\bar{t}$ events but allowing only Hypothesis I within the 4$^{\text{th}}$ PCBT bin.
"custom" n_j	×	—	—	—	—	—	—	—	$n_{j,t_{\text{had}}}(\chi^2_{\text{min, ttAll}}$, PCBT-bin 4), number of jets that belong to the hadronic top-quark found from reconstructing $t\bar{t}$ events within the 4$^{\text{th}}$ PCBT bin.
"custom" n_j	×	—	—	—	—	—	—	—	$n_{j,t_{\text{had}}}(\chi^2_{\text{min, ttAll}}$, PCBT-bin $\in \{1,2,3\}$), number of jets that belong to the hadronic top-quark found from reconstructing $t\bar{t}$ events within the 1$^{\text{st}}$, 2$^{\text{nd}}$ or 3$^{\text{rd}}$ PCBT bin.
$p_{\text{T}}^{\text{fwd},0}$	×	—	—	—	—	—	—	—	Transverse momentum of the leading forward-jet.
Sphericity	×	—	—	—	—	—	—	—	as defined in ref. [118].
$\chi^2_{\text{min,ttAll}}$	×	—	—	—	—	—	—	—	The minimum χ^2 value found from reconstructing $t\bar{t}$ events.
"custom" n_j	×	—	—	—	—	—	—	—	$n_{j,\text{not-}t_{\text{had}}}(\chi^2_{\text{min, ttl}}$, PCBT-bin $\in \{1,2,3\}$), number of jets that do not belong to the hadronic top-quark found from reconstructing $t\bar{t}$ events but allowing only Hypothesis I within the 1$^{\text{st}}$, 2$^{\text{nd}}$ or 3$^{\text{rd}}$ PCBT bin.
$p_{\text{T}}^{\text{light},1}$	×	—	—	—	—	—	—	—	Transverse momentum of the 2$^{\text{nd}}$ leading jet failing to meet the b-tagging requirement.
"custom" χ^2	×	—	—	—	—	—	—	—	$\chi^2_{\text{top-higgs}}(m_H = 111.5, m_t = 168)$, the minimum χ^2 value found from reconstructing $tHq(H \to b\bar{b})$ events, where the leptonic W from the top-quark decay is reconstructed using the neutrino reconstruction technique.
$\chi^2_{\text{min,ttl}}$	×	—	—	—	—	—	—	—	The minimum χ^2 value found from reconstructing $t\bar{t}$ events allowing only Hypothesis I.
DL1r$_{\text{light},0}$	×	—	—	—	—	—	—	—	Pseudo-continuous b-tagging distribution for the leading jet failing to meet the b-tagging requirement.
$p_{\text{T}}^{\text{light},2}$	×	—	—	—	—	—	—	—	Transverse momentum of the 3$^{\text{rd}}$ leading jet failing to meet the b-tagging requirement.
$\eta_{\text{light},0}$	×	—	—	—	—	—	—	—	Pseudo-rapidity of the leading jet failing to meet the b-tagging requirement.
"custom" χ^2	×	—	—	—	—	—	—	—	$\chi^2_{\text{top-higgs}}(m_H = 113, m_t = 165)$, the minimum χ^2 value found from reconstructing $tHq(H \to b\bar{b})$ events, where the leptonic W from the top-quark decay is reconstructed using the neutrino reconstruction technique.
$p_{\text{T}}^{\text{light},0}$	×	—	—	—	—	—	—	—	Transverse momentum of the leading jet failing to meet the b-tagging requirement.
$\Delta\eta_{\text{top-higgs}}$	×	—	—	—	—	—	—	—	The $\Delta\eta$ between the reconstructed top quark and the reconstructed Higgs boson according to the minimum χ^2 method.
"custom" n_j	×	—	—	—	—	—	—	—	$n_{j,t_{\text{had}}}(\chi^2_{\text{min, ttl}}$, PCBT-bin 0), number of jets that belong to the hadronic top-quark found from reconstructing $t\bar{t}$ events but allowing only Hypothesis I within the 0$^{\text{th}}$ PCBT bin.
$m_{t_{\text{had}}}(\chi^2_{\text{min, ttAll}})$	×	—	—	—	—	—	—	—	The mass of the reconstructed hadronic top-quark found from reconstructing $t\bar{t}$ events.

Variable	$H \to b\bar{b}$	2ℓ SS				3ℓ			Description
		BDT($t\bar{t}$)	BDT(VV)	BDT($t\bar{t}W$)	BDT(tHq)	BDT(tHq)	BDT($t\bar{t}$)	BDT($t\bar{t}W$)	
$m_{t_{\text{had}}}(\chi^2_{\text{min, ttl}})$	×	—	—	—	—	—	—	—	The mass of the reconstructed hadronic top-quark found from reconstructing $t\bar{t}$ events but allowing only Hypothesis I.
$\eta_{\text{light},2}$	×	—	—	—	—	—	—	—	Pseudo-rapidity of the 3rd leading jet failing the b-tagging requirement.
$\Delta R(q_1^W, q_2^W)$	×	—	—	—	—	—	—	—	The minimum ΔR between the two jets assigned to the hadronic W decay from reconstructing $t\bar{t}$ events.
$m(b_{\text{top}}, j_{\text{tag}})$	×	—	—	—	—	—	—	—	The invariant mass of the b-jet from top-quark decay found using a reconstruction of $tHq(H \to b\bar{b})$ events and the light-flavour jet most de-correlated from the top-quark system. The light jet is chosen such that it maximises the invariant mass $m(b_{\text{top}}, j_{\text{tag}})$.
η_{tag}	×	—	—	—	—	—	—	—	The η of the light-flavour jet, η_{tag} most de-correlated from the top-quark system. The light jet is chosen such that it maximises the invariant mass $m(b_{\text{top}}, j_{\text{tag}})$.

Table 6. List of variables considered in the training of the BDTGs in each channel. The × symbol marks in which BDTGs the variable is used. Variables labelled with "custom" are better explained in the description column.

$H \to b\bar{b}$ channel				
	Pre-fit		Post-fit	
Process	SR	CR($t\bar{t}+\geq 1b$)	SR	CR($t\bar{t}+\geq 1b$)
tHq	43 ± 7	9.1 ± 2.0	350 ± 130	72 ± 29
tWH	3.4 ± 2.0	14 ± 8	28 ± 20	110 ± 80
$t\bar{t}+\geq 1b$	6800 ± 1100	20100 ± 2600	8100 ± 1000	25600 ± 1900
$t\bar{t}+\geq 1c$	4000 ± 2400	11000 ± 6000	3900 ± 1500	10200 ± 3300
$t\bar{t}+\geq 0$ light	19300 ± 3300	23100 ± 3500	18500 ± 1100	23300 ± 2100
e/μ_{Fakes}	1700 ± 500	1600 ± 500	1700 ± 500	1600 ± 500
$t\bar{t}W$	20.1 ± 3.0	134 ± 19	20.2 ± 2.9	133 ± 19
$t\bar{t}H$	120 ± 15	683 ± 70	120 ± 15	683 ± 70
$t\bar{t}Z$	68 ± 9	340 ± 40	68 ± 9	340 ± 40
tZq	69 ± 7	20.4 ± 1.9	69 ± 6	20.4 ± 1.9
tWZ	0.20 ± 0.10	0.9 ± 0.5	0.20 ± 0.11	0.9 ± 0.5
Wt channel	970 ± 260	1500 ± 500	970 ± 250	1600 ± 500
t-channel	1070 ± 180	350 ± 120	1060 ± 160	350 ± 120
s-channel	43 ± 8	40 ± 11	42 ± 7	39 ± 10
W + jets	740 ± 310	900 ± 400	750 ± 300	890 ± 350
Z + jets	140 ± 50	100 ± 40	140 ± 50	100 ± 40
VV	48 ± 25	70 ± 40	41 ± 22	63 ± 33
other Higgs	6 ± 5	5.3 ± 2.9	7 ± 5	5.2 ± 2.8
Rare top	0.08 ± 0.04	3.3 ± 1.7	0.08 ± 0.04	3.4 ± 1.7
Total	35000 ± 5000	60000 ± 8000	35870 ± 210	65000 ± 340
Data	35869	65002	35869	65002

Table 7. Pre-fit and post-fit event yields in the SR and CR($t\bar{t}+\geq 1b$) of the $H \to b\bar{b}$ channel. Post-fit yields are after the inclusive fit in all channels. All uncertainties are included, taking into account correlations in the post-fit case.

B Pre-fit and post-fit yields tables

Pre-fit and post-fit yields of the analysis regions are reported in table 7 for the $H \to b\bar{b}$ channel. Tables 8 and 9 show the pre- and post-fit yields for the 2ℓ SS channel, respectively. Tables 10 and 11 show the pre- and post-fit yields for the 3ℓ channel, respectively.

Pre-fit 2ℓ SS channel					
Process	SR	CR($\mu_{\rm HF}$)	CR($e_{\rm HF}$)	CR($e_{\rm conv}$)	CR($t\bar{t}W$)
tHq	3.1 ± 0.5	0.65 ± 0.11	2.5 ± 0.4	0.085 ± 0.024	0.30 ± 0.06
tWH	0.09 ± 0.04	0.20 ± 0.04	0.89 ± 0.13	0.016 ± 0.006	0.39 ± 0.05
$\mu_{\rm HF}$	16 ± 5	59 ± 11	19 ± 4	0.24 ± 0.24	3.0 ± 2.0
$e_{\rm HF}$	4.9 ± 3.1	-	86 ± 17	1.3 ± 0.8	0.9 ± 0.8
$e_{\rm conv}$	3.4 ± 2.7	-	80 ± 15	47 ± 15	2.8 ± 1.4
other mis-id leptons	4 ± 4	15 ± 12	41 ± 28	3.0 ± 3.0	3.7 ± 2.6
$e_{\rm ChargeFlip}$	8.3 ± 1.9	-	220 ± 50	37 ± 11	4.4 ± 1.0
$t\bar{t}W$	14.9 ± 2.1	35 ± 4	160 ± 8	5.0 ± 0.4	131 ± 5
$t\bar{t}Z$	3.7 ± 0.6	8.0 ± 1.4	38 ± 6	1.12 ± 0.21	15.3 ± 2.2
$t\bar{t}H$	2.4 ± 0.4	7.2 ± 1.0	30 ± 4	0.77 ± 0.12	13.5 ± 2.0
tZq	14.2 ± 1.9	3.9 ± 0.5	22.0 ± 2.0	0.68 ± 0.09	1.05 ± 0.18
VV	7.3 ± 3.3	9 ± 5	50 ± 15	1.8 ± 1.5	7.2 ± 3.1
others	0.45 ± 0.13	1.1 ± 0.4	7.9 ± 2.1	0.28 ± 0.10	2.0 ± 0.5
4-tops	0.042 ± 0.014	0.050 ± 0.015	0.54 ± 0.15	0.016 ± 0.007	0.83 ± 0.24
Total	83 ± 10	138 ± 16	760 ± 80	98 ± 21	187 ± 8
Data	101	137	756	110	200

Table 8. Pre-fit event yields in the SR and CRs of the 2ℓ SS channel. The 'others' process includes tWZ, Tri-boson, s-channel, 3-tops and VH processes.

Post-fit 2ℓ SS channel					
Process	SR	CR($\mu_{\rm HF}$)	CR($e_{\rm HF}$)	CR($e_{\rm conv}$)	CR($t\bar{t}W$)
tHq	25 ± 9	5.3 ± 2.1	21 ± 8	0.67 ± 0.30	2.4 ± 0.9
tWH	0.7 ± 0.4	1.6 ± 0.7	7.3 ± 3.2	0.13 ± 0.07	3.2 ± 1.4
$\mu_{\rm HF}$	13 ± 6	47 ± 18	15 ± 7	0.22 ± 0.17	2.9 ± 1.9
$e_{\rm HF}$	2.6 ± 3.4	-	50 ± 60	0.7 ± 0.9	0.5 ± 0.7
$e_{\rm conv}$	3.8 ± 3.1	-	98 ± 35	58 ± 15	3.4 ± 1.6
other mis-id leptons	4 ± 4	15 ± 11	38 ± 25	3.3 ± 2.8	3.2 ± 2.1
$e_{\rm ChargeFlip}$	8.0 ± 1.8	-	210 ± 50	36 ± 10	4.2 ± 1.0
$t\bar{t}W$	15.0 ± 2.4	41 ± 5	178 ± 17	5.7 ± 0.6	144 ± 13
$t\bar{t}Z$	3.7 ± 0.6	7.9 ± 1.3	37 ± 6	1.07 ± 0.20	15.1 ± 2.1
$t\bar{t}H$	2.4 ± 0.4	7.3 ± 0.9	30 ± 4	0.78 ± 0.11	13.5 ± 1.9
tZq	14.1 ± 1.9	3.9 ± 0.5	22.1 ± 2.0	0.68 ± 0.09	1.03 ± 0.17
VV	6.0 ± 2.4	7.1 ± 3.5	45 ± 13	2.0 ± 1.6	6.0 ± 2.4
others	0.44 ± 0.13	1.1 ± 0.4	7.9 ± 2.1	0.28 ± 0.11	1.9 ± 0.5
4-tops	0.043 ± 0.014	0.050 ± 0.015	0.55 ± 0.15	0.017 ± 0.007	0.85 ± 0.24
Total	99 ± 8	138 ± 11	762 ± 27	109 ± 10	202 ± 12
Data	101	137	756	110	200

Table 9. Post-fit event yields in the SR and CRs of the 2ℓ SS channel. Post-fit yields are after the inclusive fit in all channels. All uncertainties are included, taking into account correlations in the post-fit case. The 'others' process includes tWZ, Tri-boson, s-channel, 3-tops and VH processes.

JHEP10(2025)093

Pre-fit 3ℓ channel					
Process	SR	CR(μ_{HF})	CR(e_{HF})	CR(e_{conv})	CR($t\bar{t}W$)
tHq	1.45 ± 0.24	0.24 ± 0.06	0.159 ± 0.030	0.025 ± 0.007	0.26 ± 0.06
tWH	0.29 ± 0.04	0.24 ± 0.04	0.150 ± 0.023	0.019 ± 0.004	0.64 ± 0.07
μ_{HF}	9 ± 4	84 ± 11	3.2 ± 1.8	0.08 ± 0.11	10 ± 7
e_{HF}	5.3 ± 2.3	2.7 ± 2.2	47 ± 9	0.16 ± 0.04	6.9 ± 3.0
e_{conv}	4.2 ± 1.8	3.5 ± 3.2	14 ± 6	14 ± 9	11 ± 8
other mis-id leptons	4.9 ± 3.0	14 ± 10	8 ± 5	1.0 ± 1.0	10 ± 8
$t\bar{t}W$	7.9 ± 0.9	13.6 ± 0.6	8.1 ± 0.8	1.97 ± 0.33	118 ± 4
tWZ	0.8 ± 0.5	1.4 ± 0.7	0.8 ± 0.5	0.6 ± 0.4	3.5 ± 1.9
$t\bar{t}Z$	14.3 ± 2.1	15.6 ± 2.4	8.2 ± 1.3	4.9 ± 1.1	37 ± 5
$t\bar{t}H$	7.7 ± 1.0	7.6 ± 1.0	4.7 ± 0.7	0.51 ± 0.16	21.0 ± 2.8
tZq	10.8 ± 1.2	9.2 ± 1.1	4.8 ± 0.6	1.8 ± 0.4	6.0 ± 0.7
tW	1.1 ± 0.7	6 ± 4	3.6 ± 2.5	0.9 ± 0.7	1.6 ± 1.2
VV	12 ± 5	22 ± 7	11.0 ± 3.5	4.8 ± 1.7	13 ± 5
others	0.24 ± 0.08	0.44 ± 0.12	0.16 ± 0.05	0.040 ± 0.012	1.0 ± 0.6
4-tops	0.14 ± 0.04	0.15 ± 0.05	0.085 ± 0.026	0.037 ± 0.013	1.7 ± 0.5
Total	80 ± 11	181 ± 17	113 ± 15	31 ± 10	242 ± 14
Data	90	175	134	26	268

Table 10. Pre-fit event yields in the SR and CRs of the 3ℓ channel. The 'others' process includes gluon-gluon fusion and vector-boson fusion Higgs boson production, Tri-boson, s-channel and t-channel single-top, 3-tops and VH processes.

Post-fit 3ℓ channel					
Process	SR	CR(μ_{HF})	CR(e_{HF})	CR(e_{conv})	CR($t\bar{t}W$)
tHq	12 ± 4	2.0 ± 0.9	1.3 ± 0.5	0.20 ± 0.09	2.2 ± 0.9
tWH	2.3 ± 0.9	2.0 ± 0.9	1.2 ± 0.5	0.15 ± 0.07	5.2 ± 2.2
μ_{HF}	8 ± 4	77 ± 18	3.0 ± 1.5	0.07 ± 0.09	9 ± 6
e_{HF}	8 ± 4	3.8 ± 2.9	68 ± 14	0.22 ± 0.08	10 ± 6
e_{conv}	3.1 ± 2.1	3 ± 4	11 ± 6	11 ± 5	9 ± 11
other mis-id leptons	3.8 ± 2.2	13 ± 8	7 ± 4	1.0 ± 0.9	9 ± 7
$t\bar{t}W$	8.3 ± 1.3	15.0 ± 1.6	9.3 ± 1.2	2.0 ± 0.4	131 ± 12
tWZ	0.9 ± 0.5	1.5 ± 0.7	0.9 ± 0.5	0.62 ± 0.33	3.6 ± 1.9
$t\bar{t}Z$	14.2 ± 2.0	15.5 ± 2.3	8.4 ± 1.3	4.6 ± 0.9	38 ± 5
$t\bar{t}H$	7.7 ± 1.0	7.6 ± 1.0	4.7 ± 0.7	0.48 ± 0.14	21.4 ± 2.8
tZq	10.7 ± 1.2	9.3 ± 1.1	4.9 ± 0.6	1.74 ± 0.32	6.0 ± 0.7
tW	1.1 ± 0.7	5 ± 4	4.0 ± 2.7	0.9 ± 0.7	1.4 ± 1.1
VV	10 ± 4	21 ± 6	10.6 ± 3.4	4.2 ± 1.3	11 ± 4
others	0.23 ± 0.08	0.43 ± 0.12	0.15 ± 0.05	0.037 ± 0.011	0.9 ± 0.4
4-tops	0.14 ± 0.04	0.15 ± 0.05	0.087 ± 0.026	0.035 ± 0.012	1.7 ± 0.5
Total	90 ± 7	177 ± 13	135 ± 11	27 ± 5	260 ± 11
Data	90	175	134	26	268

Table 11. Post-fit event yields in the SR and CRs of the 2ℓSS channel. Post-fit yields are after the inclusive fit in all channels. All uncertainties are included, taking into account correlations in the post-fit case. The 'others' process includes gluon-gluon fusion and vector-boson fusion Higgs boson production, Tri-boson, s-channel and t-channel single-top, 3-tops and VH processes.

Data Availability Statement. This article has no associated data or the data will not be deposited.

Code Availability Statement. This article has no associated code or the code will not be deposited.

References

[1] F. Englert and R. Brout, *Broken symmetry and the mass of gauge vector mesons*, *Phys. Rev. Lett.* **13** (1964) 321 [INSPIRE].

[2] P.W. Higgs, *Broken symmetries and the masses of gauge bosons*, *Phys. Rev. Lett.* **13** (1964) 508 [INSPIRE].

[3] ATLAS collaboration, *Observation of a new particle in the search for the Standard Model Higgs boson with the ATLAS detector at the LHC*, *Phys. Lett. B* **716** (2012) 1 [arXiv:1207.7214] [INSPIRE].

[4] CMS collaboration, *Observation of a new boson at a mass of 125 GeV with the CMS experiment at the LHC*, *Phys. Lett. B* **716** (2012) 30 [arXiv:1207.7235] [INSPIRE].

[5] M.E. Peskin and D.V. Schroeder, *An introduction to quantum field theory*, Addison-Wesley, Reading, U.S.A. (1995) [DOI:10.1201/9780429503559] [INSPIRE].

[6] G. Degrassi et al., *Higgs mass and vacuum stability in the Standard Model at NNLO*, *JHEP* **08** (2012) 098 [arXiv:1205.6497] [INSPIRE].

[7] D. Buttazzo et al., *Investigating the near-criticality of the Higgs boson*, *JHEP* **12** (2013) 089 [arXiv:1307.3536] [INSPIRE].

[8] C. Englert et al., *Precision measurements of Higgs couplings: implications for new physics scales*, *J. Phys. G* **41** (2014) 113001 [arXiv:1403.7191] [INSPIRE].

[9] J.F. Gunion and X.-G. He, *Determining the CP nature of a neutral Higgs boson at the LHC*, *Phys. Rev. Lett.* **76** (1996) 4468 [hep-ph/9602226] [INSPIRE].

[10] J. Ellis, D.S. Hwang, K. Sakurai and M. Takeuchi, *Disentangling Higgs-top couplings in associated production*, *JHEP* **04** (2014) 004 [arXiv:1312.5736] [INSPIRE].

[11] X.-G. He, G.-N. Li and Y.-J. Zheng, *Probing Higgs boson CP properties with $t\bar{t}H$ at the LHC and the 100 TeV pp collider*, *Int. J. Mod. Phys. A* **30** (2015) 1550156 [arXiv:1501.00012] [INSPIRE].

[12] ATLAS collaboration, *Observation of Higgs boson production in association with a top quark pair at the LHC with the ATLAS detector*, *Phys. Lett. B* **784** (2018) 173 [arXiv:1806.00425] [INSPIRE].

[13] CMS collaboration, *Observation of $t\bar{t}H$ production*, *Phys. Rev. Lett.* **120** (2018) 231801 [arXiv:1804.02610] [INSPIRE].

[14] T.M.P. Tait and C.-P. Yuan, *Single top quark production as a window to physics beyond the standard model*, *Phys. Rev. D* **63** (2000) 014018 [hep-ph/0007298] [INSPIRE].

[15] V. Barger, M. McCaskey and G. Shaughnessy, *Single top and Higgs associated production at the LHC*, *Phys. Rev. D* **81** (2010) 034020 [arXiv:0911.1556] [INSPIRE].

JHEP10(2025)093

[16] S. Biswas, E. Gabrielli and B. Mele, *Single top and Higgs associated production as a probe of the Htt coupling sign at the LHC*, JHEP **01** (2013) 088 [arXiv:1211.0499] [INSPIRE].

[17] M. Farina et al., *Lifting degeneracies in Higgs couplings using single top production in association with a Higgs boson*, JHEP **05** (2013) 022 [arXiv:1211.3736] [INSPIRE].

[18] J. Chang, K. Cheung, J.S. Lee and C.-T. Lu, *Probing the top-Yukawa coupling in associated Higgs production with a single top quark*, JHEP **05** (2014) 062 [arXiv:1403.2053] [INSPIRE].

[19] ATLAS collaboration, *CP properties of Higgs boson interactions with top quarks in the $t\bar{t}H$ and tH processes using $H \to \gamma\gamma$ with the ATLAS detector*, Phys. Rev. Lett. **125** (2020) 061802 [arXiv:2004.04545] [INSPIRE].

[20] CMS collaboration, *Measurements of Higgs boson production cross sections and couplings in the diphoton decay channel at $\sqrt{s} = 13$ TeV*, JHEP **07** (2021) 027 [arXiv:2103.06956] [INSPIRE].

[21] ATLAS collaboration, *A detailed map of Higgs boson interactions by the ATLAS experiment ten years after the discovery*, Nature **607** (2022) 52 [*Erratum ibid.* **612** (2022) E24] [arXiv:2207.00092] [INSPIRE].

[22] CMS collaboration, *A portrait of the Higgs boson by the CMS experiment ten years after the discovery*, Nature **607** (2022) 60 [arXiv:2207.00043] [INSPIRE].

[23] ATLAS and CMS collaborations, *Measurements of the Higgs boson production and decay rates and constraints on its couplings from a combined ATLAS and CMS analysis of the LHC pp collision data at $\sqrt{s} = 7$ and 8 TeV*, JHEP **08** (2016) 045 [arXiv:1606.02266] [INSPIRE].

[24] F. Demartin, F. Maltoni, K. Mawatari and M. Zaro, *Higgs production in association with a single top quark at the LHC*, Eur. Phys. J. C **75** (2015) 267 [arXiv:1504.00611] [INSPIRE].

[25] F. Demartin et al., *tWH associated production at the LHC*, Eur. Phys. J. C **77** (2017) 34 [arXiv:1607.05862] [INSPIRE].

[26] L. Evans and P. Bryant, *LHC machine*, 2008 *JINST* **3** S08001 [INSPIRE].

[27] J.M. Campbell, R. Frederix, F. Maltoni and F. Tramontano, *Next-to-leading-order predictions for t-channel single-top production at hadron colliders*, Phys. Rev. Lett. **102** (2009) 182003 [arXiv:0903.0005] [INSPIRE].

[28] F. Maltoni, G. Ridolfi and M. Ubiali, *b-initiated processes at the LHC: a reappraisal*, JHEP **04** (2012) 095 [*Erratum ibid.* **04** (2013) 095] [arXiv:1203.6393] [INSPIRE].

[29] E. Bothmann, F. Krauss and M. Schönherr, *Single top-quark production with SHERPA*, Eur. Phys. J. C **78** (2018) 220 [arXiv:1711.02568] [INSPIRE].

[30] CMS collaboration, *Search for associated production of a Higgs boson and a single top quark in proton-proton collisions at $\sqrt{s} = 13$ TeV*, Phys. Rev. D **99** (2019) 092005 [arXiv:1811.09696] [INSPIRE].

[31] CMS collaboration, *Measurement of the Higgs boson production rate in association with top quarks in final states with electrons, muons, and hadronically decaying tau leptons at $\sqrt{s} = 13$ TeV*, Eur. Phys. J. C **81** (2021) 378 [arXiv:2011.03652] [INSPIRE].

[32] CMS collaboration, *Measurement of the $t\bar{t}H$ and tH production rates in the $H \to b\bar{b}$ decay channel using proton-proton collision data at $\sqrt{s} = 13$ TeV*, JHEP **02** (2025) 097 [arXiv:2407.10896] [INSPIRE].

[33] M. Aly, T. Dado, A. Held, M. Pinamonti and L. Valery, *Trexfitter*, Zenodo, February (2025).

[34] ATLAS collaboration, *The ATLAS experiment at the CERN Large Hadron Collider*, 2008 *JINST* **3** S08003 [INSPIRE].

JHEP10(2025)093

[35] ATLAS collaboration, *ATLAS Insertable B-Layer technical design report*, CERN-LHCC-2010-013, CERN, Geneva, Switzerland (2010).

[36] ATLAS IBL collaboration, *Production and integration of the ATLAS Insertable B-Layer*, 2018 *JINST* **13** T05008 [arXiv:1803.00844] [INSPIRE].

[37] G. Avoni et al., *The new LUCID-2 detector for luminosity measurement and monitoring in ATLAS*, 2018 *JINST* **13** P07017 [INSPIRE].

[38] ATLAS collaboration, *Performance of the ATLAS trigger system in 2015*, *Eur. Phys. J. C* **77** (2017) 317 [arXiv:1611.09661] [INSPIRE].

[39] ATLAS collaboration, *Software and computing for run 3 of the ATLAS experiment at the LHC*, *Eur. Phys. J. C* **85** (2025) 234 [arXiv:2404.06335] [INSPIRE].

[40] ATLAS collaboration, *ATLAS data quality operations and performance for 2015–2018 data-taking*, 2020 *JINST* **15** P04003 [arXiv:1911.04632] [INSPIRE].

[41] ATLAS collaboration, *Performance of electron and photon triggers in ATLAS during LHC run 2*, *Eur. Phys. J. C* **80** (2020) 47 [arXiv:1909.00761] [INSPIRE].

[42] ATLAS collaboration, *Performance of the ATLAS muon triggers in run 2*, 2020 *JINST* **15** P09015 [arXiv:2004.13447] [INSPIRE].

[43] T. Sjostrand, S. Mrenna and P.Z. Skands, *A brief introduction to PYTHIA 8.1*, *Comput. Phys. Commun.* **178** (2008) 852 [arXiv:0710.3820] [INSPIRE].

[44] T. Sjöstrand et al., *An introduction to PYTHIA 8.2*, *Comput. Phys. Commun.* **191** (2015) 159 [arXiv:1410.3012] [INSPIRE].

[45] R.D. Ball et al., *Parton distributions with LHC data*, *Nucl. Phys. B* **867** (2013) 244 [arXiv:1207.1303] [INSPIRE].

[46] ATLAS collaboration, *The Pythia 8 A3 tune description of ATLAS minimum bias and inelastic measurements incorporating the Donnachie-Landshoff diffractive model*, ATL-PHYS-PUB-2016-017, CERN, Geneva, Switzerland (2016).

[47] Particle Data Group collaboration, *Review of particle physics*, *Phys. Rev. D* **110** (2024) 030001 [INSPIRE].

[48] D.J. Lange, *The EvtGen particle decay simulation package*, *Nucl. Instrum. Meth. A* **462** (2001) 152 [INSPIRE].

[49] J. Alwall et al., *The automated computation of tree-level and next-to-leading order differential cross sections, and their matching to parton shower simulations*, *JHEP* **07** (2014) 079 [arXiv:1405.0301] [INSPIRE].

[50] NNPDF collaboration, *Parton distributions for the LHC run II*, *JHEP* **04** (2015) 040 [arXiv:1410.8849] [INSPIRE].

[51] ATLAS collaboration, *ATLAS Pythia 8 tunes to 7 TeV data*, ATL-PHYS-PUB-2014-021, CERN, Geneva, Switzerland (2014).

[52] LHC Higgs Cross Section Working Group collaboration, *Handbook of LHC Higgs cross sections: 4. Deciphering the nature of the Higgs sector*, *CERN Yellow Rep. Monogr.* **2** (2017) 1 [arXiv:1610.07922] [INSPIRE].

[53] ATLAS collaboration, *SM Higgs production cross sections at $\sqrt{s} = 13$ TeV*, https://twiki.cern.ch/twiki/bin/view/LHCPhysics/CERNYellowReportPageAt13TeV (2024).

[54] J. Butterworth et al., *PDF4LHC recommendations for LHC run II*, *J. Phys. G* **43** (2016) 023001 [arXiv:1510.03865] [INSPIRE].

[55] S. Frixione et al., *Single-top hadroproduction in association with a W boson*, *JHEP* **07** (2008) 029 [arXiv:0805.3067] [INSPIRE].

[56] ATLAS collaboration, *Studies on top-quark Monte Carlo modelling for Top2016*, ATL-PHYS-PUB-2016-020, CERN, Geneva, Switzerland (2016).

[57] M. Bahr et al., *Herwig++ physics and manual*, *Eur. Phys. J. C* **58** (2008) 639 [arXiv:0803.0883] [INSPIRE].

[58] J. Bellm et al., *Herwig 7.0/Herwig++ 3.0 release note*, *Eur. Phys. J. C* **76** (2016) 196 [arXiv:1512.01178] [INSPIRE].

[59] L.A. Harland-Lang, A.D. Martin, P. Motylinski and R.S. Thorne, *Parton distributions in the LHC era: MMHT 2014 PDFs*, *Eur. Phys. J. C* **75** (2015) 204 [arXiv:1412.3989] [INSPIRE].

[60] S. Frixione, P. Nason and G. Ridolfi, *A positive-weight next-to-leading-order Monte Carlo for heavy flavour hadroproduction*, *JHEP* **09** (2007) 126 [arXiv:0707.3088] [INSPIRE].

[61] P. Nason, *A new method for combining NLO QCD with shower Monte Carlo algorithms*, *JHEP* **11** (2004) 040 [hep-ph/0409146] [INSPIRE].

[62] S. Frixione, P. Nason and C. Oleari, *Matching NLO QCD computations with parton shower simulations: the POWHEG method*, *JHEP* **11** (2007) 070 [arXiv:0709.2092] [INSPIRE].

[63] S. Alioli, P. Nason, C. Oleari and E. Re, *A general framework for implementing NLO calculations in shower Monte Carlo programs: the POWHEG BOX*, *JHEP* **06** (2010) 043 [arXiv:1002.2581] [INSPIRE].

[64] M. Beneke, P. Falgari, S. Klein and C. Schwinn, *Hadronic top-quark pair production with NNLL threshold resummation*, *Nucl. Phys. B* **855** (2012) 695 [arXiv:1109.1536] [INSPIRE].

[65] M. Cacciari et al., *Top-pair production at hadron colliders with next-to-next-to-leading logarithmic soft-gluon resummation*, *Phys. Lett. B* **710** (2012) 612 [arXiv:1111.5869] [INSPIRE].

[66] P. Bärnreuther, M. Czakon and A. Mitov, *Percent level precision physics at the Tevatron: first genuine NNLO QCD corrections to $q\bar{q} \to t\bar{t} + X$*, *Phys. Rev. Lett.* **109** (2012) 132001 [arXiv:1204.5201] [INSPIRE].

[67] M. Czakon and A. Mitov, *NNLO corrections to top-pair production at hadron colliders: the all-fermionic scattering channels*, *JHEP* **12** (2012) 054 [arXiv:1207.0236] [INSPIRE].

[68] M. Czakon and A. Mitov, *NNLO corrections to top pair production at hadron colliders: the quark-gluon reaction*, *JHEP* **01** (2013) 080 [arXiv:1210.6832] [INSPIRE].

[69] M. Czakon, P. Fiedler and A. Mitov, *Total top-quark pair-production cross section at hadron colliders through $O(\alpha_S^4)$*, *Phys. Rev. Lett.* **110** (2013) 252004 [arXiv:1303.6254] [INSPIRE].

[70] M. Czakon and A. Mitov, *Top++: a program for the calculation of the top-pair cross-section at hadron colliders*, *Comput. Phys. Commun.* **185** (2014) 2930 [arXiv:1112.5675] [INSPIRE].

[71] S. Höche et al., *A study of QCD radiation in VBF Higgs production with Vincia and Pythia*, *SciPost Phys.* **12** (2022) 010 [arXiv:2106.10987] [INSPIRE].

[72] F. Buccioni et al., *OpenLoops 2*, *Eur. Phys. J. C* **79** (2019) 866 [arXiv:1907.13071] [INSPIRE].

[73] F. Cascioli, P. Maierhofer and S. Pozzorini, *Scattering amplitudes with OpenLoops*, *Phys. Rev. Lett.* **108** (2012) 111601 [arXiv:1111.5206] [INSPIRE].

[74] A. Denner, S. Dittmaier and L. Hofer, *Collier: a fortran-based Complex One-Loop LIbrary in Extended Regularizations*, *Comput. Phys. Commun.* **212** (2017) 220 [arXiv:1604.06792] [INSPIRE].

[75] H.B. Hartanto, B. Jager, L. Reina and D. Wackeroth, *Higgs boson production in association with top quarks in the POWHEG BOX*, *Phys. Rev. D* **91** (2015) 094003 [arXiv:1501.04498] [INSPIRE].

[76] SHERPA collaboration, *Event generation with Sherpa 2.2*, *SciPost Phys.* **7** (2019) 034 [arXiv:1905.09127] [INSPIRE].

[77] R. Frederix and S. Frixione, *Merging meets matching in MC@NLO*, *JHEP* **12** (2012) 061 [arXiv:1209.6215] [INSPIRE].

[78] R. Frederix and I. Tsinikos, *On improving NLO merging for $t\bar{t}W$ production*, *JHEP* **11** (2021) 029 [arXiv:2108.07826] [INSPIRE].

[79] ATLAS collaboration, *Modelling of the $t\bar{t}H$ and $t\bar{t}V$ $(V = W, Z)$ processes for $\sqrt{s} = 13$ TeV ATLAS analyses*, ATL-PHYS-PUB-2016-005, CERN, Geneva, Switzerland (2016).

[80] S. Hoeche, F. Krauss, M. Schonherr and F. Siegert, *QCD matrix elements + parton showers: the NLO case*, *JHEP* **04** (2013) 027 [arXiv:1207.5030] [INSPIRE].

[81] S. Alioli, P. Nason, C. Oleari and E. Re, *NLO single-top production matched with shower in POWHEG: s- and t-channel contributions*, *JHEP* **09** (2009) 111 [*Erratum ibid.* **02** (2010) 011] [arXiv:0907.4076] [INSPIRE].

[82] E. Re, *Single-top Wt-channel production matched with parton showers using the POWHEG method*, *Eur. Phys. J. C* **71** (2011) 1547 [arXiv:1009.2450] [INSPIRE].

[83] T. Gleisberg and S. Hoeche, *Comix, a new matrix element generator*, *JHEP* **12** (2008) 039 [arXiv:0808.3674] [INSPIRE].

[84] C. Anastasiou, L.J. Dixon, K. Melnikov and F. Petriello, *High precision QCD at hadron colliders: electroweak gauge boson rapidity distributions at NNLO*, *Phys. Rev. D* **69** (2004) 094008 [hep-ph/0312266] [INSPIRE].

[85] S. Hoeche, F. Krauss, M. Schonherr and F. Siegert, *A critical appraisal of NLO+PS matching methods*, *JHEP* **09** (2012) 049 [arXiv:1111.1220] [INSPIRE].

[86] S. Catani, F. Krauss, R. Kuhn and B.R. Webber, *QCD matrix elements + parton showers*, *JHEP* **11** (2001) 063 [hep-ph/0109231] [INSPIRE].

[87] S. Hoeche, F. Krauss, S. Schumann and F. Siegert, *QCD matrix elements and truncated showers*, *JHEP* **05** (2009) 053 [arXiv:0903.1219] [INSPIRE].

[88] P. Nason and G. Zanderighi, *W^+W^-, WZ and ZZ production in the POWHEG-BOX-V2*, *Eur. Phys. J. C* **74** (2014) 2702 [arXiv:1311.1365] [INSPIRE].

[89] ATLAS collaboration, *Measurement of the Z/γ^* boson transverse momentum distribution in pp collisions at $\sqrt{s} = 7$ TeV with the ATLAS detector*, *JHEP* **09** (2014) 145 [arXiv:1406.3660] [INSPIRE].

[90] H.-L. Lai et al., *New parton distributions for collider physics*, *Phys. Rev. D* **82** (2010) 074024 [arXiv:1007.2241] [INSPIRE].

[91] J. Pumplin et al., *New generation of parton distributions with uncertainties from global QCD analysis*, *JHEP* **07** (2002) 012 [hep-ph/0201195] [INSPIRE].

[92] S. Alioli, P. Nason, C. Oleari and E. Re, *NLO Higgs boson production via gluon fusion matched with shower in POWHEG*, *JHEP* **04** (2009) 002 [arXiv:0812.0578] [INSPIRE].

JHEP10(2025)093

[93] P. Nason and C. Oleari, *NLO Higgs boson production via vector-boson fusion matched with shower in POWHEG*, *JHEP* **02** (2010) 037 [arXiv:0911.5299] [INSPIRE].

[94] ATLAS collaboration, *The ATLAS simulation infrastructure*, *Eur. Phys. J. C* **70** (2010) 823 [arXiv:1005.4568] [INSPIRE].

[95] GEANT4 collaboration, *GEANT4 — a simulation toolkit*, *Nucl. Instrum. Meth. A* **506** (2003) 250 [INSPIRE].

[96] ATLAS collaboration, *The simulation principle and performance of the ATLAS fast calorimeter simulation FastCaloSim*, ATL-PHYS-PUB-2010-013, CERN, Geneva, Switzerland (2010).

[97] ATLAS collaboration, *Vertex reconstruction performance of the ATLAS detector at $\sqrt{s} = 13$ TeV*, ATL-PHYS-PUB-2015-026, CERN, Geneva, Switzerland (2015).

[98] ATLAS collaboration, *Electron and photon performance measurements with the ATLAS detector using the 2015–2017 LHC proton-proton collision data*, 2019 *JINST* **14** P12006 [arXiv:1908.00005] [INSPIRE].

[99] ATLAS collaboration, *Muon reconstruction and identification efficiency in ATLAS using the full run 2 pp collision data set at $\sqrt{s} = 13$ TeV*, *Eur. Phys. J. C* **81** (2021) 578 [arXiv:2012.00578] [INSPIRE].

[100] ATLAS collaboration, *Studies of the muon momentum calibration and performance of the ATLAS detector with pp collisions at $\sqrt{s} = 13$ TeV*, *Eur. Phys. J. C* **83** (2023) 686 [arXiv:2212.07338] [INSPIRE].

[101] ATLAS collaboration, *Evidence for the associated production of the Higgs boson and a top quark pair with the ATLAS detector*, *Phys. Rev. D* **97** (2018) 072003 [arXiv:1712.08891] [INSPIRE].

[102] ATLAS collaboration, *Electron reconstruction and identification in the ATLAS experiment using the 2015 and 2016 LHC proton-proton collision data at $\sqrt{s} = 13$ TeV*, *Eur. Phys. J. C* **79** (2019) 639 [arXiv:1902.04655] [INSPIRE].

[103] ATLAS collaboration, *Jet reconstruction and performance using particle flow with the ATLAS detector*, *Eur. Phys. J. C* **77** (2017) 466 [arXiv:1703.10485] [INSPIRE].

[104] M. Cacciari, G.P. Salam and G. Soyez, *The anti-k_t jet clustering algorithm*, *JHEP* **04** (2008) 063 [arXiv:0802.1189] [INSPIRE].

[105] M. Cacciari, G.P. Salam and G. Soyez, *FastJet user manual*, *Eur. Phys. J. C* **72** (2012) 1896 [arXiv:1111.6097] [INSPIRE].

[106] ATLAS collaboration, *Jet energy scale and resolution measured in proton–proton collisions at $\sqrt{s} = 13$ TeV with the ATLAS detector*, *Eur. Phys. J. C* **81** (2021) 689 [arXiv:2007.02645] [INSPIRE].

[107] ATLAS collaboration, *Performance of pile-up mitigation techniques for jets in pp collisions at $\sqrt{s} = 8$ TeV using the ATLAS detector*, *Eur. Phys. J. C* **76** (2016) 581 [arXiv:1510.03823] [INSPIRE].

[108] ATLAS collaboration, *Identification and rejection of pile-up jets at high pseudorapidity with the ATLAS detector*, *Eur. Phys. J. C* **77** (2017) 580 [*Erratum ibid.* **77** (2017) 712] [arXiv:1705.02211] [INSPIRE].

[109] ATLAS collaboration, *Selection of jets produced in 13 TeV proton-proton collisions with the ATLAS detector*, ATLAS-CONF-2015-029, CERN, Geneva, Switzerland (2015).

[110] ATLAS collaboration, *ATLAS flavour-tagging algorithms for the LHC run 2 pp collision dataset*, Eur. Phys. J. C **83** (2023) 681 [arXiv:2211.16345] [INSPIRE].

[111] ATLAS collaboration, *Identification of jets containing b-hadrons with recurrent neural networks at the ATLAS experiment*, ATL-PHYS-PUB-2017-003, CERN, Geneva, Switzerland (2017).

[112] ATLAS collaboration, *Reconstruction, energy calibration, and identification of hadronically decaying tau leptons in the ATLAS experiment for run-2 of the LHC*, ATL-PHYS-PUB-2015-045, CERN, Geneva, Switzerland (2015).

[113] ATLAS collaboration, *Measurement of the tau lepton reconstruction and identification performance in the ATLAS experiment using pp collisions at $\sqrt{s} = 13$ TeV*, ATLAS-CONF-2017-029, CERN, Geneva, Switzerland (2017).

[114] ATLAS collaboration, *Identification of hadronic tau lepton decays using neural networks in the ATLAS experiment*, ATL-PHYS-PUB-2019-033, CERN, Geneva, Switzerland (2019).

[115] ATLAS collaboration, *Reconstruction, identification, and calibration of hadronically decaying tau leptons with the ATLAS detector for the LHC run 3 and reprocessed run 2 data*, ATL-PHYS-PUB-2022-044, CERN, Geneva, Switzerland (2022).

[116] ATLAS collaboration, *Performance of missing transverse momentum reconstruction with the ATLAS detector using proton-proton collisions at $\sqrt{s} = 13$ TeV*, Eur. Phys. J. C **78** (2018) 903 [arXiv:1802.08168] [INSPIRE].

[117] T. Chen and C. Guestrin, *XGBoost: a scalable tree boosting system*, in *Proceedings of the 22nd ACM SIGKDD International Conference on Knowledge Discovery and Data Mining, KDD '16, (New York, NY, U.S.A.)*, Association for Computing Machinery, U.S.A. (2016), p. 785 [DOI:10.1145/2939672.2939785] [arXiv:1603.02754] [INSPIRE].

[118] ATLAS collaboration, *Measurement of event shapes at large momentum transfer with the ATLAS detector in pp collisions at $\sqrt{s} = 7$ TeV*, Eur. Phys. J. C **72** (2012) 2211 [arXiv:1206.2135] [INSPIRE].

[119] ATLAS collaboration, *Tools for estimating fake/non-prompt lepton backgrounds with the ATLAS detector at the LHC*, 2023 *JINST* **18** T11004 [arXiv:2211.16178] [INSPIRE].

[120] ATLAS collaboration, *The performance of missing transverse momentum reconstruction and its significance with the ATLAS detector using 140 fb^{-1} of $\sqrt{s} = 13$ TeV pp collisions*, Eur. Phys. J. C **85** (2025) 606 [arXiv:2402.05858] [INSPIRE].

[121] ATLAS collaboration, *ATLAS b-jet identification performance and efficiency measurement with $t\bar{t}$ events in pp collisions at $\sqrt{s} = 13$ TeV*, Eur. Phys. J. C **79** (2019) 970 [arXiv:1907.05120] [INSPIRE].

[122] ATLAS collaboration, *Measurement of the c-jet mistagging efficiency in $t\bar{t}$ events using pp collision data at $\sqrt{s} = 13$ TeV collected with the ATLAS detector*, Eur. Phys. J. C **82** (2022) 95 [arXiv:2109.10627] [INSPIRE].

[123] ATLAS collaboration, *Calibration of the light-flavour jet mistagging efficiency of the b-tagging algorithms with Z+jets events using 139 fb^{-1} of ATLAS proton–proton collision data at $\sqrt{s} = 13$ TeV*, Eur. Phys. J. C **83** (2023) 728 [arXiv:2301.06319] [INSPIRE].

[124] ATLAS collaboration, *Luminosity determination in pp collisions at $\sqrt{s} = 13$ TeV using the ATLAS detector at the LHC*, Eur. Phys. J. C **83** (2023) 982 [arXiv:2212.09379] [INSPIRE].

[125] ATLAS collaboration, *Studies on top-quark Monte Carlo modelling with Sherpa and MG5_aMC@NLO*, ATL-PHYS-PUB-2017-007, CERN, Geneva, Switzerland (2017).

[126] E. Bothmann, M. Schönherr and S. Schumann, *Reweighting QCD matrix-element and parton-shower calculations*, *Eur. Phys. J. C* **76** (2016) 590 [arXiv:1606.08753] [INSPIRE].

[127] N. Kidonakis, *Two-loop soft anomalous dimensions for single top quark associated production with a W^- or H^-*, *Phys. Rev. D* **82** (2010) 054018 [arXiv:1005.4451] [INSPIRE].

[128] F.A. Berends, H. Kuijf, B. Tausk and W.T. Giele, *On the production of a W and jets at hadron colliders*, *Nucl. Phys. B* **357** (1991) 32 [INSPIRE].

[129] ATLAS collaboration, *Study of ttbb and ttW background modelling for ttH analyses*, ATL-PHYS-PUB-2022-026, CERN, Geneva, Switzerland (2022) [INSPIRE].

[130] ATLAS collaboration, *Measurement of top-quark pair production in association with charm quarks in proton–proton collisions at $\sqrt{s} = 13$ TeV with the ATLAS detector*, *Phys. Lett. B* **860** (2025) 139177 [arXiv:2409.11305] [INSPIRE].

[131] ROOT collaboration, *HistFactory: a tool for creating statistical models for use with RooFit and RooStats*, CERN-OPEN-2012-016, New York U., New York, NY, U.S.A. (2012) [DOI:10.17181/CERN-OPEN-2012-016].

[132] R.J. Barlow and C. Beeston, *Fitting using finite Monte Carlo samples*, *Comput. Phys. Commun.* **77** (1993) 219 [INSPIRE].

[133] R.D. Cousins, *Generalization of chisquare goodness-offit test for binned data using saturated models, with application to histograms*, https://api.semanticscholar.org/CorpusID:5936965 (2013).

[134] A. Pinto et al., *Uncertainty components in profile likelihood fits*, *Eur. Phys. J. C* **84** (2024) 593 [arXiv:2307.04007] [INSPIRE].

[135] ATLAS collaboration, *ATLAS computing acknowledgements*, ATL-SOFT-PUB-2025-001, CERN, Geneva, Switzerland (2025).

[136] G.C. Fox and S. Wolfram, *Observables for the analysis of event shapes in e^+e^- annihilation and other processes*, *Phys. Rev. Lett.* **41** (1978) 1581 [INSPIRE].

[137] C. Bernaciak, M.S.A. Buschmann, A. Butter and T. Plehn, *Fox-Wolfram moments in Higgs physics*, *Phys. Rev. D* **87** (2013) 073014 [arXiv:1212.4436] [INSPIRE].

JHEP10(2025)093

The ATLAS collaboration

G. Aad[104], E. Aakvaag[17], B. Abbott[123], S. Abdelhameed[119a], K. Abeling[55], N.J. Abicht[49], S.H. Abidi[30], M. Aboelela[45], A. Aboulhorma[36e], H. Abramowicz[157], Y. Abulaiti[120], B.S. Acharya[69a,69b,m], A. Ackermann[63a], C. Adam Bourdarios[4], L. Adamczyk[87a], S.V. Addepalli[149], M.J. Addison[103], J. Adelman[118], A. Adiguzel[22c], T. Adye[137], A.A. Affolder[139], Y. Afik[40], M.N. Agaras[13], A. Aggarwal[102], C. Agheorghiesei[28c], F. Ahmadov[39,ad], S. Ahuja[97], X. Ai[143b], G. Aielli[76a,76b], A. Aikot[169], M. Ait Tamlihat[36e], B. Aitbenchikh[36a], M. Akbiyik[102], T.P.A. Åkesson[100], A.V. Akimov[151], D. Akiyama[174], N.N. Akolkar[25], S. Aktas[172], G.L. Alberghi[24b], J. Albert[171], U. Alberti[20], P. Albicocco[53], G.L. Albouy[60], S. Alderweireldt[52], Z.L. Alegria[124], M. Aleksa[37], I.N. Aleksandrov[39], C. Alexa[28b], T. Alexopoulos[10], F. Alfonsi[24b], M. Algren[56], M. Alhroob[173], B. Ali[135], H.M.J. Ali[93,w], S. Ali[32], S.W. Alibocus[94], M. Aliev[34c], G. Alimonti[71a], W. Alkakhi[55], C. Allaire[66], B.M.M. Allbrooke[152], J.S. Allen[103], J.F. Allen[52], P.P. Allport[21], A. Aloisio[72a,72b], F. Alonso[92], C. Alpigiani[142], Z.M.K. Alsolami[93], A. Alvarez Fernandez[102], M. Alves Cardoso[56], M.G. Alviggi[72a,72b], M. Aly[103], Y. Amaral Coutinho[83b], A. Ambler[106], C. Amelung[37], M. Amerl[103], C.G. Ames[111], T. Amezza[130], D. Amidei[108], B. Amini[54], K. Amirie[161], A. Amirkhanov[39], S.P. Amor Dos Santos[133a], K.R. Amos[169], D. Amperiadou[158], S. An[84], C. Anastopoulos[145], T. Andeen[11], J.K. Anders[94], A.C. Anderson[59], A. Andreazza[71a,71b], S. Angelidakis[9], A. Angerami[42], A.V. Anisenkov[39], A. Annovi[74a], C. Antel[37], E. Antipov[151], M. Antonelli[53], F. Anulli[75a], M. Aoki[84], T. Aoki[159], M.A. Aparo[152], L. Aperio Bella[48], M. Apicella[31], C. Appelt[157], A. Apyan[27], M. Arampatzi[10], S.J. Arbiol Val[88], C. Arcangeletti[53], A.T.H. Arce[51], J-F. Arguin[110], S. Argyropoulos[158], J.-H. Arling[48], O. Arnaez[4], H. Arnold[151], G. Artoni[75a,75b], H. Asada[113], K. Asai[121], S. Asatryan[179], N.A. Asbah[37], R.A. Ashby Pickering[173], A.M. Aslam[97], K. Assamagan[30], R. Astalos[29a], K.S.V. Astrand[100], S. Atashi[165], R.J. Atkin[34a], H. Atmani[36f], P.A. Atmasiddha[131], K. Augsten[135], A.D. Auriol[41], V.A. Austrup[103], A.S. Avad[96], G. Avolio[37], K. Axiotis[56], A. Azzam[13], D. Babal[29b], H. Bachacou[138], K. Bachas[158,q], A. Bachiu[35], E. Bachmann[50], M.J. Backes[63a], A. Badea[40], T.M. Baer[108], P. Bagnaia[75a,75b], M. Bahmani[19], D. Bahner[54], K. Bai[126], J.T. Baines[137], L. Baines[96], O.K. Baker[178], E. Bakos[16], D. Bakshi Gupta[8], L.E. Balabram Filho[83b], V. Balakrishnan[123], R. Balasubramanian[4], E.M. Baldin[38], P. Balek[87a], E. Ballabene[24b,24a], F. Balli[138], L.M. Baltes[63a], W.K. Balunas[33], J. Balz[102], I. Bamwidhi[119b], E. Banas[88], M. Bandieramonte[132], A. Bandyopadhyay[25], S. Bansal[25], L. Barak[157], M. Barakat[48], E.L. Barberio[107], D. Barberis[18b], M. Barbero[104], M.Z. Barel[117], T. Barillari[112], M-S. Barisits[37], T. Barklow[149], P. Baron[136], D.A. Baron Moreno[103], A. Baroncelli[62], A.J. Barr[129], J.D. Barr[98], F. Barreiro[101], J. Barreiro Guimarães da Costa[14], M.G. Barros Teixeira[133a], S. Barsov[38], F. Bartels[63a], R. Bartoldus[149], A.E. Barton[93], P. Bartos[29a], M. Baselga[49], S. Bashiri[88], A. Bassalat[66,b], M.J. Basso[162a], S. Bataju[45], R. Bate[170], R.L. Bates[59], S. Batlamous[101], M. Battaglia[139], D. Battulga[19], M. Bauce[75a,75b], M. Bauer[79], P. Bauer[25], L.T. Bayer[48], L.T. Bazzano Hurrell[31], J.B. Beacham[112], T. Beau[130], J.Y. Beaucamp[92], P.H. Beauchemin[164], P. Bechtle[25], H.P. Beck[20,p], K. Becker[173], A.J. Beddall[82],

JHEP10(2025)093

V.A. Bednyakov[39], C.P. Bee[151], L.J. Beemster[16], M. Begalli[83d], M. Begel[30], J.K. Behr[48], J.F. Beirer[37], F. Beisiegel[25], M. Belfkir[119b], G. Bella[157], L. Bellagamba[24b], A. Bellerive[35], C.D. Bellgraph[68], P. Bellos[21], K. Beloborodov[38], I. Benaoumeur[21], D. Benchekroun[36a], F. Bendebba[36a], Y. Benhammou[157], K.C. Benkendorfer[61], L. Beresford[48], M. Beretta[53], E. Bergeaas Kuutmann[167], N. Berger[4], B. Bergmann[135], J. Beringer[18a], G. Bernardi[5], C. Bernius[149], F.U. Bernlochner[25], A. Berrocal Guardia[13], T. Berry[97], P. Berta[136], A. Berthold[50], A. Berti[133a], R. Bertrand[104], S. Bethke[112], A. Betti[75a,75b], A.J. Bevan[96], L. Bezio[56], N.K. Bhalla[54], S. Bharthuar[112], S. Bhatta[151], P. Bhattarai[149], Z.M. Bhatti[120], K.D. Bhide[54], V.S. Bhopatkar[124], R.M. Bianchi[132], G. Bianco[24b,24a], O. Biebel[111], M. Biglietti[77a], C.S. Billingsley[45], Y. Bimgdi[36f], M. Bindi[55], A. Bingham[177], A. Bingul[22b], C. Bini[75a,75b], G.A. Bird[33], M. Birman[175], M. Biros[136], S. Biryukov[152], T. Bisanz[49], E. Bisceglie[24b,24a], J.P. Biswal[137], D. Biswas[147], I. Bloch[48], A. Blue[59], U. Blumenschein[96], V.S. Bobrovnikov[39], L. Boccardo[57b,57a], M. Boehler[54], B. Boehm[172], D. Bogavac[13], A.G. Bogdanchikov[38], L.S. Boggia[130], V. Boisvert[97], P. Bokan[37], T. Bold[87a], M. Bomben[5], M. Bona[96], M. Boonekamp[138], A.G. Borbély[59], I.S. Bordulev[38], G. Borissov[93], D. Bortoletto[129], D. Boscherini[24b], M. Bosman[13], K. Bouaouda[36a], N. Bouchhar[169], L. Boudet[4], J. Boudreau[132], E.V. Bouhova-Thacker[93], D. Boumediene[41], R. Bouquet[57b,57a], A. Boveia[122], J. Boyd[37], D. Boye[30], I.R. Boyko[39], L. Bozianu[56], J. Bracinik[21], N. Brahimi[4], G. Brandt[177], O. Brandt[33], B. Brau[105], J.E. Brau[126], R. Brener[175], L. Brenner[117], R. Brenner[167], S. Bressler[175], G. Brianti[78a,78b], D. Britton[59], D. Britzger[112], I. Brock[25], R. Brock[109], G. Brooijmans[42], A.J. Brooks[68], E.M. Brooks[162b], E. Brost[30], L.M. Brown[171,162a], L.E. Bruce[61], T.L. Bruckler[129], P.A. Bruckman de Renstrom[88], B. Brüers[48], A. Bruni[24b], G. Bruni[24b], D. Brunner[47a,47b], M. Bruschi[24b], N. Bruscino[75a,75b], T. Buanes[17], Q. Buat[142], D. Buchin[112], A.G. Buckley[59], O. Bulekov[82], B.A. Bullard[149], S. Burdin[94], C.D. Burgard[49], A.M. Burger[91], B. Burghgrave[8], O. Burlayenko[54], J. Burleson[168], J.C. Burzynski[148], E.L. Busch[42], V. Büscher[102], P.J. Bussey[59], J.M. Butler[26], C.M. Buttar[59], J.M. Butterworth[98], W. Buttinger[137], C.J. Buxo Vazquez[109], A.R. Buzykaev[39], S. Cabrera Urbán[169], L. Cadamuro[66], H. Cai[37], Y. Cai[24b,114c,24a], Y. Cai[114a], V.M.M. Cairo[37], O. Cakir[3a], N. Calace[37], P. Calafiura[18a], G. Calderini[130], P. Calfayan[35], L. Calic[100], G. Callea[59], L.P. Caloba[83b], D. Calvet[41], S. Calvet[41], R. Camacho Toro[130], S. Camarda[37], D. Camarero Munoz[27], P. Camarri[76a,76b], C. Camincher[171], M. Campanelli[98], A. Camplani[43], V. Canale[72a,72b], A.C. Canbay[3a], E. Canonero[97], J. Cantero[169], Y. Cao[168], F. Capocasa[27], M. Capua[44b,44a], A. Carbone[71a,71b], R. Cardarelli[76a], J.C.J. Cardenas[8], M.P. Cardiff[27], G. Carducci[44b,44a], T. Carli[37], G. Carlino[72a], J.I. Carlotto[13], B.T. Carlson[132,r], E.M. Carlson[171], J. Carmignani[94], L. Carminati[71a,71b], A. Carnelli[4], M. Carnesale[37], S. Caron[116], E. Carquin[140g], I.B. Carr[107], S. Carrá[73a,73b], G. Carratta[24b,24a], C. Carrion Martinez[169], A.M. Carroll[126], M.P. Casado[13,h], P. Casolaro[72a,72b], M. Caspar[48], W.R. Castiglioni[40], F.L. Castillo[4], L. Castillo Garcia[13], V. Castillo Gimenez[169], N.F. Castro[133a,133e], A. Catinaccio[37], J.R. Catmore[128], T. Cavaliere[4], V. Cavaliere[30], L.J. Caviedes Betancourt[23b], E. Celebi[82], S. Cella[37], V. Cepaitis[56], K. Cerny[125], A.S. Cerqueira[83a], A. Cerri[74a,74b,am], L. Cerrito[76a,76b], F. Cerutti[18a], B. Cervato[71a,71b],

A. Cervelli[24b], G. Cesarini[53], S.A. Cetin[82], P.M. Chabrillat[130], R. Chakkappai[66], S. Chakraborty[173], A. Chambers[61], J. Chan[18a], W.Y. Chan[159], J.D. Chapman[33], E. Chapon[138], B. Chargeishvili[155b], D.G. Charlton[21], C. Chauhan[136], Y. Che[114a], S. Chekanov[6], S.V. Chekulaev[162a], G.A. Chelkov[39,a], B. Chen[157], B. Chen[171], H. Chen[114a], H. Chen[30], J. Chen[144a], J. Chen[148], M. Chen[129], S. Chen[89], S.J. Chen[114a], X. Chen[144a], X. Chen[15,ah], Z. Chen[62], C.L. Cheng[176], H.C. Cheng[64a], S. Cheong[149], A. Cheplakov[39], E. Cherepanova[117], R. Cherkaoui El Moursli[36e], E. Cheu[7], K. Cheung[65], L. Chevalier[138], V. Chiarella[53], G. Chiarelli[74a], G. Chiodini[70a], A.S. Chisholm[21], A. Chitan[28b], M. Chitishvili[169], M.V. Chizhov[39,s], K. Choi[11], Y. Chou[142], E.Y.S. Chow[116], K.L. Chu[175], M.C. Chu[64a], X. Chu[14,114c], Z. Chubinidze[53], J. Chudoba[134], J.J. Chwastowski[88], D. Cieri[112], K.M. Ciesla[87a], V. Cindro[95], A. Ciocio[18a], F. Cirotto[72a,72b], Z.H. Citron[175], M. Citterio[71a], D.A. Ciubotaru[28b], A. Clark[56], P.J. Clark[52], N. Clarke Hall[98], C. Clarry[161], S.E. Clawson[48], C. Clement[47a,47b], Y. Coadou[104], M. Cobal[69a,69c], A. Coccaro[57b], R.F. Coelho Barrue[133a], R. Coelho Lopes De Sa[105], S. Coelli[71a], L.S. Colangeli[161], B. Cole[42], P. Collado Soto[101], J. Collot[60], R. Coluccia[70a,70b], P. Conde Muiño[133a,133g], M.P. Connell[34c], S.H. Connell[34c], E.I. Conroy[129], M. Contreras Cossio[11], F. Conventi[72a,aj], A.M. Cooper-Sarkar[129], L. Corazzina[75a,75b], F.A. Corchia[24b,24a], A. Cordeiro Oudot Choi[142], L.D. Corpe[41], M. Corradi[75a,75b], F. Corriveau[106,ab], A. Cortes-Gonzalez[159], M.J. Costa[169], F. Costanza[4], D. Costanzo[145], J. Couthures[4], G. Cowan[97], K. Cranmer[176], L. Cremer[49], D. Cremonini[24b,24a], S. Crépé-Renaudin[60], F. Crescioli[130], T. Cresta[73a,73b], M. Cristinziani[147], M. Cristoforetti[78a,78b], V. Croft[117], G. Crosetti[44b,44a], A. Cueto[101], H. Cui[98], Z. Cui[7], B.M. Cunnett[152], W.R. Cunningham[59], F. Curcio[169], J.R. Curran[52], M.J. Da Cunha Sargedas De Sousa[57b,57a], J.V. Da Fonseca Pinto[83b], C. Da Via[103], W. Dabrowski[87a], T. Dado[37], S. Dahbi[154], T. Dai[108], D. Dal Santo[20], C. Dallapiccola[105], M. Dam[43], G. D'amen[30], V. D'Amico[111], J. Damp[102], J.R. Dandoy[35], M. D'Andrea[57b,57a], D. Dannheim[37], G. D'anniballe[74a,74b], M. Danninger[148], V. Dao[151], G. Darbo[57b], S.J. Das[30], F. Dattola[48], S. D'Auria[71a,71b], A. D'Avanzo[72a,72b], T. Davidek[136], J. Davidson[173], I. Dawson[96], K. De[8], C. De Almeida Rossi[161], R. De Asmundis[72a], N. De Biase[48], S. De Castro[24b,24a], N. De Groot[116], P. de Jong[117], H. De la Torre[118], A. De Maria[114a], A. De Salvo[75a], U. De Sanctis[76a,76b], F. De Santis[70a,70b], A. De Santo[152], J.B. De Vivie De Regie[60], J. Debevc[95], D.V. Dedovich[39], J. Degens[94], A.M. Deiana[45], J. Del Peso[101], L. Delagrange[130], F. Deliot[138], C.M. Delitzsch[49], M. Della Pietra[72a,72b], D. Della Volpe[56], A. Dell'Acqua[37], L. Dell'Asta[71a,71b], M. Delmastro[4], C.C. Delogu[102], P.A. Delsart[60], S. Demers[178], M. Demichev[39], S.P. Denisov[38], H. Denizli[22a,l], L. D'Eramo[41], D. Derendarz[88], F. Derue[130], P. Dervan[94,*], A.M. Desai[1], K. Desch[25], F.A. Di Bello[57b,57a], A. Di Ciaccio[76a,76b], L. Di Ciaccio[4], A. Di Domenico[75a,75b], C. Di Donato[72a,72b], A. Di Girolamo[37], G. Di Gregorio[37], A. Di Luca[78a,78b], B. Di Micco[77a,77b], R. Di Nardo[77a,77b], K.F. Di Petrillo[40], M. Diamantopoulou[35], F.A. Dias[117], M.A. Diaz[140a,140b], A.R. Didenko[39], M. Didenko[169], S.D. Diefenbacher[18a], E.B. Diehl[108], S. Díez Cornell[48], C. Diez Pardos[147], C. Dimitriadi[150], A. Dimitrievska[21], A. Dimri[151], Y. Ding[62], J. Dingfelder[25], T. Dingley[129], I-M. Dinu[28b], S.J. Dittmeier[63b], F. Dittus[37],

M. Divisek[136], B. Dixit[94], F. Djama[104], T. Djobava[155b], C. Doglioni[103,100], A. Dohnalova[29a], Z. Dolezal[136], K. Domijan[87a], K.M. Dona[40], M. Donadelli[83d], B. Dong[109], J. Donini[41], A. D'Onofrio[72a,72b], M. D'Onofrio[94], J. Dopke[137], A. Doria[72a], N. Dos Santos Fernandes[133a], I.A. Dos Santos Luz[83e], P. Dougan[103], M.T. Dova[92], A.T. Doyle[59], M.P. Drescher[55], E. Dreyer[175], I. Drivas-koulouris[10], M. Drnevich[120], D. Du[62], T.A. du Pree[117], Z. Duan[114a], M. Dubau[4], F. Dubinin[39], M. Dubovsky[29a], E. Duchovni[175], G. Duckeck[111], P.K. Duckett[98], O.A. Ducu[28b], D. Duda[52], A. Dudarev[37], M.M. Dudek[88], E.R. Duden[27], M. D'uffizi[103], L. Duflot[66], M. Dührssen[37], I. Duminica[28g], A.E. Dumitriu[28b], M. Dunford[63a], K. Dunne[47a,47b], A. Duperrin[104], H. Duran Yildiz[3a], A. Durglishvili[155b], G.I. Dyckes[18a], M. Dyndal[87a], B.S. Dziedzic[37], Z.O. Earnshaw[152], G.H. Eberwein[129], B. Eckerova[29a], S. Eggebrecht[55], E. Egidio Purcino De Souza[83e], G. Eigen[17], K. Einsweiler[18a], T. Ekelof[167], P.A. Ekman[100], S. El Farkh[36b], Y. El Ghazali[62], H. El Jarrari[37], A. El Moussaouy[36a], D. Elitez[37], M. Ellert[167], F. Ellinghaus[177], T.A. Elliot[97], N. Ellis[37], J. Elmsheuser[30], M. Elsawy[119a], M. Elsing[37], D. Emeliyanov[137], Y. Enari[84], S. Epari[110], D. Ernani Martins Neto[88], F. Ernst[37], M. Errenst[177], M. Escalier[66], C. Escobar[169], E. Etzion[157], G. Evans[133a,133b], H. Evans[68], L.S. Evans[48], A. Ezhilov[38], S. Ezzarqtouni[36a], F. Fabbri[24b,24a], L. Fabbri[24b,24a], G. Facini[98], V. Fadeyev[139], R.M. Fakhrutdinov[38], D. Fakoudis[102], S. Falciano[75a], L.F. Falda Ulhoa Coelho[133a], F. Fallavollita[112], G. Falsetti[44b,44a], J. Faltova[136], C. Fan[168], K.Y. Fan[64b], Y. Fan[14], Y. Fang[14,114c], M. Fanti[71a,71b], M. Faraj[69a,69b], Z. Farazpay[99], A. Farbin[8], A. Farilla[77a], K. Farman[154], T. Farooque[109], J.N. Farr[178], S.M. Farrington[137,52], F. Fassi[36e], D. Fassouliotis[9], L. Fayard[66], P. Federic[136], P. Federicova[134], O.L. Fedin[38,a], M. Feickert[176], L. Feligioni[104], D.E. Fellers[18a], C. Feng[143a], Y. Feng[14], Z. Feng[117], M.J. Fenton[165], L. Ferencz[48], B. Fernandez Barbadillo[93], P. Fernandez Martinez[67], M.J.V. Fernoux[104], J. Ferrando[93], A. Ferrari[167], P. Ferrari[117,116], R. Ferrari[73a], D. Ferrere[56], C. Ferretti[108], M.P. Fewell[1], D. Fiacco[75a,75b], F. Fiedler[102], P. Fiedler[135], S. Filimonov[39], M.S. Filip[28b,t], A. Filipčič[95], E.K. Filmer[162a], F. Filthaut[116], M.C.N. Fiolhais[133a,133c,c], L. Fiorini[169], W.C. Fisher[109], T. Fitschen[103], P.M. Fitzhugh[138], I. Fleck[147], P. Fleischmann[108], T. Flick[177], M. Flores[34d,ag], L.R. Flores Castillo[64a], L. Flores Sanz De Acedo[37], F.M. Follega[78a,78b], N. Fomin[33], J.H. Foo[161], A. Formica[138], A.C. Forti[103], E. Fortin[37], A.W. Fortman[18a], L. Foster[18a], L. Fountas[9,i], D. Fournier[66], H. Fox[93], P. Francavilla[74a,74b], S. Francescato[61], S. Franchellucci[56], M. Franchini[24b,24a], S. Franchino[63a], D. Francis[37], L. Franco[116], L. Franconi[48], M. Franklin[61], G. Frattari[27], Y.Y. Frid[157], J. Friend[59], N. Fritzsche[37], A. Froch[56], D. Froidevaux[37], J.A. Frost[129], Y. Fu[109], S. Fuenzalida Garrido[140g], M. Fujimoto[151], K.Y. Fung[64a], E. Furtado De Simas Filho[83e], M. Furukawa[159], J. Fuster[169], A. Gaa[55], A. Gabrielli[24b,24a], A. Gabrielli[161], P. Gadow[37], G. Gagliardi[57b,57a], L.G. Gagnon[18a], S. Gaid[85b], S. Galantzan[157], J. Gallagher[1], E.J. Gallas[129], A.L. Gallen[167], B.J. Gallop[137], K.K. Gan[122], S. Ganguly[159], Y. Gao[52], A. Garabaglu[142], F.M. Garay Walls[140a,140b], C. García[169], A. Garcia Alonso[117], A.G. Garcia Caffaro[178], J.E. García Navarro[169], M.A. Garcia Ruiz[23b], M. Garcia-Sciveres[18a], G.L. Gardner[131], R.W. Gardner[40], N. Garelli[164], R.B. Garg[149], J.M. Gargan[33], C.A. Garner[161], C.M. Garvey[34a], V.K. Gassmann[164], G. Gaudio[73a], V. Gautam[13], P. Gauzzi[75a,75b], J. Gavranovic[95], I.L. Gavrilenko[133a], A. Gavrilyuk[38], C. Gay[170], G. Gaycken[126], E.N. Gazis[10], A. Gekow[122], C. Gemme[57b], M.H. Genest[60], A.D. Gentry[115], S. George[97], T. Geralis[46], A.A. Gerwin[123], P. Gessinger-Befurt[37], M.E. Geyik[177], M. Ghani[173], K. Ghorbanian[96], A. Ghosal[147], A. Ghosh[165], A. Ghosh[7], B. Giacobbe[24b], S. Giagu[75a,75b], T. Giani[117], A. Giannini[62], S.M. Gibson[97], M. Gignac[139], D.T. Gil[87b], A.K. Gilbert[87a], B.J. Gilbert[42], D. Gillberg[35], G. Gilles[117], D.M. Gingrich[2,ai], M.P. Giordani[69a,69c], P.F. Giraud[138], G. Giugliarelli[69a,69c], D. Giugni[71a], F. Giuli[76a,76b], I. Gkialas[9,i], L.K. Gladilin[38], C. Glasman[101], M. Glazewska[20], R.M. Gleason[165], G. Glemža[48], M. Glisic[126], I. Gnesi[44b], Y. Go[30], M. Goblirsch-Kolb[37], B. Gocke[49], D. Godin[110], B. Gokturk[22a], S. Goldfarb[107], T. Golling[56], M.G.D. Gololo[34c], D. Golubkov[38], J.P. Gombas[109], A. Gomes[133a,133b], G. Gomes Da Silva[147], A.J. Gomez Delegido[37], R. Gonçalo[133a], L. Gonella[21], A. Gongadze[155c], F. Gonnella[21], J.L. Gonski[149], R.Y. González Andana[52], S. González de la Hoz[169], M.V. Gonzalez Rodrigues[48], R. Gonzalez Suarez[167], S. Gonzalez-Sevilla[56], L. Goossens[37], B. Gorini[37], E. Gorini[70a,70b], A. Gorišek[95], T.C. Gosart[131], A.T. Goshaw[51], M.I. Gostkin[39], S. Goswami[124], C.A. Gottardo[37], S.A. Gotz[111], M. Gouighri[36b], A.G. Goussiou[142], N. Govender[34c], R.P. Grabarczyk[129], I. Grabowska-Bold[87a], K. Graham[35], E. Gramstad[128], S. Grancagnolo[70a,70b], C.M. Grant[1], P.M. Gravila[28f], F.G. Gravili[70a,70b], H.M. Gray[18a], M. Greco[112], M.J. Green[1], C. Grefe[25], A.S. Grefsrud[17], I.M. Gregor[48], K.T. Greif[165], P. Grenier[149], S.G. Grewe[112], A.A. Grillo[139], K. Grimm[32], S. Grinstein[13,x], J.-F. Grivaz[66], E. Gross[175], J. Grosse-Knetter[55], L. Guan[108], G. Guerrieri[37], R. Guevara[128], R. Gugel[102], J.A.M. Guhit[108], A. Guida[19], E. Guilloton[173], S. Guindon[37], F. Guo[14,114c], J. Guo[144a], L. Guo[48], L. Guo[114b,v], Y. Guo[108], Y. Guo[42], A. Gupta[49], R. Gupta[132], S. Gupta[27], S. Gurbuz[25], S.S. Gurdasani[48], G. Gustavino[75a,75b], P. Gutierrez[123], L.F. Gutierrez Zagazeta[131], M. Gutsche[50], C. Gutschow[98], C. Gwenlan[129], C.B. Gwilliam[94], E.S. Haaland[128], A. Haas[120], M. Habedank[59], C. Haber[18a], H.K. Hadavand[8], A. Haddad[41], A. Hadef[50], A.I. Hagan[93], J.J. Hahn[147], E.H. Haines[98], M. Haleem[172], J. Haley[124], G.D. Hallewell[104], K. Hamano[171], H. Hamdaoui[167], M. Hamer[25], S.E.D. Hammoud[66], E.J. Hampshire[97], J. Han[143a], L. Han[114a], L. Han[62], S. Han[14], K. Hanagaki[84], M. Hance[139], D.A. Hangal[42], H. Hanif[148], M.D. Hank[131], J.B. Hansen[43], P.H. Hansen[43], D. Harada[56], T. Harenberg[177], S. Harkusha[179], M.L. Harris[105], Y.T. Harris[25], J. Harrison[13], N.M. Harrison[122], P.F. Harrison[173], M.L.E. Hart[98], N.M. Hartman[112], N.M. Hartmann[111], R.Z. Hasan[97,137], Y. Hasegawa[146], F. Haslbeck[129], S. Hassan[17], R. Hauser[109], M. Haviernik[136], C.M. Hawkes[21], R.J. Hawkings[37], Y. Hayashi[159], D. Hayden[109], C. Hayes[108], R.L. Hayes[117], C.P. Hays[129], J.M. Hays[96], H.S. Hayward[94], M. He[14,114c], Y. He[48], Y. He[98], N.B. Heatley[96], V. Hedberg[100], C. Heidegger[54], K.K. Heidegger[54], J. Heilman[35], S. Heim[48], T. Heim[18a], J.J. Heinrich[126], L. Heinrich[112], J. Hejbal[134], M. Helbig[50], A. Held[176], S. Hellesund[17], C.M. Helling[170], S. Hellman[47a,47b], A.M. Henriques Correia[37], H. Herde[100], Y. Hernández Jiménez[151], L.M. Herrmann[25], T. Herrmann[50], G. Herten[54], R. Hertenberger[111], L. Hervas[37], M.E. Hesping[102], N.P. Hessey[162a], J. Hessler[112], M. Hidaoui[36b], N. Hidic[136], E. Hill[161], T.S. Hillersoy[17], S.J. Hillier[21], J.R. Hinds[109],

F. Hinterkeuser[25], M. Hirose[127], S. Hirose[163], D. Hirschbuehl[177], T.G. Hitchings[103], B. Hiti[95], J. Hobbs[151], R. Hobincu[28e], N. Hod[175], A.M. Hodges[168], M.C. Hodgkinson[145], B.H. Hodkinson[129], A. Hoecker[37], D.D. Hofer[108], J. Hofer[169], J. Hofner[102], M. Holzbock[37], L.B.A.H. Hommels[33], V. Homsak[129], B.P. Honan[103], J.J. Hong[68], T.M. Hong[132], B.H. Hooberman[168], W.H. Hopkins[6], M.C. Hoppesch[168], Y. Horii[113], M.E. Horstmann[112], S. Hou[154], M.R. Housenga[168], J. Howarth[59], J. Hoya[6], M. Hrabovsky[125], T. Hryn'ova[4], P.J. Hsu[65], S.-C. Hsu[142], T. Hsu[66], M. Hu[18a], Q. Hu[62], S. Huang[33], X. Huang[14,114c], Y. Huang[136], Y. Huang[114b], Y. Huang[14], Z. Huang[66], Z. Hubacek[135], F. Huegging[25], T.B. Huffman[129], M. Hufnagel Maranha De Faria[83a], C.A. Hugli[48], M. Huhtinen[37], S.K. Huiberts[17], R. Hulsken[106], C.E. Hultquist[18a], D.L. Humphreys[105], N. Huseynov[12], J. Huston[109], J. Huth[61], L. Huth[48], R. Hyneman[7], G. Iacobucci[56], G. Iakovidis[30], L. Iconomidou-Fayard[66], J.P. Iddon[37], P. Iengo[72a,72b], R. Iguchi[159], Y. Iiyama[159], T. Iizawa[159], Y. Ikegami[84], D. Iliadis[158], N. Ilic[161], H. Imam[36a], G. Inacio Goncalves[83d], S.A. Infante Cabanas[140c], T. Ingebretsen Carlson[47a,47b], J.M. Inglis[96], G. Introzzi[73a,73b], M. Iodice[77a], V. Ippolito[75a,75b], R.K. Irwin[94], M. Ishino[159], W. Islam[176], C. Issever[19], S. Istin[22a,ao], K. Itabashi[84], H. Ito[174], R. Iuppa[78a,78b], A. Ivina[175], V. Izzo[72a], P. Jacka[135], P. Jackson[1], P. Jain[48], K. Jakobs[54], T. Jakoubek[175], J. Jamieson[59], W. Jang[159], S. Jankovych[136], M. Javurkova[105], P. Jawahar[103], L. Jeanty[126], J. Jejelava[155a,ae], P. Jenni[54,f], C.E. Jessiman[35], C. Jia[143a], H. Jia[170], J. Jia[151], X. Jia[112,114c], Z. Jia[114a], C. Jiang[52], Q. Jiang[64b], S. Jiggins[48], M. Jimenez Ortega[169], J. Jimenez Pena[13], S. Jin[114a], A. Jinaru[28b], O. Jinnouchi[141], P. Johansson[145], K.A. Johns[7], J.W. Johnson[139], F.A. Jolly[48], D.M. Jones[152], E. Jones[48], K.S. Jones[8], P. Jones[33], R.W.L. Jones[93], T.J. Jones[94], H.L. Joos[55], R. Joshi[122], J. Jovicevic[16], X. Ju[18a], J.J. Junggeburth[37], T. Junkermann[63a], A. Juste Rozas[13,x], M.K. Juzek[88], S. Kabana[140f], A. Kaczmarska[88], S.A. Kadir[149], M. Kado[112], H. Kagan[122], M. Kagan[149], A. Kahn[131], C. Kahra[102], T. Kaji[159], E. Kajomovitz[156], N. Kakati[175], N. Kakoty[13], I. Kalaitzidou[54], S. Kandel[8], N.J. Kang[139], D. Kar[34h], E. Karentzos[25], K. Karki[8], O. Karkout[117], S.N. Karpov[39], Z.M. Karpova[39], V. Kartvelishvili[93], A.N. Karyukhin[38], E. Kasimi[158], J. Katzy[48], S. Kaur[35], K. Kawade[146], M.P. Kawale[123], C. Kawamoto[89], T. Kawamoto[62], E.F. Kay[37], F.I. Kaya[164], S. Kazakos[109], V.F. Kazanin[38], J.M. Keaveney[34a], R. Keeler[171], G.V. Kehris[61], J.S. Keller[35], J.M. Kelly[171], J.J. Kempster[152], O. Kepka[134], J. Kerr[162b], B.P. Kerridge[137], B.P. Kerševan[95], L. Keszeghova[29a], R.A. Khan[132], A. Khanov[124], A.G. Kharlamov[38], T. Kharlamova[38], E.E. Khoda[142], M. Kholodenko[133a], T.J. Khoo[19], G. Khoriauli[172], Y. Khoulaki[36a], J. Khubua[155b,*], Y.A.R. Khwaira[130], B. Kibirige[34h], D. Kim[6], D.W. Kim[47a,47b], Y.K. Kim[40], N. Kimura[98], M.K. Kingston[55], A. Kirchhoff[55], C. Kirfel[25], F. Kirfel[25], J. Kirk[137], A.E. Kiryunin[112], S. Kita[163], O. Kivernyk[25], M. Klassen[164], C. Klein[35], L. Klein[172], M.H. Klein[45], S.B. Klein[56], U. Klein[94], A. Klimentov[30], T. Klioutchnikova[37], P. Kluit[117], S. Kluth[112], E. Kneringer[79], T.M. Knight[161], A. Knue[49], M. Kobel[50], D. Kobylianskii[175], S.F. Koch[129], M. Kocian[149], P. Kodyš[136], D.M. Koeck[126], T. Koffas[35], O. Kolay[50], I. Koletsou[4], T. Komarek[88], K. Köneke[55], A.X.Y. Kong[1], T. Kono[121], N. Konstantinidis[98], P. Kontaxakis[56], B. Konya[100],

JHEP10(2025)093

R. Kopeliansky[42], S. Koperny[87a], K. Korcyl[88], K. Kordas[158,d], A. Korn[98], S. Korn[55], I. Korolkov[13], N. Korotkova[38], B. Kortman[117], O. Kortner[112], S. Kortner[112], W.H. Kostecka[118], M. Kostov[29a], V.V. Kostyukhin[147], A. Kotsokechagia[37], A. Kotwal[51], A. Koulouris[37], A. Kourkoumeli-Charalampidi[73a,73b], C. Kourkoumelis[9], E. Kourlitis[112], O. Kovanda[126], R. Kowalewski[171], W. Kozanecki[126], A.S. Kozhin[38], V.A. Kramarenko[38], G. Kramberger[95], P. Kramer[25], M.W. Krasny[130], A. Krasznahorkay[105], A.C. Kraus[118], J.W. Kraus[177], J.A. Kremer[48], N.B. Krengel[147], T. Kresse[50], L. Kretschmann[177], J. Kretzschmar[94], P. Krieger[161], K. Krizka[21], K. Kroeninger[49], H. Kroha[112], J. Kroll[134], J. Kroll[131], K.S. Krowpman[109], U. Kruchonak[39], H. Krüger[25], N. Krumnack[81], M.C. Kruse[51], O. Kuchinskaia[39], S. Kuday[3a], S. Kuehn[37], R. Kuesters[54], T. Kuhl[48], V. Kukhtin[39], Y. Kulchitsky[39], S. Kuleshov[140d,140b], J. Kull[1], E.V. Kumar[111], M. Kumar[34h], N. Kumari[48], P. Kumari[162b], A. Kupco[134], A. Kupich[38], O. Kuprash[54], H. Kurashige[86], L.L. Kurchaninov[162a], O. Kurdysh[4], Y.A. Kurochkin[38], A. Kurova[38], M. Kuze[141], A.K. Kvam[105], J. Kvita[125], N.G. Kyriacou[142], C. Lacasta[169], F. Lacava[75a,75b], H. Lacker[19], D. Lacour[130], N.N. Lad[98], E. Ladygin[39], A. Lafarge[41], B. Laforge[130], T. Lagouri[178], F.Z. Lahbabi[36a], S. Lai[55,37], W.S. Lai[98], J.E. Lambert[171], S. Lammers[68], W. Lampl[7], C. Lampoudis[158,d], G. Lamprinoudis[102], A.N. Lancaster[118], E. Lançon[30], U. Landgraf[54], M.P.J. Landon[96], V.S. Lang[54], O.K.B. Langrekken[128], A.J. Lankford[165], F. Lanni[37], K. Lantzsch[25], A. Lanza[73a], M. Lanzac Berrocal[169], J.F. Laporte[138], T. Lari[71a], D. Larsen[17], L. Larson[11], F. Lasagni Manghi[24b], M. Lassnig[37], S.D. Lawlor[145], R. Lazaridou[165], M. Lazzaroni[71a,71b], E.T.T. Le[165], H.D.M. Le[109], E.M. Le Boulicaut[178], L.T. Le Pottier[18a], B. Leban[24b,24a], F. Ledroit-Guillon[60], T.F. Lee[162b], L.L. Leeuw[34c], M. Lefebvre[171], C. Leggett[18a], G. Lehmann Miotto[37], M. Leigh[56], W.A. Leight[105], W. Leinonen[116], A. Leisos[158,u], M.A.L. Leite[83c], C.E. Leitgeb[19], R. Leitner[136], K.J.C. Leney[45], T. Lenz[25], S. Leone[74a], C. Leonidopoulos[52], A. Leopold[150], J.H. Lepage Bourbonnais[35], R. Les[109], C.G. Lester[33], M. Levchenko[38], J. Levêque[4], L.J. Levinson[175], G. Levrini[24b,24a], M.P. Lewicki[88], C. Lewis[142], D.J. Lewis[4], L. Lewitt[145], A. Li[30], B. Li[143a], C. Li[108], C-Q. Li[112], H. Li[143a], H. Li[103], H. Li[15], H. Li[62], H. Li[143a], J. Li[144a], K. Li[14], L. Li[144a], R. Li[178], S. Li[14,114c], S. Li[144b,144a], T. Li[5], X. Li[106], Y. Li[14], Z. Li[159], Z. Li[14,114c], Z. Li[62], S. Liang[14,114c], Z. Liang[14], M. Liberatore[138], B. Liberti[76a], G.B. Libotte[83d], K. Lie[64c], J. Lieber Marin[83e], H. Lien[68], H. Lin[108], S.F. Lin[151], L. Linden[111], R.E. Lindley[7], J.H. Lindon[37], J. Ling[61], E. Lipeles[131], A. Lipniacka[17], A. Lister[170], J.D. Little[68], B. Liu[14], B.X. Liu[114b], D. Liu[144b,144a], D. Liu[139], E.H.L. Liu[21], J.K.K. Liu[120], K. Liu[144b], K. Liu[144b,144a], M. Liu[62], M.Y. Liu[62], P. Liu[14], Q. Liu[144b,142,144a], S. Liu[151], X. Liu[62], X. Liu[143a], Y. Liu[114b,114c], Y. Liu[168], Y.L. Liu[143a], Y.W. Liu[62], Z. Liu[66,k], S.L. Lloyd[96], E.M. Lobodzinska[48], P. Loch[7], E. Lodhi[161], K. Lohwasser[145], E. Loiacono[48], J.D. Lomas[21], J.D. Long[42], I. Longarini[165], R. Longo[168], A. Lopez Solis[13], N.A. Lopez-canelas[7], N. Lorenzo Martinez[4], A.M. Lory[111], M. Losada[119a], G. Löschcke Centeno[4], X. Lou[47a,47b], X. Lou[14,114c], A. Lounis[66], P.A. Love[93], M. Lu[66], S. Lu[131], Y.J. Lu[154], H.J. Lubatti[142], C. Luci[75a,75b], F.L. Lucio Alves[114a], F. Luehring[68], B.S. Lunday[131], O. Lundberg[150], J. Lunde[37], N.A. Luongo[6], M.S. Lutz[37], A.B. Lux[26], D. Lynn[30], R. Lysak[134], V. Lysenko[135], E. Lytken[100], V. Lyubushkin[39],

JHEP10(2025)093

T. Lyubushkina[39], M.M. Lyukova[151], M.Firdaus M. Soberi[52], H. Ma[30], K. Ma[62], L.L. Ma[143a], W. Ma[62], Y. Ma[124], J.C. MacDonald[102], P.C. Machado De Abreu Farias[83e], D. Macina[37], R. Madar[41], T. Madula[98], J. Maeda[86], T. Maeno[30], P.T. Mafa[34c,j], H. Maguire[145], M. Maheshwari[33], V. Maiboroda[66], A. Maio[133a,133b,133d], K. Maj[87a], O. Majersky[48], S. Majewski[126], R. Makhmanazarov[38], N. Makovec[66], V. Maksimovic[16], B. Malaescu[130], J. Malamant[128], Pa. Malecki[88], V.P. Maleev[38], F. Malek[60,o], M. Mali[95], D. Malito[97], U. Mallik[80,*], A. Maloizel[5], S. Maltezos[10], A. Malvezzi Lopes[83d], S. Malyukov[39], J. Mamuzic[95], G. Mancini[53], M.N. Mancini[27], G. Manco[73a,73b], J.P. Mandalia[96], S.S. Mandarry[152], I. Mandić[95], L. Manhaes de Andrade Filho[83a], I.M. Maniatis[175], J. Manjarres Ramos[91], D.C. Mankad[175], A. Mann[111], T. Manoussos[37], M.N. Mantinan[40], S. Manzoni[37], L. Mao[144a], X. Mapekula[34c], A. Marantis[158], R.R. Marcelo Gregorio[96], G. Marchiori[5], C. Marcon[71a], E. Maricic[16], M. Marinescu[48], S. Marium[48], M. Marjanovic[123], A. Markhoos[54], M. Markovitch[66], M.K. Maroun[105], M.C. Marr[148], G.T. Marsden[103], E.J. Marshall[93], Z. Marshall[18a], S. Marti-Garcia[169], J. Martin[98], T.A. Martin[137], V.J. Martin[52], B. Martin dit Latour[17], L. Martinelli[75a,75b], M. Martinez[13,x], P. Martinez Agullo[169], V.I. Martinez Outschoorn[105], P. Martinez Suarez[37], S. Martin-Haugh[137], G. Martinovicova[136], V.S. Martoiu[28b], A.C. Martyniuk[98], A. Marzin[37], D. Mascione[78a,78b], L. Masetti[102], J. Masik[103], A.L. Maslennikov[39], S.L. Mason[42], P. Massarotti[72a,72b], P. Mastrandrea[74a,74b], A. Mastroberardino[44b,44a], T. Masubuchi[127], T.T. Mathew[126], J. Matousek[136], D.M. Mattern[49], J. Maurer[28b], T. Maurin[59], A.J. Maury[66], B. Maček[95], C. Mavungu Tsava[104], D.A. Maximov[38], A.E. May[103], E. Mayer[41], R. Mazini[34h], I. Maznas[118], S.M. Mazza[139], E. Mazzeo[37], J.P. Mc Gowan[171], S.P. Mc Kee[108], C.A. Mc Lean[6], C.C. McCracken[170], E.F. McDonald[107], A.E. McDougall[117], L.F. Mcelhinney[93], J.A. Mcfayden[152], R.P. McGovern[131], R.P. Mckenzie[34h], T.C. Mclachlan[48], D.J. Mclaughlin[98], S.J. McMahon[137], C.M. Mcpartland[94], R.A. McPherson[171,ab], S. Mehlhase[111], A. Mehta[94], D. Melini[169], B.R. Mellado Garcia[34h], A.H. Melo[55], F. Meloni[48], A.M. Mendes Jacques Da Costa[103], L. Meng[93], S. Menke[112], M. Mentink[37], E. Meoni[44b,44a], G. Mercado[118], S. Merianos[158], C. Merlassino[69a,69c], C. Meroni[71a,71b], J. Metcalfe[6], A.S. Mete[6], E. Meuser[102], C. Meyer[68], J-P. Meyer[138], Y. Miao[114a], R.P. Middleton[137], M. Mihovilovic[66], L. Mijović[52], G. Mikenberg[175], M. Mikestikova[134], M. Mikuž[95], H. Mildner[102], A. Milic[37], D.W. Miller[40], E.H. Miller[149], A. Milov[175], D.A. Milstead[47a,47b], T. Min[114a], A.A. Minaenko[38], I.A. Minashvili[155b], A.I. Mincer[120], B. Mindur[87a], M. Mineev[39], Y. Mino[89], L.M. Mir[13], M. Miralles Lopez[59], M. Mironova[18a], M. Missio[41], A. Mitra[173], V.A. Mitsou[169], Y. Mitsumori[113], O. Miu[161], P.S. Miyagawa[96], T. Mkrtchyan[37], M. Mlinarevic[98], T. Mlinarevic[98], M. Mlynarikova[136], L. Mlynarska[87a], C. Mo[144a], S. Mobius[20], M.H. Mohamed Farook[115], S. Mohapatra[42], S. Mohiuddin[124], G. Mokgatitswane[34h], L. Moleri[175], U. Molinatti[129], L.G. Mollier[20], B. Mondal[134], S. Mondal[135], K. Mönig[48], E. Monnier[104], L. Monsonis Romero[169], J. Montejo Berlingen[13], A. Montella[47a,47b], M. Montella[122], F. Montereali[77a,77b], F. Monticelli[92], S. Monzani[69a,69c], A. Morancho Tarda[43], N. Morange[66], A.L. Moreira De Carvalho[48], M. Moreno Llácer[169], C. Moreno Martinez[56], J.M. Moreno Perez[23b], P. Morettini[57b], S. Morgenstern[37], M. Morii[61], M. Morinaga[159],

M. Moritsu[90], F. Morodei[75a,75b], P. Moschovakos[37], B. Moser[54], M. Mosidze[155b], T. Moskalets[45], P. Moskvitina[116], J. Moss[32], P. Moszkowicz[87a], A. Moussa[36d], Y. Moyal[175], H. Moyano Gomez[13], E.J.W. Moyse[105], T.G. Mroz[88], O. Mtintsilana[34h], S. Muanza[104], M. Mucha[25], J. Mueller[132], R. Müller[37], G.A. Mullier[167], A.J. Mullin[33], J.J. Mullin[51], A.C. Mullins[45], A.E. Mulski[61], D.P. Mungo[161], D. Munoz Perez[169], F.J. Munoz Sanchez[103], W.J. Murray[173,137], M. Muškinja[95], C. Mwewa[48], A.G. Myagkov[38,a], A.J. Myers[8], G. Myers[108], M. Myska[135], B.P. Nachman[149], K. Nagai[129], K. Nagano[84], R. Nagasaka[159], J.L. Nagle[30,al], E. Nagy[104], A.M. Nairz[37], Y. Nakahama[84], K. Nakamura[84], K. Nakkalil[5], A. Nandi[63b], H. Nanjo[127], E.A. Narayanan[45], Y. Narukawa[159], I. Naryshkin[38], L. Nasella[71a,71b], S. Nasri[119b], C. Nass[25], G. Navarro[23a], A. Nayaz[19], P.Y. Nechaeva[38], S. Nechaeva[24b,24a], F. Nechansky[134], L. Nedic[129], T.J. Neep[21], A. Negri[73a,73b], M. Negrini[24b], C. Nellist[117], C. Nelson[106], K. Nelson[108], S. Nemecek[134], M. Nessi[37,g], M.S. Neubauer[168], J. Newell[94], P.R. Newman[21], Y.W.Y. Ng[168], B. Ngair[119a], H.D.N. Nguyen[110], J.D. Nichols[123], R.B. Nickerson[129], R. Nicolaidou[138], J. Nielsen[139], M. Niemeyer[55], J. Niermann[37], N. Nikiforou[37], V. Nikolaenko[38,a], I. Nikolic-Audit[130], P. Nilsson[30], I. Ninca[48], G. Ninio[157], A. Nisati[75a], R. Nisius[112], N. Nitika[175], J-E. Nitschke[50], E.K. Nkadimeng[34b], T. Nobe[159], D. Noll[18a], T. Nommensen[153], M.B. Norfolk[145], B.J. Norman[35], L.C. Nosler[18a], M. Noury[36a], J. Novak[95], T. Novak[95], R. Novotny[135], L. Nozka[125], K. Ntekas[165], D. Ntounis[149], N.M.J. Nunes De Moura Junior[83b], J. Ocariz[130], I. Ochoa[133a], S. Oerdek[48,y], J.T. Offermann[40], A. Ogrodnik[88], A. Oh[103], C.C. Ohm[150], H. Oide[84], M.L. Ojeda[37], Y. Okumura[159], L.F. Oleiro Seabra[133a], I. Oleksiyuk[56], G. Oliveira Correa[13], D. Oliveira Damazio[30], J.L. Oliver[165], R. Omar[68], Ö.O. Öncel[54], A.P. O'Neill[20], A. Onofre[133a,133e,e], P.U.E. Onyisi[11], M.J. Oreglia[40], D. Orestano[77a,77b], R. Orlandini[77a,77b], R.S. Orr[161], L.M. Osojnak[42], Y. Osumi[113], G. Otero y Garzon[31], H. Otono[90], M. Ouchrif[36d], F. Ould-Saada[128], T. Ovsiannikova[142], M. Owen[59], R.E. Owen[137], V.E. Ozcan[22a], F. Ozturk[88], N. Ozturk[8], S. Ozturk[82], H.A. Pacey[129], K. Pachal[162a], A. Pacheco Pages[13], C. Padilla Aranda[13], G. Padovano[75a,75b], S. Pagan Griso[18a], G. Palacino[68], A. Palazzo[70a,70b], J. Pampel[25], J. Pan[178], T. Pan[64a], D.K. Panchal[11], C.E. Pandini[60], J.G. Panduro Vazquez[137], H.D. Pandya[1], H. Pang[138], P. Pani[48], G. Panizzo[69a,69c], L. Panwar[130], L. Paolozzi[56], S. Parajuli[168], A. Paramonov[6], C. Paraskevopoulos[53], D. Paredes Hernandez[64b], A. Pareti[73a,73b], K.R. Park[42], T.H. Park[112], F. Parodi[57b,57a], J.A. Parsons[42], U. Parzefall[54], B. Pascual Dias[41], L. Pascual Dominguez[101], E. Pasqualucci[75a], S. Passaggio[57b], F. Pastore[97], P. Patel[88], U.M. Patel[51], J.R. Pater[103], T. Pauly[37], F. Pauwels[136], C.I. Pazos[164], M. Pedersen[128], R. Pedro[133a], S.V. Peleganchuk[38], O. Penc[134], S. Peng[15], G.D. Penn[178], K.E. Penski[111], M. Penzin[38], B.S. Peralva[83d], A.P. Pereira Peixoto[142], L. Pereira Sanchez[149], D.V. Perepelitsa[30,al], G. Perera[105], E. Perez Codina[37], M. Perganti[10], H. Pernegger[37], S. Perrella[75a,75b], K. Peters[48], R.F.Y. Peters[103], B.A. Petersen[37], T.C. Petersen[43], E. Petit[104], V. Petousis[135], A.R. Petri[71a,71b], C. Petridou[158,d], T. Petru[136], A. Petrukhin[147], M. Pettee[18a], A. Petukhov[82], K. Petukhova[37], R. Pezoa[140g], L. Pezzotti[24b,24a], G. Pezzullo[178], L. Pfaffenbichler[37], A.J. Pfleger[79], T.M. Pham[176], T. Pham[107], P.W. Phillips[137], G. Piacquadio[151], E. Pianori[18a], F. Piazza[126],

JHEP10(2025)093

R. Piegaia[31], D. Pietreanu[28b], A.D. Pilkington[103], M. Pinamonti[69a,69c], J.L. Pinfold[2], B.C. Pinheiro Pereira[133a], J. Pinol Bel[13], A.E. Pinto Pinoargote[130], L. Pintucci[69a,69c], K.M. Piper[152], A. Pirttikoski[56], D.A. Pizzi[35], L. Pizzimento[64b], A. Plebani[33], M.-A. Pleier[30], V. Pleskot[136], E. Plotnikova[39], G. Poddar[96], R. Poettgen[100], L. Poggioli[130], S. Polacek[136], G. Polesello[73a], A. Poley[148], A. Polini[24b], C.S. Pollard[173], Z.B. Pollock[122], E. Pompa Pacchi[123], N.I. Pond[98], D. Ponomarenko[68], L. Pontecorvo[37], S. Popa[28a], G.A. Popeneciu[28d], A. Poreba[37], D.M. Portillo Quintero[162a], S. Pospisil[135], M.A. Postill[145], P. Postolache[28c], K. Potamianos[173], P.A. Potepa[87a], I.N. Potrap[39], C.J. Potter[33], H. Potti[153], J. Poveda[169], M.E. Pozo Astigarraga[37], R. Pozzi[37], A. Prades Ibanez[76a,76b], S.R. Pradhan[145], J. Pretel[171], D. Price[103], M. Primavera[70a], L. Primomo[69a,69c], M.A. Principe Martin[101], R. Privara[125], T. Procter[87b], M.L. Proffitt[142], N. Proklova[131], K. Prokofiev[64c], G. Proto[112], J. Proudfoot[6], M. Przybycien[87a], W.W. Przygoda[87b], A. Psallidas[46], J.E. Puddefoot[145], D. Pudzha[53], H.I. Purnell[1], D. Pyatiizbyantseva[116], J. Qian[108], R. Qian[109], D. Qichen[129], Y. Qin[13], T. Qiu[52], A. Quadt[55], M. Queitsch-Maitland[103], G. Quetant[56], R.P. Quinn[170], G. Rabanal Bolanos[61], D. Rafanoharana[112], F. Raffaeli[76a,76b], F. Ragusa[71a,71b], J.L. Rainbolt[40], S. Rajagopalan[30], E. Ramakoti[39], L. Rambelli[57b,57a], I.A. Ramirez-Berend[35], K. Ran[48,114c], D.S. Rankin[131], N.P. Rapheeha[34h], H. Rasheed[28b], D.F. Rassloff[63a], A. Rastogi[18a], S. Rave[102], S. Ravera[57b,57a], B. Ravina[37], I. Ravinovich[175], M. Raymond[37], A.L. Read[128], N.P. Readioff[145], D.M. Rebuzzi[73a,73b], A.S. Reed[59], K. Reeves[27], J.A. Reidelsturz[177], D. Reikher[37], A. Rej[49], C. Rembser[37], H. Ren[62], M. Renda[28b], F. Renner[48], A.G. Rennie[59], M. Repik[56], A.L. Rescia[57b,57a], S. Resconi[71a], M. Ressegotti[57b,57a], S. Rettie[117], W.F. Rettie[35], M.M. Revering[33], E. Reynolds[18a], O.L. Rezanova[39], P. Reznicek[136], H. Riani[36d], N. Ribaric[51], B. Ricci[69a,69c], E. Ricci[78a,78b], R. Richter[112], S. Richter[47a,47b], E. Richter-Was[87b], M. Ridel[130], S. Ridouani[36d], P. Rieck[120], P. Riedler[37], E.M. Riefel[47a,47b], J.O. Rieger[117], M. Rijssenbeek[151], M. Rimoldi[37], L. Rinaldi[24b,24a], P. Rincke[167,55], G. Ripellino[167], I. Riu[13], J.C. Rivera Vergara[171], F. Rizatdinova[124], E. Rizvi[96], B.R. Roberts[18a], S.S. Roberts[139], D. Robinson[33], M. Robles Manzano[102], A. Robson[59], A. Rocchi[76a,76b], C. Roda[74a,74b], S. Rodriguez Bosca[37], Y. Rodriguez Garcia[23a], A.M. Rodríguez Vera[118], S. Roe[37], J.T. Roemer[37], O. Røhne[128], R.A. Rojas[37], C.P.A. Roland[130], A. Romaniouk[79], E. Romano[73a,73b], M. Romano[24b], A.C. Romero Hernandez[168], N. Rompotis[94], L. Roos[130], S. Rosati[75a], B.J. Rosser[40], E. Rossi[129], E. Rossi[72a,72b], L.P. Rossi[61], L. Rossini[54], R. Rosten[122], M. Rotaru[28b], B. Rottler[54], D. Rousseau[66], D. Rousso[48], S. Roy-Garand[161], A. Rozanov[104], Z.M.A. Rozario[59], Y. Rozen[156], A. Rubio Jimenez[169], V.H. Ruelas Rivera[19], T.A. Ruggeri[1], A. Ruggiero[129], A. Ruiz-Martinez[169], A. Rummler[37], Z. Rurikova[54], N.A. Rusakovich[39], S. Ruscelli[49], H.L. Russell[171], G. Russo[75a,75b], J.P. Rutherfoord[7], S. Rutherford Colmenares[33], M. Rybar[136], P. Rybczynski[87a], A. Ryzhov[45], J.A. Sabater Iglesias[56], H.F-W. Sadrozinski[139], F. Safai Tehrani[75a], S. Saha[1], M. Sahinsoy[82], B. Sahoo[175], A. Saibel[169], B.T. Saifuddin[123], M. Saimpert[138], G.T. Saito[83c], M. Saito[159], T. Saito[159], A. Sala[71a,71b], A. Salnikov[149], J. Salt[169], A. Salvador Salas[157], F. Salvatore[152], A. Salzburger[37], D. Sammel[54], E. Sampson[93], D. Sampsonidis[158,d], D. Sampsonidou[126], M.A.A. Samy[59], J. Sánchez[169],

V. Sanchez Sebastian[169], H. Sandaker[128], C.O. Sander[48], J.A. Sandesara[176], M. Sandhoff[177], C. Sandoval[23b], L. Sanfilippo[63a], D.P.C. Sankey[137], T. Sano[89], A. Sansoni[53], M. Santana Queiroz[18b], L. Santi[37], C. Santoni[41], H. Santos[133a,133b], A. Santra[175], E. Sanzani[24b,24a], K.A. Saoucha[85b], J.G. Saraiva[133a,133d], J. Sardain[7], O. Sasaki[84], K. Sato[163], C. Sauer[37], E. Sauvan[4], P. Savard[161,ai], R. Sawada[159], C. Sawyer[137], L. Sawyer[99], C. Sbarra[24b], A. Sbrizzi[24b,24a], T. Scanlon[98], J. Schaarschmidt[142], U. Schäfer[102], A.C. Schaffer[66,45], D. Schaile[111], R.D. Schamberger[151], C. Scharf[19], M.M. Schefer[20], V.A. Schegelsky[38], D. Scheirich[136], M. Schernau[140f], C. Scheulen[56], C. Schiavi[57b,57a], M. Schioppa[44b,44a], B. Schlag[149], S. Schlenker[37], J. Schmeing[177], E. Schmidt[112], M.A. Schmidt[177], K. Schmieden[25], C. Schmitt[102], N. Schmitt[102], S. Schmitt[48], N.A. Schneider[111], L. Schoeffel[138], A. Schoening[63b], P.G. Scholer[35], E. Schopf[147], M. Schott[25], S. Schramm[56], T. Schroer[56], H-C. Schultz-Coulon[63a], M. Schumacher[54], B.A. Schumm[139], Ph. Schune[138], H.R. Schwartz[7], A. Schwartzman[149], T.A. Schwarz[108], Ph. Schwemling[138], R. Schwienhorst[109], F.G. Sciacca[20], A. Sciandra[30], G. Sciolla[27], F. Scuri[74a], C.D. Sebastiani[37], K. Sedlaczek[118], S.C. Seidel[115], A. Seiden[139], B.D. Seidlitz[42], C. Seitz[48], J.M. Seixas[83b], G. Sekhniaidze[72a], L. Selem[60], N. Semprini-Cesari[24b,24a], A. Semushin[179], D. Sengupta[56], V. Senthilkumar[169], L. Serin[66], M. Sessa[72a,72b], H. Severini[123], F. Sforza[57b,57a], A. Sfyrla[56], Q. Sha[14], E. Shabalina[55], H. Shaddix[118], A.H. Shah[33], R. Shaheen[150], J.D. Shahinian[131], M. Shamim[37], L.Y. Shan[14], M. Shapiro[18a], A. Sharma[37], A.S. Sharma[170], P. Sharma[30], P.B. Shatalov[38], K. Shaw[152], S.M. Shaw[103], Q. Shen[14], D.J. Sheppard[148], P. Sherwood[98], L. Shi[98], X. Shi[14], S. Shimizu[84], C.O. Shimmin[178], I.P.J. Shipsey[129,*], S. Shirabe[90], M. Shiyakova[39,z], M.J. Shochet[40], D.R. Shope[128], B. Shrestha[123], S. Shrestha[122,an], I. Shreyber[39], M.J. Shroff[171], P. Sicho[134], A.M. Sickles[168], E. Sideras Haddad[34h,166], A.C. Sidley[117], A. Sidoti[24b], F. Siegert[50], Dj. Sijacki[16], F. Sili[92], J.M. Silva[52], I. Silva Ferreira[83b], M.V. Silva Oliveira[30], S.B. Silverstein[47a], S. Simion[66], R. Simoniello[37], E.L. Simpson[103], H. Simpson[152], L.R. Simpson[6], S. Simsek[82], S. Sindhu[55], P. Sinervo[161], S.N. Singh[27], S. Singh[30], S. Sinha[48], S. Sinha[103], M. Sioli[24b,24a], K. Sioulas[9], I. Siral[37], E. Sitnikova[48], J. Sjölin[47a,47b], A. Skaf[55], E. Skorda[21], P. Skubic[123], M. Slawinska[88], I. Slazyk[17], I. Sliusar[128], V. Smakhtin[175], B.H. Smart[137], S.Yu. Smirnov[140b], Y. Smirnov[82], L.N. Smirnova[38,a], O. Smirnova[100], A.C. Smith[42], D.R. Smith[165], J.L. Smith[103], M.B. Smith[35], R. Smith[149], H. Smitmanns[102], M. Smizanska[93], K. Smolek[135], P. Smolyanskiy[135], A.A. Snesarev[39], H.L. Snoek[117], S. Snyder[30], R. Sobie[171,ab], A. Soffer[157], C.A. Solans Sanchez[37], E.Yu. Soldatov[39], U. Soldevila[169], A.A. Solodkov[34h], S. Solomon[27], A. Soloshenko[39], K. Solovieva[54], O.V. Solovyanov[41], P. Sommer[50], A. Sonay[13], A. Sopczak[135], A.L. Sopio[52], F. Sopkova[29b], J.D. Sorenson[115], I.R. Sotarriva Alvarez[141], V. Sothilingam[63a], O.J. Soto Sandoval[140c,140b], S. Sottocornola[68], R. Soualah[85a], Z. Soumaimi[36e], D. South[48], N. Soybelman[175], S. Spagnolo[70a,70b], M. Spalla[112], D. Sperlich[54], B. Spisso[72a,72b], D.P. Spiteri[59], L. Splendori[104], M. Spousta[136], E.J. Staats[35], R. Stamen[63a], E. Stanecka[88], W. Stanek-Maslouska[48], M.V. Stange[50], B. Stanislaus[18a], M.M. Stanitzki[48], B. Stapf[48], E.A. Starchenko[38], G.H. Stark[139], J. Stark[91], P. Staroba[134], P. Starovoitov[85b], R. Staszewski[88],

C. Stauch[111], G. Stavropoulos[46], A. Stefl[37], A. Stein[102], P. Steinberg[30], B. Stelzer[148,162a], H.J. Stelzer[132], O. Stelzer[162a], H. Stenzel[58], T.J. Stevenson[152], G.A. Stewart[37], J.R. Stewart[124], G. Stoicea[28b], M. Stolarski[133a], S. Stonjek[112], A. Straessner[50], J. Strandberg[150], S. Strandberg[47a,47b], M. Stratmann[177], M. Strauss[123], T. Strebler[104], P. Strizenec[29b], R. Ströhmer[172], D.M. Strom[126], R. Stroynowski[45], A. Strubig[47a,47b], S.A. Stucci[30], B. Stugu[17], J. Stupak[123], N.A. Styles[48], D. Su[149], S. Su[62], X. Su[62], D. Suchy[29a], A.D. Sudhakar Ponnu[55], K. Sugizaki[131], V.V. Sulin[38], D.M.S. Sultan[129], L. Sultanaliyeva[25], S. Sultansoy[3b], S. Sun[176], W. Sun[14], N. Sur[100], M.R. Sutton[152], M. Svatos[134], P.N. Swallow[33], M. Swiatlowski[162a], T. Swirski[172], A. Swoboda[37], I. Sykora[29a], M. Sykora[136], T. Sykora[136], D. Ta[102], K. Tackmann[48,y], A. Taffard[165], R. Tafirout[162a], Y. Takubo[84], M. Talby[104], A.A. Talyshev[38], K.C. Tam[64b], N.M. Tamir[157], A. Tanaka[159], J. Tanaka[159], R. Tanaka[66], M. Tanasini[151], Z. Tao[170], S. Tapia Araya[140g], S. Tapprogge[102], A. Tarek Abouelfadl Mohamed[37], S. Tarem[156], K. Tariq[14], G. Tarna[37], G.F. Tartarelli[71a], M.J. Tartarin[91], P. Tas[136], M. Tasevsky[134], E. Tassi[44b,44a], A.C. Tate[168], Y. Tayalati[36e,aa], G.N. Taylor[107], W. Taylor[162b], R.J. Taylor Vara[169], A.S. Tegetmeier[91], P. Teixeira-Dias[97], J.J. Teoh[161], K. Terashi[159], J. Terron[101], S. Terzo[13], M. Testa[53], R.J. Teuscher[161,ab], A. Thaler[79], O. Theiner[56], T. Theveneaux-Pelzer[104], D.W. Thomas[97], J.P. Thomas[21], E.A. Thompson[18a], P.D. Thompson[21], E. Thomson[131], R.E. Thornberry[45], C. Tian[62], Y. Tian[56], V. Tikhomirov[82], Yu.A. Tikhonov[39], S. Timoshenko[38], D. Timoshyn[136], E.X.L. Ting[1], P. Tipton[178], A. Tishelman-Charny[30], K. Todome[141], S. Todorova-Nova[136], L. Toffolin[69a,69c], M. Togawa[84], J. Tojo[90], S. Tokár[29a], O. Toldaiev[68], G. Tolkachev[104], M. Tomoto[84], L. Tompkins[149,n], E. Torrence[126], H. Torres[91], D.I. Torres Arza[140g], E. Torró Pastor[169], M. Toscani[31], C. Tosciri[40], M. Tost[11], D.R. Tovey[145], T. Trefzger[172], P.M. Tricarico[13], A. Tricoli[30], I.M. Trigger[162a], S. Trincaz-Duvoid[130], D.A. Trischuk[27], A. Tropina[39], L. Truong[34c], M. Trzebinski[88], A. Trzupek[88], F. Tsai[151], M. Tsai[108], A. Tsiamis[158], P.V. Tsiareshka[39], S. Tsigaridas[162a], A. Tsirigotis[158,u], V. Tsiskaridze[155a], E.G. Tskhadadze[155a], Y. Tsujikawa[89], I.I. Tsukerman[38], V. Tsulaia[18a], S. Tsuno[84], K. Tsuri[121], D. Tsybychev[151], Y. Tu[64b], A. Tudorache[28b], V. Tudorache[28b], S.B. Tuncay[129], S. Turchikhin[57b,57a], I. Turk Cakir[3a], R. Turra[71a], T. Turtuvshin[39,ac], P.M. Tuts[42], S. Tzamarias[158,d], Y. Uematsu[84], F. Ukegawa[163], P.A. Ulloa Poblete[140c,140b], E.N. Umaka[30], G. Unal[37], A. Undrus[30], G. Unel[165], J. Urban[29b], P. Urrejola[140e], G. Usai[8], R. Ushioda[160], M. Usman[110], F. Ustuner[52], Z. Uysal[82], V. Vacek[135], B. Vachon[106], T. Vafeiadis[37], A. Vaitkus[98], C. Valderanis[111], E. Valdes Santurio[47a,47b], M. Valente[37], S. Valentinetti[24b,24a], A. Valero[169], E. Valiente Moreno[169], A. Vallier[91], J.A. Valls Ferrer[169], D.R. Van Arneman[117], A. Van Der Graaf[49], H.Z. Van Der Schyf[34h], P. Van Gemmeren[6], M. Van Rijnbach[37], S. Van Stroud[98], I. Van Vulpen[117], P. Vana[136], M. Vanadia[76a,76b], U.M. Vande Voorde[150], W. Vandelli[37], E.R. Vandewall[124], D. Vannicola[157], L. Vannoli[53], R. Vari[75a], M. Varma[178], E.W. Varnes[7], C. Varni[118], D. Varouchas[66], L. Varriale[169], K.E. Varvell[153], M.E. Vasile[28b], L. Vaslin[84], M.D. Vassilev[149], A. Vasyukov[39], L.M. Vaughan[124], R. Vavricka[136], T. Vazquez Schroeder[13], J. Veatch[32], V. Vecchio[103], M.J. Veen[105], I. Veliscek[30], I. Velkovska[95], L.M. Veloce[161], F. Veloso[133a,133c], S. Veneziano[75a], A. Ventura[70a,70b], A. Verbytskyi[112], M. Verducci[74a,74b],

C. Vergis[96], M. Verissimo De Araujo[83b], W. Verkerke[117], J.C. Vermeulen[117], C. Vernieri[149], M. Vessella[165], M.C. Vetterli[148,ai], A. Vgenopoulos[102], N. Viaux Maira[140g,af], T. Vickey[145], O.E. Vickey Boeriu[145], G.H.A. Viehhauser[129], L. Vigani[63b], M. Vigl[112], M. Villa[24b,24a], M. Villaplana Perez[169], E.M. Villhauer[40], E. Vilucchi[53], M. Vincent[169], M.G. Vincter[35], A. Visibile[117], A. Visive[117], C. Vittori[37], I. Vivarelli[24b,24a], M.I. Vivas Albornoz[48], E. Voevodina[112], F. Vogel[111], J.C. Voigt[50], P. Vokac[135], Yu. Volkotrub[87b], L. Vomberg[25], E. Von Toerne[25], B. Vormwald[37], K. Vorobev[51], M. Vos[169], K. Voss[147], M. Vozak[37], L. Vozdecky[123], N. Vranjes[16], M. Vranjes Milosavljevic[16], M. Vreeswijk[117], N.K. Vu[144b,144a], R. Vuillermet[37], O. Vujinovic[102], I. Vukotic[40], I.K. Vyas[35], J.F. Wack[33], S. Wada[163], C. Wagner[149], J.M. Wagner[18a], W. Wagner[177], S. Wahdan[177], H. Wahlberg[92], C.H. Waits[123], J. Walder[137], R. Walker[111], K. Walkingshaw Pass[59], W. Walkowiak[147], A. Wall[131], E.J. Wallin[100], T. Wamorkar[18a], K. Wandall-Christensen[169], A. Wang[62], A.Z. Wang[139], C. Wang[102], C. Wang[11], H. Wang[18a], J. Wang[64c], P. Wang[103], P. Wang[98], R. Wang[61], R. Wang[6], S.M. Wang[154], S. Wang[14], T. Wang[116], T. Wang[62], W.T. Wang[129], W. Wang[14], X. Wang[168], X. Wang[144a], X. Wang[48], Y. Wang[114a], Y. Wang[62], Z. Wang[108], Z. Wang[144b], Z. Wang[108], C. Wanotayaroj[84], A. Warburton[106], A.L. Warnerbring[147], S. Waterhouse[97], A.T. Watson[21], H. Watson[52], M.F. Watson[21], E. Watton[37], G. Watts[142], B.M. Waugh[98], J.M. Webb[54], C. Weber[30], H.A. Weber[19], M.S. Weber[20], S.M. Weber[63a], C. Wei[62], Y. Wei[54], A.R. Weidberg[129], E.J. Weik[120], J. Weingarten[49], C. Weiser[54], C.J. Wells[48], T. Wenaus[30], T. Wengler[37], N.S. Wenke[112], N. Wermes[25], M. Wessels[63a], A.M. Wharton[93], A.S. White[61], A. White[8], M.J. White[1], D. Whiteson[165], L. Wickremasinghe[127], W. Wiedenmann[176], M. Wielers[137], R. Wierda[150], C. Wiglesworth[43], H.G. Wilkens[37], J.J.H. Wilkinson[33], D.M. Williams[42], H.H. Williams[131], S. Williams[33], S. Willocq[105], B.J. Wilson[103], D.J. Wilson[103], P.J. Windischhofer[40], F.I. Winkel[31], F. Winklmeier[126], B.T. Winter[54], M. Wittgen[149], M. Wobisch[99], T. Wojtkowski[60], Z. Wolffs[117], J. Wollrath[37], M.W. Wolter[88], H. Wolters[133a,133c], M.C. Wong[139], E.L. Woodward[42], S.D. Worm[48], B.K. Wosiek[88], K.W. Woźniak[88], S. Wozniewski[55], K. Wraight[59], C. Wu[161], C. Wu[21], J. Wu[159], M. Wu[114b], M. Wu[116], S.L. Wu[176], S. Wu[14,ak], X. Wu[62], Y.Q. Wu[161], Y. Wu[62], Z. Wu[4], Z. Wu[114a], J. Wuerzinger[112], T.R. Wyatt[103], B.M. Wynne[52], S. Xella[43], L. Xia[114a], M. Xie[62], A. Xiong[126], D. Xu[14], H. Xu[62], L. Xu[62], R. Xu[131], T. Xu[108], Y. Xu[142], Z. Xu[52], R. Xue[132], B. Yabsley[153], S. Yacoob[34a], Y. Yamaguchi[84], E. Yamashita[159], H. Yamauchi[163], T. Yamazaki[18a], Y. Yamazaki[86], S. Yan[59], Z. Yan[105], H.J. Yang[144a,144b], H.T. Yang[62], S. Yang[62], T. Yang[64c], X. Yang[37], X. Yang[14], Y. Yang[159], Y. Yang[62], W-M. Yao[18a], C.L. Yardley[152], J. Ye[14], S. Ye[30], X. Ye[62], Y. Yeh[98], I. Yeletskikh[39], B. Yeo[18b], M.R. Yexley[98], T.P. Yildirim[129], K. Yorita[174], C.J.S. Young[37], C. Young[149], N.D. Young[126], Y. Yu[62], J. Yuan[14,114c], M. Yuan[108], R. Yuan[144b,144a], L. Yue[98], M. Zaazoua[62], B. Zabinski[88], I. Zahir[36a], A. Zaio[57b,57a], Z.K. Zak[88], T. Zakareishvili[169], S. Zambito[56], J.A. Zamora Saa[140d], J. Zang[159], R. Zanzottera[71a,71b], O. Zaplatilek[135], C. Zeitnitz[177], H. Zeng[14], J.C. Zeng[168], D.T. Zenger Jr[27], O. Zenin[38], T. Ženiš[29a], S. Zenz[96], D. Zerwas[66], M. Zhai[14,114c], D.F. Zhang[145], G. Zhang[14,ak], J. Zhang[143a], J. Zhang[6], K. Zhang[14,114c], L. Zhang[62],

JHEP10(2025)093

L. Zhang[114a], P. Zhang[14,114c], R. Zhang[114a], S. Zhang[91], T. Zhang[159], Y. Zhang[142], Y. Zhang[98], Y. Zhang[62], Y. Zhang[114a], Z. Zhang[18a], Z. Zhang[143a], Z. Zhang[66], H. Zhao[142], T. Zhao[143a], Y. Zhao[35], Z. Zhao[62], Z. Zhao[62], A. Zhemchugov[39], J. Zheng[114a], K. Zheng[168], X. Zheng[62], Z. Zheng[149], D. Zhong[168], B. Zhou[108], H. Zhou[7], N. Zhou[144a], Y. Zhou[15], Y. Zhou[114a], Y. Zhou[7], C.G. Zhu[143a], J. Zhu[108], X. Zhu[144b], Y. Zhu[144a], Y. Zhu[62], X. Zhuang[14], K. Zhukov[68], N.I. Zimine[39], J. Zinsser[63b], M. Ziolkowski[147], L. Živković[16], A. Zoccoli[24b,24a], K. Zoch[61], A. Zografos[37], T.G. Zorbas[145], O. Zormpa[46], L. Zwalinski[37]

[1] *Department of Physics, University of Adelaide, Adelaide; Australia*
[2] *Department of Physics, University of Alberta, Edmonton AB; Canada*
[3] [(a)] *Department of Physics, Ankara University, Ankara;*[(b)] *Division of Physics, TOBB University of Economics and Technology, Ankara; Türkiye*
[4] *LAPP, Université Savoie Mont Blanc, CNRS/IN2P3, Annecy; France*
[5] *APC, Université Paris Cité, CNRS/IN2P3, Paris; France*
[6] *High Energy Physics Division, Argonne National Laboratory, Argonne IL; United States of America*
[7] *Department of Physics, University of Arizona, Tucson AZ; United States of America*
[8] *Department of Physics, University of Texas at Arlington, Arlington TX; United States of America*
[9] *Physics Department, National and Kapodistrian University of Athens, Athens; Greece*
[10] *Physics Department, National Technical University of Athens, Zografou; Greece*
[11] *Department of Physics, University of Texas at Austin, Austin TX; United States of America*
[12] *Institute of Physics, Azerbaijan Academy of Sciences, Baku; Azerbaijan*
[13] *Institut de Física d'Altes Energies (IFAE), Barcelona Institute of Science and Technology, Barcelona; Spain*
[14] *Institute of High Energy Physics, Chinese Academy of Sciences, Beijing; China*
[15] *Physics Department, Tsinghua University, Beijing; China*
[16] *Institute of Physics, University of Belgrade, Belgrade; Serbia*
[17] *Department for Physics and Technology, University of Bergen, Bergen; Norway*
[18] [(a)] *Physics Division, Lawrence Berkeley National Laboratory, Berkeley CA;*[(b)] *University of California, Berkeley CA; United States of America*
[19] *Institut für Physik, Humboldt Universität zu Berlin, Berlin; Germany*
[20] *Albert Einstein Center for Fundamental Physics and Laboratory for High Energy Physics, University of Bern, Bern; Switzerland*
[21] *School of Physics and Astronomy, University of Birmingham, Birmingham; United Kingdom*
[22] [(a)] *Department of Physics, Bogazici University, Istanbul;*[(b)] *Department of Physics Engineering, Gaziantep University, Gaziantep;*[(c)] *Department of Physics, Istanbul University, Istanbul; Türkiye*
[23] [(a)] *Facultad de Ciencias y Centro de Investigaciónes, Universidad Antonio Nariño, Bogotá;*[(b)] *Departamento de Física, Universidad Nacional de Colombia, Bogotá; Colombia*
[24] [(a)] *Dipartimento di Fisica e Astronomia A. Righi, Università di Bologna, Bologna;*[(b)] *INFN Sezione di Bologna; Italy*
[25] *Physikalisches Institut, Universität Bonn, Bonn; Germany*
[26] *Department of Physics, Boston University, Boston MA; United States of America*
[27] *Department of Physics, Brandeis University, Waltham MA; United States of America*
[28] [(a)] *Transilvania University of Brasov, Brasov;*[(b)] *Horia Hulubei National Institute of Physics and Nuclear Engineering, Bucharest;*[(c)] *Department of Physics, Alexandru Ioan Cuza University of Iasi, Iasi;*[(d)] *National Institute for Research and Development of Isotopic and Molecular Technologies, Physics Department, Cluj-Napoca;*[(e)] *National University of Science and Technology Politechnica, Bucharest;*[(f)] *West University in Timisoara, Timisoara;*[(g)] *Faculty of Physics, University of Bucharest, Bucharest; Romania*
[29] [(a)] *Faculty of Mathematics, Physics and Informatics, Comenius University, Bratislava;*[(b)] *Department of Subnuclear Physics, Institute of Experimental Physics of the Slovak Academy of Sciences, Kosice; Slovak Republic*
[30] *Physics Department, Brookhaven National Laboratory, Upton NY; United States of America*

JHEP10(2025)093

[31] Universidad de Buenos Aires, Facultad de Ciencias Exactas y Naturales, Departamento de Física, y CONICET, Instituto de Física de Buenos Aires (IFIBA), Buenos Aires; Argentina
[32] California State University, CA; United States of America
[33] Cavendish Laboratory, University of Cambridge, Cambridge; United Kingdom
[34] [(a)] Department of Physics, University of Cape Town, Cape Town;[(b)] iThemba Labs, Western Cape;[(c)] Department of Mechanical Engineering Science, University of Johannesburg, Johannesburg;[(d)] National Institute of Physics, University of the Philippines Diliman (Philippines);[(e)] Department of Physics, Stellenbosch University, Matieland;[(f)] University of South Africa, Department of Physics, Pretoria;[(g)] University of Zululand, KwaDlangezwa;[(h)] School of Physics, University of the Witwatersrand, Johannesburg; South Africa
[35] Department of Physics, Carleton University, Ottawa ON; Canada
[36] [(a)] Faculté des Sciences Ain Chock, Université Hassan II de Casablanca;[(b)] Faculté des Sciences, Université Ibn-Tofail, Kénitra;[(c)] Faculté des Sciences Semlalia, Université Cadi Ayyad, LPHEA-Marrakech;[(d)] LPMR, Faculté des Sciences, Université Mohamed Premier, Oujda;[(e)] Faculté des sciences, Université Mohammed V, Rabat;[(f)] Institute of Applied Physics, Mohammed VI Polytechnic University, Ben Guerir; Morocco
[37] CERN, Geneva; Switzerland
[38] Affiliated with an institute formerly covered by a cooperation agreement with CERN
[39] Affiliated with an international laboratory covered by a cooperation agreement with CERN
[40] Enrico Fermi Institute, University of Chicago, Chicago IL; United States of America
[41] LPC, Université Clermont Auvergne, CNRS/IN2P3, Clermont-Ferrand; France
[42] Nevis Laboratory, Columbia University, Irvington NY; United States of America
[43] Niels Bohr Institute, University of Copenhagen, Copenhagen; Denmark
[44] [(a)] Dipartimento di Fisica, Università della Calabria, Rende;[(b)] INFN Gruppo Collegato di Cosenza, Laboratori Nazionali di Frascati; Italy
[45] Physics Department, Southern Methodist University, Dallas TX; United States of America
[46] National Centre for Scientific Research "Demokritos", Agia Paraskevi; Greece
[47] [(a)] Department of Physics, Stockholm University;[(b)] Oskar Klein Centre, Stockholm; Sweden
[48] Deutsches Elektronen-Synchrotron DESY, Hamburg and Zeuthen; Germany
[49] Fakultät Physik, Technische Universität Dortmund, Dortmund; Germany
[50] Institut für Kern- und Teilchenphysik, Technische Universität Dresden, Dresden; Germany
[51] Department of Physics, Duke University, Durham NC; United States of America
[52] SUPA — School of Physics and Astronomy, University of Edinburgh, Edinburgh; United Kingdom
[53] INFN e Laboratori Nazionali di Frascati, Frascati; Italy
[54] Physikalisches Institut, Albert-Ludwigs-Universität Freiburg, Freiburg; Germany
[55] II. Physikalisches Institut, Georg-August-Universität Göttingen, Göttingen; Germany
[56] Département de Physique Nucléaire et Corpusculaire, Université de Genève, Genève; Switzerland
[57] [(a)] Dipartimento di Fisica, Università di Genova, Genova;[(b)] INFN Sezione di Genova; Italy
[58] II. Physikalisches Institut, Justus-Liebig-Universität Giessen, Giessen; Germany
[59] SUPA — School of Physics and Astronomy, University of Glasgow, Glasgow; United Kingdom
[60] LPSC, Université Grenoble Alpes, CNRS/IN2P3, Grenoble INP, Grenoble; France
[61] Laboratory for Particle Physics and Cosmology, Harvard University, Cambridge MA; United States of America
[62] Department of Modern Physics and State Key Laboratory of Particle Detection and Electronics, University of Science and Technology of China, Hefei; China
[63] [(a)] Kirchhoff-Institut für Physik, Ruprecht-Karls-Universität Heidelberg, Heidelberg;[(b)] Physikalisches Institut, Ruprecht-Karls-Universität Heidelberg, Heidelberg; Germany
[64] [(a)] Department of Physics, Chinese University of Hong Kong, Shatin, N.T., Hong Kong;[(b)] Department of Physics, University of Hong Kong, Hong Kong;[(c)] Department of Physics and Institute for Advanced Study, Hong Kong University of Science and Technology, Clear Water Bay, Kowloon, Hong Kong; China
[65] Department of Physics, National Tsing Hua University, Hsinchu; Taiwan
[66] IJCLab, Université Paris-Saclay, CNRS/IN2P3, 91405, Orsay; France
[67] Centro Nacional de Microelectrónica (IMB-CNM-CSIC), Barcelona; Spain
[68] Department of Physics, Indiana University, Bloomington IN; United States of America

JHEP10(2025)093

[69] [(a)] *INFN Gruppo Collegato di Udine, Sezione di Trieste, Udine;* [(b)] *ICTP, Trieste;* [(c)] *Dipartimento Politecnico di Ingegneria e Architettura, Università di Udine, Udine; Italy*
[70] [(a)] *INFN Sezione di Lecce;* [(b)] *Dipartimento di Matematica e Fisica, Università del Salento, Lecce; Italy*
[71] [(a)] *INFN Sezione di Milano;* [(b)] *Dipartimento di Fisica, Università di Milano, Milano; Italy*
[72] [(a)] *INFN Sezione di Napoli;* [(b)] *Dipartimento di Fisica, Università di Napoli, Napoli; Italy*
[73] [(a)] *INFN Sezione di Pavia;* [(b)] *Dipartimento di Fisica, Università di Pavia, Pavia; Italy*
[74] [(a)] *INFN Sezione di Pisa;* [(b)] *Dipartimento di Fisica E. Fermi, Università di Pisa, Pisa; Italy*
[75] [(a)] *INFN Sezione di Roma;* [(b)] *Dipartimento di Fisica, Sapienza Università di Roma, Roma; Italy*
[76] [(a)] *INFN Sezione di Roma Tor Vergata;* [(b)] *Dipartimento di Fisica, Università di Roma Tor Vergata, Roma; Italy*
[77] [(a)] *INFN Sezione di Roma Tre;* [(b)] *Dipartimento di Matematica e Fisica, Università Roma Tre, Roma; Italy*
[78] [(a)] *INFN-TIFPA;* [(b)] *Università degli Studi di Trento, Trento; Italy*
[79] *Universität Innsbruck, Department of Astro and Particle Physics, Innsbruck; Austria*
[80] *University of Iowa, Iowa City IA; United States of America*
[81] *Department of Physics and Astronomy, Iowa State University, Ames IA; United States of America*
[82] *Istinye University, Sariyer, Istanbul; Türkiye*
[83] [(a)] *Departamento de Engenharia Elétrica, Universidade Federal de Juiz de Fora (UFJF), Juiz de Fora;* [(b)] *Universidade Federal do Rio De Janeiro COPPE/EE/IF, Rio de Janeiro;* [(c)] *Instituto de Física, Universidade de São Paulo, São Paulo;* [(d)] *Rio de Janeiro State University, Rio de Janeiro;* [(e)] *Federal University of Bahia, Bahia; Brazil*
[84] *KEK, High Energy Accelerator Research Organization, Tsukuba; Japan*
[85] [(a)] *Khalifa University of Science and Technology, Abu Dhabi;* [(b)] *University of Sharjah, Sharjah; United Arab Emirates*
[86] *Graduate School of Science, Kobe University, Kobe; Japan*
[87] [(a)] *AGH University of Krakow, Faculty of Physics and Applied Computer Science, Krakow;* [(b)] *Marian Smoluchowski Institute of Physics, Jagiellonian University, Krakow; Poland*
[88] *Institute of Nuclear Physics Polish Academy of Sciences, Krakow; Poland*
[89] *Faculty of Science, Kyoto University, Kyoto; Japan*
[90] *Research Center for Advanced Particle Physics and Department of Physics, Kyushu University, Fukuoka; Japan*
[91] *L2IT, Université de Toulouse, CNRS/IN2P3, UPS, Toulouse; France*
[92] *Instituto de Física La Plata, Universidad Nacional de La Plata and CONICET, La Plata; Argentina*
[93] *Physics Department, Lancaster University, Lancaster; United Kingdom*
[94] *Oliver Lodge Laboratory, University of Liverpool, Liverpool; United Kingdom*
[95] *Department of Experimental Particle Physics, Jožef Stefan Institute and Department of Physics, University of Ljubljana, Ljubljana; Slovenia*
[96] *Department of Physics and Astronomy, Queen Mary University of London, London; United Kingdom*
[97] *Department of Physics, Royal Holloway University of London, Egham; United Kingdom*
[98] *Department of Physics and Astronomy, University College London, London; United Kingdom*
[99] *Louisiana Tech University, Ruston LA; United States of America*
[100] *Fysiska institutionen, Lunds universitet, Lund; Sweden*
[101] *Departamento de Física Teorica C-15 and CIAFF, Universidad Autónoma de Madrid, Madrid; Spain*
[102] *Institut für Physik, Universität Mainz, Mainz; Germany*
[103] *School of Physics and Astronomy, University of Manchester, Manchester; United Kingdom*
[104] *CPPM, Aix-Marseille Université, CNRS/IN2P3, Marseille; France*
[105] *Department of Physics, University of Massachusetts, Amherst MA; United States of America*
[106] *Department of Physics, McGill University, Montreal QC; Canada*
[107] *School of Physics, University of Melbourne, Victoria; Australia*
[108] *Department of Physics, University of Michigan, Ann Arbor MI; United States of America*
[109] *Department of Physics and Astronomy, Michigan State University, East Lansing MI; United States of America*
[110] *Group of Particle Physics, University of Montreal, Montreal QC; Canada*
[111] *Fakultät für Physik, Ludwig-Maximilians-Universität München, München; Germany*

[112] *Max-Planck-Institut für Physik (Werner-Heisenberg-Institut), München; Germany*
[113] *Graduate School of Science and Kobayashi-Maskawa Institute, Nagoya University, Nagoya; Japan*
[114] [(a)] *Department of Physics, Nanjing University, Nanjing;* [(b)] *School of Science, Shenzhen Campus of Sun Yat-sen University;* [(c)] *University of Chinese Academy of Science (UCAS), Beijing; China*
[115] *Department of Physics and Astronomy, University of New Mexico, Albuquerque NM; United States of America*
[116] *Institute for Mathematics, Astrophysics and Particle Physics, Radboud University/Nikhef, Nijmegen; Netherlands*
[117] *Nikhef National Institute for Subatomic Physics and University of Amsterdam, Amsterdam; Netherlands*
[118] *Department of Physics, Northern Illinois University, DeKalb IL; United States of America*
[119] [(a)] *New York University Abu Dhabi, Abu Dhabi;* [(b)] *United Arab Emirates University, Al Ain; United Arab Emirates*
[120] *Department of Physics, New York University, New York NY; United States of America*
[121] *Ochanomizu University, Otsuka, Bunkyo-ku, Tokyo; Japan*
[122] *Ohio State University, Columbus OH; United States of America*
[123] *Homer L. Dodge Department of Physics and Astronomy, University of Oklahoma, Norman OK; United States of America*
[124] *Department of Physics, Oklahoma State University, Stillwater OK; United States of America*
[125] *Palacký University, Joint Laboratory of Optics, Olomouc; Czech Republic*
[126] *Institute for Fundamental Science, University of Oregon, Eugene, OR; United States of America*
[127] *Graduate School of Science, University of Osaka, Osaka; Japan*
[128] *Department of Physics, University of Oslo, Oslo; Norway*
[129] *Department of Physics, Oxford University, Oxford; United Kingdom*
[130] *LPNHE, Sorbonne Université, Université Paris Cité, CNRS/IN2P3, Paris; France*
[131] *Department of Physics, University of Pennsylvania, Philadelphia PA; United States of America*
[132] *Department of Physics and Astronomy, University of Pittsburgh, Pittsburgh PA; United States of America*
[133] [(a)] *Laboratório de Instrumentação e Física Experimental de Partículas — LIP, Lisboa;* [(b)] *Departamento de Física, Faculdade de Ciências, Universidade de Lisboa, Lisboa;* [(c)] *Departamento de Física, Universidade de Coimbra, Coimbra;* [(d)] *Centro de Física Nuclear da Universidade de Lisboa, Lisboa;* [(e)] *Departamento de Física, Escola de Ciências, Universidade do Minho, Braga;* [(f)] *Departamento de Física Teórica y del Cosmos, Universidad de Granada, Granada (Spain);* [(g)] *Departamento de Física, Instituto Superior Técnico, Universidade de Lisboa, Lisboa; Portugal*
[134] *Institute of Physics of the Czech Academy of Sciences, Prague; Czech Republic*
[135] *Czech Technical University in Prague, Prague; Czech Republic*
[136] *Charles University, Faculty of Mathematics and Physics, Prague; Czech Republic*
[137] *Particle Physics Department, Rutherford Appleton Laboratory, Didcot; United Kingdom*
[138] *IRFU, CEA, Université Paris-Saclay, Gif-sur-Yvette; France*
[139] *Santa Cruz Institute for Particle Physics, University of California Santa Cruz, Santa Cruz CA; United States of America*
[140] [(a)] *Departamento de Física, Pontificia Universidad Católica de Chile, Santiago;* [(b)] *Millennium Institute for Subatomic physics at high energy frontier (SAPHIR), Santiago;* [(c)] *Instituto de Investigación Multidisciplinario en Ciencia y Tecnología, y Departamento de Física, Universidad de La Serena;* [(d)] *Universidad Andres Bello, Department of Physics, Santiago;* [(e)] *Universidad San Sebastian, Recoleta;* [(f)] *Instituto de Alta Investigación, Universidad de Tarapacá, Arica;* [(g)] *Departamento de Física, Universidad Técnica Federico Santa María, Valparaíso; Chile*
[141] *Department of Physics, Institute of Science, Tokyo; Japan*
[142] *Department of Physics, University of Washington, Seattle WA; United States of America*
[143] [(a)] *Institute of Frontier and Interdisciplinary Science and Key Laboratory of Particle Physics and Particle Irradiation (MOE), Shandong University, Qingdao;* [(b)] *School of Physics, Zhengzhou University; China*
[144] [(a)] *State Key Laboratory of Dark Matter Physics, School of Physics and Astronomy, Shanghai Jiao Tong University, Key Laboratory for Particle Astrophysics and Cosmology (MOE), SKLPPC, Shanghai;* [(b)] *State Key Laboratory of Dark Matter Physics, Tsung-Dao Lee Institute, Shanghai Jiao Tong University, Shanghai; China*

JHEP10(2025)093

[145] *Department of Physics and Astronomy, University of Sheffield, Sheffield; United Kingdom*
[146] *Department of Physics, Shinshu University, Nagano; Japan*
[147] *Department Physik, Universität Siegen, Siegen; Germany*
[148] *Department of Physics, Simon Fraser University, Burnaby BC; Canada*
[149] *SLAC National Accelerator Laboratory, Stanford CA; United States of America*
[150] *Department of Physics, Royal Institute of Technology, Stockholm; Sweden*
[151] *Departments of Physics and Astronomy, Stony Brook University, Stony Brook NY; United States of America*
[152] *Department of Physics and Astronomy, University of Sussex, Brighton; United Kingdom*
[153] *School of Physics, University of Sydney, Sydney; Australia*
[154] *Institute of Physics, Academia Sinica, Taipei; Taiwan*
[155] [(a)] *E. Andronikashvili Institute of Physics, Iv. Javakhishvili Tbilisi State University, Tbilisi;*[(b)] *High Energy Physics Institute, Tbilisi State University, Tbilisi;*[(c)] *University of Georgia, Tbilisi; Georgia*
[156] *Department of Physics, Technion, Israel Institute of Technology, Haifa; Israel*
[157] *Raymond and Beverly Sackler School of Physics and Astronomy, Tel Aviv University, Tel Aviv; Israel*
[158] *Department of Physics, Aristotle University of Thessaloniki, Thessaloniki; Greece*
[159] *International Center for Elementary Particle Physics and Department of Physics, University of Tokyo, Tokyo; Japan*
[160] *Graduate School of Science and Technology, Tokyo Metropolitan University, Tokyo; Japan*
[161] *Department of Physics, University of Toronto, Toronto ON; Canada*
[162] [(a)] *TRIUMF, Vancouver BC;*[(b)] *Department of Physics and Astronomy, York University, Toronto ON; Canada*
[163] *Division of Physics and Tomonaga Center for the History of the Universe, Faculty of Pure and Applied Sciences, University of Tsukuba, Tsukuba; Japan*
[164] *Department of Physics and Astronomy, Tufts University, Medford MA; United States of America*
[165] *Department of Physics and Astronomy, University of California Irvine, Irvine CA; United States of America*
[166] *University of West Attica, Athens; Greece*
[167] *Department of Physics and Astronomy, University of Uppsala, Uppsala; Sweden*
[168] *Department of Physics, University of Illinois, Urbana IL; United States of America*
[169] *Instituto de Física Corpuscular (IFIC), Centro Mixto Universidad de Valencia — CSIC, Valencia; Spain*
[170] *Department of Physics, University of British Columbia, Vancouver BC; Canada*
[171] *Department of Physics and Astronomy, University of Victoria, Victoria BC; Canada*
[172] *Fakultät für Physik und Astronomie, Julius-Maximilians-Universität Würzburg, Würzburg; Germany*
[173] *Department of Physics, University of Warwick, Coventry; United Kingdom*
[174] *Waseda University, Tokyo; Japan*
[175] *Department of Particle Physics and Astrophysics, Weizmann Institute of Science, Rehovot; Israel*
[176] *Department of Physics, University of Wisconsin, Madison WI; United States of America*
[177] *Fakultät für Mathematik und Naturwissenschaften, Fachgruppe Physik, Bergische Universität Wuppertal, Wuppertal; Germany*
[178] *Department of Physics, Yale University, New Haven CT; United States of America*
[179] *Yerevan Physics Institute, Yerevan; Armenia*

[a] *Also at Affiliated with an institute formerly covered by a cooperation agreement with CERN*
[b] *Also at An-Najah National University, Nablus; Palestine*
[c] *Also at Borough of Manhattan Community College, City University of New York, New York NY; United States of America*
[d] *Also at Center for Interdisciplinary Research and Innovation (CIRI-AUTH), Thessaloniki; Greece*
[e] *Also at Centre of Physics of the Universities of Minho and Porto (CF-UM-UP); Portugal*
[f] *Also at CERN, Geneva; Switzerland*
[g] *Also at Département de Physique Nucléaire et Corpusculaire, Université de Genève, Genève; Switzerland*
[h] *Also at Departament de Fisica de la Universitat Autonoma de Barcelona, Barcelona; Spain*
[i] *Also at Department of Financial and Management Engineering, University of the Aegean, Chios; Greece*
[j] *Also at Department of Mathematical Sciences, University of South Africa, Johannesburg; South Africa*

[k] Also at Department of Modern Physics and State Key Laboratory of Particle Detection and Electronics, University of Science and Technology of China, Hefei; China
[l] Also at Department of Physics, Bolu Abant Izzet Baysal University, Bolu; Türkiye
[m] Also at Department of Physics, King's College London, London; United Kingdom
[n] Also at Department of Physics, Stanford University, Stanford CA; United States of America
[o] Also at Department of Physics, Stellenbosch University; South Africa
[p] Also at Department of Physics, University of Fribourg, Fribourg; Switzerland
[q] Also at Department of Physics, University of Thessaly; Greece
[r] Also at Department of Physics, Westmont College, Santa Barbara; United States of America
[s] Also at Faculty of Physics, Sofia University, 'St. Kliment Ohridski', Sofia; Bulgaria
[t] Also at Faculty of Physics, University of Bucharest; Romania
[u] Also at Hellenic Open University, Patras; Greece
[v] Also at Henan University; China
[w] Also at Imam Mohammad Ibn Saud Islamic University; Saudi Arabia
[x] Also at Institucio Catalana de Recerca i Estudis Avancats, ICREA, Barcelona; Spain
[y] Also at Institut für Experimentalphysik, Universität Hamburg, Hamburg; Germany
[z] Also at Institute for Nuclear Research and Nuclear Energy (INRNE) of the Bulgarian Academy of Sciences, Sofia; Bulgaria
[aa] Also at Institute of Applied Physics, Mohammed VI Polytechnic University, Ben Guerir; Morocco
[ab] Also at Institute of Particle Physics (IPP); Canada
[ac] Also at Institute of Physics and Technology, Mongolian Academy of Sciences, Ulaanbaatar; Mongolia
[ad] Also at Institute of Physics, Azerbaijan Academy of Sciences, Baku; Azerbaijan
[ae] Also at Institute of Theoretical Physics, Ilia State University, Tbilisi; Georgia
[af] Also at Millennium Institute for Subatomic physics at high energy frontier (SAPHIR), Santiago; Chile
[ag] Also at National Institute of Physics, University of the Philippines Diliman (Philippines); Philippines
[ah] Also at The Collaborative Innovation Center of Quantum Matter (CICQM), Beijing; China
[ai] Also at TRIUMF, Vancouver BC; Canada
[aj] Also at Università di Napoli Parthenope, Napoli; Italy
[ak] Also at University of Chinese Academy of Sciences (UCAS), Beijing; China
[al] Also at University of Colorado Boulder, Department of Physics, Colorado; United States of America
[am] Also at University of Sienna; Italy
[an] Also at Washington College, Chestertown, MD; United States of America
[ao] Also at Yeditepe University, Physics Department, Istanbul; Türkiye
[*] Deceased